Improving the Delivery and Efficacy of a Cancer Therapeutic via Extracellular Matrix Modification

by

Wilson Mok

B.S. Chemical Engineering
University of California, Berkeley (2002)

SUBMITTED TO THE DEPARTMENT OF CHEMICAL ENGINEERING IN PARTIAL FULLFILLMENT OF THE REQUIREMENTS FOR THE DEGREE OF

DOCTOR OF PHILOSOPHY IN CHEMICAL ENGINEERING
AT THE
MASSACHUSETTS INSTITUTE OF TECHNOLOGY
[February 2008]
October 2007

Signature of Author: _____
Department of Chemical Engineering
October 10, 2007

Certified by: _____
Rakesh K. Jain
Andrew Werk Cook Professor of Tumor Biology, Harvard Medical School
Thesis Supervisor

Certified by: _____
Robert S. Langer
Institute Professor
Thesis Supervisor

Accepted by: _____
William M. Deen
Professor of Chemical Engineering
Chairman, Committee for Graduate Students

Improving the Delivery and Efficacy of a Cancer Therapeutic via Extracellular Matrix Modification

by

Wilson Mok

Submitted to the Department of Chemical Engineering on October 10, 2007
in Partial Fullfillment of the Requirements for the Degree of
Doctor of Philosophy in Chemical Engineering

ABSTRACT

The extracellular matrix (ECM) has been shown to be a significant source of hindrance to the transport of macromolecules in solid tumors. This thesis shows that by limiting their interstitial transport, the tumor ECM can reduce the efficacy of cancer therapeutics. Furthermore, techniques for overcoming this transport barrier and improving the effectiveness of existing cancer therapetuics are developed. Mathematical modeling was utilized to characterize the distribution of a therapeutic herpes simplex virus (HSV) vector in solid tumors. The model showed that the spread of virus following intratumoral injection is severely limited by rapid binding and limited diffusion. Importantly, the model demonstrates that an improvement in virus diffusion can enhance its distribution significantly. *In vivo* multiphoton imaging of fibrillar collagen type I and injected HSV vectors largely supported the model predictions. Injected viral particles could not penetrate dense networks of fibrillar collagen. Both the initial distribution and subsequent propagation of these replication-competent vectors were limited by collagen. Degradation of tumor collagen with bacterial collagenase enhanced the distribution and efficacy of the virus. To develop a technique that is clinically applicable, human collagenases were screened for similar activity. Matrix metalloproteinase (MMP) -1 and -8 were identified as viable candidates and tested for their ability to degrade collagen and enhance diffusion in tumors. When overexpressed in tumors, neither MMP significantly altered collagen content or diffusive transport. However, these MMPs have multiple matrix substrates and were found to deplete the tumor of sulfated glycosaminoglycans (GAGs). This, in turn, increased the hydraulic conductivity of these tumors, enhancing the distribution and efficacy of infused oncolytic HSV. Genetic mutations were employed to enhance the activity of these enzymes, but impaired intracellular processing and inactivating autoproteolytic degradation reduced overall activity. Thus, our work demonstrates the importance of the tumor extracellular matrix in regulating the distribution and efficacy of cancer therapeutics. Methods to modulate both tumor collagen and sulfated GAGs are developed to enhance interstitial transport and improve the treatment of solid tumors.

Thesis Supervisor: Rakesh K. Jain
Title: Andrew Werk Cook Professor of Tumor Biology, Harvard Medical School

Thesis Supervisor: Robert S. Langer
Title: Institute Professor

Biographical Sketch

EDUCATION

2002	University of California at Berkeley, *Magna Cum Laude*, Chemical Engineering, B.S.

PROFESSIONAL EXPERIENCE

2/99-5/00	Undergraduate Researcher, Department of Chemistry UC Berkeley, Berkeley, CA Advisor: Ronald Cohen
5/00-8/00	Research Intern, Pharmaceutical Development Department Merck & Co., West Point, PA
9/00-5/02	Undergraduate Researcher, Department of Chemical Engineering UC Berkeley, Berkeley, CA Advisor: David Schaffer
2/03-present	Research Fellow, Massachussetts General Hospital, Boston, MA Advisor: Rakesh K. Jain
9/05-12/05	Teaching Assistant: Tumor Pathophysiology and Transport Phenomena Department of Chemical Engineering, MIT, Cambridge, MA
11/05-12/05	Teaching Assistant: Introduction to Biocatalysis Department of Chemical Engineering, MIT, Cambridge, MA
1/06-2/06	Teaching Assistant: Statistical Design of Experiments Department of Chemical Engineering, MIT, Cambridge, MA

HONORS AND AWARDS

Elected to Tau Beta Pi (2000)
Merck Engineering and Technology Fellowship (2000)
UC Berkeley President's Undergraduate Fellowship (2002)
UC Berkeley Outstanding Senior Award, American Institute of Chemical Engineers (2002)
MIT Presidential Fellowship (2002)
National Science Foundation Graduate Fellowship (2002, declined)
Whitaker Foundation Graduate Fellowship (2002)

PUBLICATIONS

McKee, T. D.*, Grandi, P.*, **Mok, W.***, Alexandrakis, G., Insin, N., Zimmer, J. P., Bawendi, M. G., Boucher, Y., Breakefield, X. O., and Jain, R. K. Degradation of fibrillar collagen in a human melanoma xenograft improves the efficacy of an oncolytic herpes simplex virus vector. Cancer Res, *66:* 2509-2513, 2006. * authors contributed equally

Manuscripts in press:

W. Mok, Y. Boucher and R.K. Jain, "Matrix Metalloproteinase-1 and -8 Improve the Distribution and Efficacy of an Oncolytic Virus." *Cancer Research*

Manuscripts submitted for review:

W. Mok and R.K. Jain, "Modeling of Herpes Simplex Virus Distribution in Solid Tumors: Implications for Cancer Therapy."

Acknowledgements

I would first like to thank my family: my parents Kevin and Winnie and my brother Kenny. To be honest, I cannot recall a single conversation in which I discussed my research with any of them. Yet they are more responsible for this work than anyone else. They instilled in me the principles of hard work, persistence and patience. These were essential traits for me to complete this thesis. I have done an exceedingly poor job of expressing to my parents the appreciation I feel for the sacrifices they have made for me and the valuable lessons they have taught me. I hope that by dedicating this thesis to them I can begin to make up for that.

I would like to thank my advisor Rakesh K. Jain for his support. His belief in my abilities has been palpable and has given me the self-assurance to explore entirely new topics and to persevere through the challenges that have arisen. I thank him for his unwavering confidence in me. I would like to thank Yves Boucher for guiding me through the experimental work. I am grateful to him for being unfailingly generous with his time. I would like to thank the members of my thesis committee, Professors Robert Langer (MIT), William Deen (MIT) and Xandra Breakefield (HMS). They have provided me with invaluable advice and encouragement. I would also like to thank the NIH and the Whitaker Foundation for funding my graduate work.

My friends in the Steele Lab have taught me everything I know about cancer. I feel tremendously privileged to say that I have not worked with another group of people so dedicated to their projects and to their colleagues. They have truly been a source of inspiration and I thank them for this. In particular I would like to thank my fellow graduate students: Patrick Au, Josh Tam, Ryan Lanning, Janet Tse, Ming-Zher Poh, Benjamin Diop and Vikash Chauhan. They have all been generous with their time, especially as I have been wrapping this up. Thank you for making the lab a really enjoyable place and keeping me company on many a late night. I would like to single out Patrick for always making time to help me analyze data and for providing brilliant ideas in those countless instances in which I had none of my own. I would like to thank Sylvie Roberge for her help with animal studies and dedication to the projects we worked on together. I would also like to thank Julia Kahn, Carolyn Smith, Eve Smith, Melanie Fortier, Grace Gorospe and Song Xu for their outstanding technical support. I am grateful to Tim Padera, Lance Munn, Gang Cheng and Ed Brown for their expertise and for providing input on my research. I would like to thank Phyllis McNally for all the help she has provided and for keeping the lab a functioning and fun place. I would also like to thank Trevor McKee for the help he gave me when I started in the lab.

I have benefited enormously from the generous support of my outside collaborators. I would like to thank Paola Grandi (University of Pittsburgh), Okay Saydam (MGH), Bakhos Tannous (MGH), Cornel Fraefel (University of Zurich) and Khalid Shah (MGH) for help with the viruses. I am grateful to Roopali Roy, Alexis Exarhopoulos and Robert Doiron at Children's Hospital for help with collagenase activity assays. I would like to thank Marsha Moses (Children's Hospital) and Stephen Krane (MGH) for their input on MMPs. I would also like to thank Moungi Bawendi (MIT) for providing Q-dot loaded

microspheres, David Tarin (UCSD) for MMP-8 constructs, Carlos Lopez Otin (University of Oviedo) for MMP-13 constructs, John Mort (Shriners Hospital for Children) for recombinant cathepsin K, E. Antonio Chiocca and Yoshi Saeki (Ohio State University) for HSV vectors and Eunice Lee (Shriners Hospital for Children) for collagen antibodies.

Finally, I would like to thank my friends on both coasts. Thank you for sharing in the highs and lows and for your endless encouragement and support. I really could not have done this without you all. And especially, thanks to Cindy and Sharon for so closely sharing with me this tiring, maddening, enlightening and rewarding experience.

Table of Contents

List of Figures

List of Tables

Chapter 1: Background and Specific Aims

Introduction

Cancer is the second leading cause of death in the U.S., accounting for nearly a quarter of all deaths in 2004. The American Cancer Society estimates that 559,650 Americans will die from cancer this year and over 1.4 million new cases will be diagnosed (1). More than 85% of cancer patients have solid tumors. Traditionally, chemotherapeutics have been used in combination with surgery and radiation to treat solid tumors. However, systemic treatment with these non-specific chemical agents frequently causes considerable morbidity. Novel therapeutics such as antibodies and viral vectors have recently been developed to provide more targeted treatment. However, these therapeutics face transport barriers not experienced by small molecule chemotherapeutics due to their larger size and unique physicochemical properties.

In order for a cancer therapeutic to be effective, sufficient amounts must be delivered to its target, often the cancer cells. There are various mass transfer barriers associated with delivery of targeted therapeutics to tumor cells (2, 3). A therapeutic agent injected intravenously first must distribute throughout the tumor microvascular space and extravasate across the microvessel wall. Alternatively, these steps can be overcome by direct injection into the tumor. However, the transport of intratumorally infused therapeutics can be limited by extracellular matrix components. Fibrillar collagens may impede uniform distribution by acting as structural barriers and glycosaminoglycans can hinder fluid flow during infusion (4, 5).

Therapeutics delivered both locally and systemically then face barriers to transport in the interstitial space of the tumor. Except in the tumor margin, interstitial transport is

meditated mainly by diffusion and not convection, a consequence of the uniformly high interstitial fluid pressure within tumors (6, 7). While diffusion is relatively rapid for small molecule chemotherapeutics, it can be a slow process for novel targeted therapeutics which can be orders of magnitude larger. Hindered diffusion may limit the distribution and thus effectiveness of these therapeutics. Fibrillar collagen I is one of the primary constituents of the tumor extracellular matrix (ECM) and collagen I content and structure have been correlated with limited diffusion (8-12). Modulating the tumor extracellular matrix to improve the transport of therapeutics during and after intratumoral infusion is the focus of this thesis.

Specific Aims

Hypothesis: Delivery of a matrix-modulating enzyme to the tumor interstitium can improve the interstitial transport, distribution and efficacy of a macromolecular cancer therapeutic.

Specific Aim 1: Develop a mathematical model to characterize the relative effect of binding and diffusion on the distribution of a herpes simplex virus (HSV) vector in solid tumors.

A mathematical model has yet to be developed to describe the relative role of binding and diffusion on the distribution of HSV vectors in a solid tumor. Such a model will provide us with a greater understanding of the physical underpinnings governing the distribution of therapeutic viruses in tumors. Furthermore, it would provide us with an estimate of the

effect that improvements in diffusion would have on intratumor virus distribution, as well as provide other targets for improving viral delivery.

Specific Aim 1a: Perform in vitro experiments to determine rate constants for binding and degradation.

The rate constant for HSV binding to its cell surface receptor will be determined *in vitro* for human cancer cells. Virus will be incubated with cells and the concentration of virus remaining in the supernatant will be monitored over time. To determine the rate of degradation, virus will be incubated with tumor cell conditioned media and the concentration monitored over time.

Specific Aim 1b: Develop a 1D model incorporating virus binding, diffusion and degradation and analyze their relative roles in virus distribution.

Parameters obtained in Aim 1a and from the literature will be used to generate a 1D model of virus distribution in a solid tumor. The scenario of direct intratumor injection of the virus into the center of the tumor will be modeled to reflect experimental conditions. The relative effects of binding, diffusion and degradation on virus distribution will be assessed. A sensitivity analysis will be performed to determine how changes in tumor and virus parameters affect the distribution of virus in the tumor.

Specific Aim 2: Determine the effect of bacterial collagenase on the distribution and efficacy of an oncolytic HSV vector.

Fibrillar collagen has been shown to be the cause of severe diffusional hindrance of tracer molecules in tumors and bacterial collagenase has been used to degrade collagen and increase the diffusion coefficient of these tracers. This study intends to show that these findings have relevance to cancer therapy by providing evidence that (1) fibrillar collagen limits the effectiveness of a macromolecular cancer therapeutic by hindering its interstitial transport and (2) bacterial collagenase can be used to enhance therapeutic efficacy.

Specific Aim 2a: Determine how fibrillar collagen affects the distribution and efficacy of intratumorally injected HSV vectors.

Human tumors will be grown in the dorsal skinfold chamber of mice and EGFP-labeled HSV vectors will be injected intratumorally. Fibrillar collagen (second harmonic generation (SHG)) and virus (EGFP) will be imaged simultaneously multiphoton microscopy following injection. The effect of fibrillar collagen on virus distribution will be quantified by image analysis. Fluorescently-labeled tracer molecules of different sizes will be injected for comparison. For oncolytic viruses, imaging will be performed up to two weeks following injection to observe virus replication and spread.

Specific Aim 2b: Assess the effect of bacterial collagenase on the distribution of intratumorally injected HSV vectors.

Tumors will be injected with virus in combination with bacterial collagenase and imaged as before. The effect of bacterial collagenase on initial virus distribution and subsequent spread throughout the tumor will be assessed by image analysis.

Specific Aim 2c: Determine if bacterial collagenase can enhance the efficacy of intratumorally injected oncolytic HSV vectors.

Tumors will be grown subcutaneously in the flank of mice. They will be treated with two injections of either PBS, bacterial collagenase, oncolytic virus or oncolytic virus in combination with bacterial collagenase. Tumor size will be measured following treatment and the delay in tumor growth compared for different treatments. The effect of bacterial collagenase on metastasis will also be assessed.

Specific Aim 3: Determine the effect of acute delivery of recombinant human collagenases on tumor collagen, interstitial diffusion and the efficacy of oncolytic HSV therapy.

In order to apply the matrix modifying technique clinically, human collagenases must ultimately be used. Here we screen various human collagenases for their ability to degrade collagen *in vivo* and improve the transport and efficacy of a therapeutic. As in Aim 2, recombinant collagenases will be applied directly to tumors.

Specific Aim 3a: Screen human collagenases for the ability to degrade collagen in vitro and in vivo.

Various human collagenases will be screened for their ability to degrade fibrillar type I collagen in an *in vitro* assay. Promising candidates will be tested *in vivo*. Recombinant human collagenase will be superfused onto the surface of tumors grown in the dorsal chamber. SHG imaging will be performed at various time points after superfusion and the total collagen content quantified by image analysis.

Specific Aim 3b: Determine the effect of recombinant human collagenases on interstitial diffusion.

Recombinant human collagenase will be superfused onto the surface of tumors grown in the dorsal chamber. At an appropriate time point following treatment (determined in Aim 3a), a fluorescently-labeled tracer molecule will be intratumorally injected. The diffusion coefficient of the tracer will be measured with fluorescence recovery after photobleaching (FRAP) and compared for different treatments.

Specific Aim 3c: Determine the effect of recombinant human collagenases on the efficacy of oncolytic HSV therapy.

Tumors will be grown subcutaneously in the leg of mice. At a given size, tumors will be treated with an intratumor injection of either PBS, oncolytic virus alone or virus in combination with a recombinant human collagenase. Tumor volume will be measured every several days following treatment and the tumor growth delay compared.

Specific Aim 4: Determine the effect of chronic delivery of MMP-1 and -8 on the tumor extracellular matrix, interstitial transport and the efficacy of oncolytic HSV therapy.

An alternative approach to delivering a collagenase to the tumor as a recombinant protein is to express it in tumor cells. In practice, this can be achieved either by expressing collagenase in tumor cells by stable transfection or by incorporating the collagenase gene in the viral genome of the oncolytic vector. One advantage to this method is that the collagenase is delivered chronically to the tumor, increasing the effective dose. We will develop tumors and oncolytic viruses which express MMP-1 and MMP-8 (both found in Aim 3a to be suitable enzymes). As these enzymes can degrade multiple ECM substrates, the effect on collagen and other matrix components will be determined. Since chronic expression of these enzymes may have profound effects on the structure and composition of the tumor matrix, the effect on both diffusive and convective transport will be assessed

Specific Aim 4a: Generate tumors overexpressing MMP-1 and -8.

Tumor cells will be stably transfected with each MMP. MMP-expressing tumors will be grown subcutaneously in the flank of mice. Tumors will be harvested and western blot performed to confirm collagenase expression *in vivo*.

Specific Aim 4b: Determine the effect of MMP-1 and -8 overexpression on tumor extracellular matrix content.

MMP-expressing tumors will be grown in the dorsal chamber. When the tumors reach a given size, SHG imaging will be performed and total collagen content will be quantified by image analysis. Additionally, collagen and hyaluronic acid (HA) content will be

assessed with immunohistochemistry. MMP-expressing tumors will be grown subcutaneously in the flank of mice. Tumors will be harvested, fixed and immunostained for type I collagen and HA. Stained sections will be imaged and analysis performed to determine the total collagen and HA content. The sulfated glycosaminoglycan (GAG) content will be determined with a biochemical assay.

Specific Aim 4c: Determine the effect of MMP-1 and -8 overexpression on tumor interstitial transport.

MMP-expressing tumors will be grown in the dorsal chamber. When the tumors reach a given size, a fluorescently-labeled tracer molecule will be intratumorally injected. The diffusion coefficient of the tracer will be measured with FRAP and compared for different collagenases. Hydraulic conductivity will be determined in each tumor type by measuring the rate of fluid flow through tissue sections under an applied pressure gradient.

Specific Aim 4d: Determine the effect of MMP-1 and -8 overexpression on the efficacy of oncolytic HSV therapy.

MMP-expressing tumors will be grown subcutaneously in the leg of mice. For each MMP-expressing and control tumor, the following growth delay assay will be performed. At a given size, tumors will be treated with an intratumor injection of either PBS or oncolytic virus. Tumor volume will be measured every several days following treatment. The growth delay induced by oncolytic HSV treatment will be compared between MMP-

expressing and control tumors. If appropriate, histological analysis will performed to determine the distribution of HSV particles in each tumor type.

Specific Aim 4e: Generate recombinant oncolytic HSV vectors which express MMP-1 and -8 and determine the effect on therapeutic efficacy.

MMP-expressing oncolytic HSV vectors will be generated using homologous recombination. The MMP-1 and -8 expression cassettes will be inserted in the *ICP6* locus of the HSV genome. MMP expression will be confirmed by western blot of tumor cells infected in culture. Wild type tumors will be grown subcutaneously in the flank of mice and will be treated with intratumor injections of each recombinant oncolytic HSV vector. Tumor volume will be measured and the effect of MMP expression on growth delay assessed.

Specific Aim 5: Generate constitutively active forms of MMPs to enhance ECM modulation in vivo.

Human collagenases of the MMP family are secreted as inactive zymogens that require cleavage of their propeptide domains to become activate. Thus, insufficient activation in the interstitial space (due to lack of appropriate proteases) may limit the collagen degradation achieved. In this aim, truncated forms of MMPs are developed to bypass this activation step and augment collagen degradation in tumors.

Specific Aim 5a: Generate truncated forms of each MMP which lack the propeptide domain and test the ability of these truncated proteins to degrade fibrillar collagen.

Truncated forms of each MMP will be generated by PCR and subcloned into an appropriate expression vector. 293ET cells will be transiently transfected and western blots performed on the conditioned media to confirm expression and secretion of the truncated MMP. An *in vitro* collagenase assay will be used to assess the activity relative to the wild type enzymes.

Specific Aim 5b: Generate forms of each truncated MMP which contain stabilizing mutations in the hinge region and test for the ability of these mutants to degrade fibrillar collagen.

Active forms of MMPs may go through inactivating autoproteolytic degradation. The site of intramolecular cleavage in is the hinge domain. Site-directed mutagenesis will be performed on the truncated forms of each MMP (generated in Aim 5a) to stabilize the recombinant enzymes. Mutations will be generated by PCR. 293ET cells will be transiently transfected and western blots performed on the conditioned media to confirm expression and secretion of the mutated MMPs. An *in vitro* collagenase assay will be used to assess the activity relative to the truncated and wild type enzymes.

Background

Composition of tumor extracellular matrix

Solid tumors consist of two interconnected compartments: the malignant cells and the stroma in which they are dispersed. Stroma is induced by tumor-host interactions and is required for tumor growth and survival (13). It consists mainly of interstitial connective tissue but also includes the blood vessels that provide the tumor cells with nutrients and allow for gas exchange and waste disposal. The major components include leaked plasma; proteoglycans (PGs) and glycosaminoglycans (GAGs); interstitial collagens (types I, III, and V); fibrin; fibronectin; connective tissue cells such as fibroblasts; and inflammatory cells (13).

Tumor stroma generation is attributed to the hyperpermeability of the tumor vasculature (14). Plasma proteins, particularly fibrinogen and other clotting factors, extravasate and rapidly clot, forming a gel of crosslinked fibrin (15). This provisional matrix entraps extravasated plasma proteins and water. Furthermore, it stimulates the inward invasion of endothelial cells and fibroblasts (16, 17), which results in the transformation of the provisional matrix into a more highly cellular and vascular matrix (15). Structural proteins such as interstitial collagens are synthesized, resulting in the mature collagenous stroma.

Collagen type I is the major fibrous protein in the interstitial matrix and is produced by host stromal cells in most tumors (15, 18). The type I collagen monomer is a 300 nm long, 1.5 nm diameter protein consisting of three subunits, two αI chains and one αII

chain, associated in a right-handed triple helix. Procollagen is discharged vectorially into extracellular compartments to promote fibril formation in a desired location (19). N- and C- proteinases cleave the propeptide segments forming tropocollagen (also called collagen); this process leads to the formation of stable fibrils (20). Fibril diameters range from 50-200 nm and lengths are up to several micrometers. Fibril assembly occurs in fibril forming compartments and fusion of these narrow compartments can lead to the formation of fibers (21, 22).

The tumor interstitial matrix contains several other components besides collagen. The other major components of the tumor interstitial matrix include: hyaluronic acid (HA); sulfated GAGs, which bind to PG core proteins; and fibronectin, which allows cells to bind collagen via cell surface integrins (23). The hydrated gel of HA, together with collagen, provides structural integrity to the matrix and resistance to compressive forces (24, 25). PGs such as decorin and versican function to organize the matrix by binding to collagen and HA, respectively (26). The interstitial matrix can be quite variable from one tumor to another: while some have very little matrix material, others, such as desmoplastic carcinomas of the breast and colon, generate excessive amounts of fibrillar collagen and elastin that separate the tumor nodules (27, 28). In general, tumors contain higher levels of GAGs and PGs than normal tissues (29, 30) and the PGs tend to be larger and have longer GAG side chains (31, 32).

Tumor interstitial transport

This thesis focuses on the last mass transfer barrier for therapeutics targeted for cancer cells: transport through the interstitial space. Therapeutics that have either transported

across the microvascular wall or have been injected directly into the tumor distribute in the interstitium via convection and diffusion. However, it has been found that molecular therapeutics do not distribute uniformly in tumors, with low concentrations reaching tumor cells distant from the vasculature (33-37). There are two major reasons for this. First, interstitial fluid pressure (IFP) is uniformly elevated in solid tumors, dropping to lower levels only in the tumor periphery and surrounding tissue (38). This is caused by both the increased permeability of blood vessels (39) and the lack of functional intratumor lymphatics (6, 7), which lead to an accumulation of fluid in the tumor interstitium. As a result there are almost no pressure gradients between the vasculature and surrounding tissue and convection is negligible except at the tumor periphery (38, 40, 41). Interstitial transport of molecular therapeutics is therefore governed mainly by diffusion. This is a much slower process, especially for large therapeutics such as liposomes, viral vectors and proteins (Fig. 1.1).

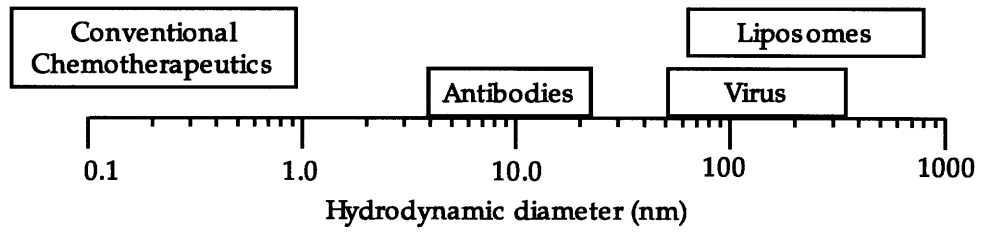

Figure 1.1. Size distribution of cancer therapeutic agents. While conventional chemotherapeutics are generally less than a nanometer in diameter, antibodies are an order of magnitude larger and viruses and liposomes are two to three orders of magnitude larger.

The second factor contributing to poor interstitial transport is the ECM – composed of collagen, proteoglycans and glycoproteins – which provides resistance to fluid and solute movement (42-44). The diffusion of solutes is considerably slower through connective tissue than water (45). Fluid flow has also been shown to be hindered by GAGs in tissue (4, 5). Measurements of the hydraulic conductivity of a variety of tissues has established a negative monotonic relationship with total GAG content (43, 46). Degradation of the non-sulfated GAG HA with hyaluronidase has been shown to increase hydraulic conductivity in several tissues (4, 47). The sulfated GAGs have been implicated, as well. The application of trypsin to deplete corneal stroma of sulfated GAGs resulted in a greater increase in hydraulic conductivity than with hyaluronidase (47).

Based on these findings, resistance to fluid flow and diffusion has been traditionally linked to GAGs. It was thought that fibrillar components such as collagen and elastin have little influence since they form large pore networks. However, this interpretation was challenged by the observation that tissue permeability is significantly lower than measurements made *in vitro* with GAG networks of similar concentration. Subsequent studies have shown that, indeed, matrix factors other than GAGs cannot be ignored in the analysis of interstitial transport (43, 44, 48). Levick observed that fibrillar components such as collagen may significantly influence transport in tissue because of hydrodynamic drag and the tortuous nature of the flow path, as well as by affecting the distribution and effective concentration of GAGs (43).

Tumor tissue may exhibit distinctive interstitial transport characteristics since tumor progression involves a wound healing-like stage with extensive synthesis of ECM

constituents (14, 18, 30). The composition of the tumor interstitial matrix differs in both composition and structure from that of the host and varies from one type to another (30, 49). The unique nature of the tumor interstitial matrix merits a specific study of tumor tissue to determine the relative roles of various ECM components as barriers to diffusive transport. The method used to measure diffusion coefficients has been fluorescence recovery after photobleaching (FRAP) (50, 51). In this method, the effective diffusion coefficient of a fluorescently-labeled tracer is measured by creating a photobleached pattern with a laser and performing image analysis on the diffusion-mediated recovery of the photobleached area. FRAP has been used to study diffusive transport in gels (12), spheroids (9) and *in vivo* tumor tissue (10, 11, 51).

Netti *et al.* (10) measured the diffusion coefficient of IgG in several tumors *in vivo* and found that it correlated with collagen, but not GAG or HA, content. Histological data showed that tumors with a low IgG diffusion coefficient had a well organized collagen network compared to other tumors. Pluen *et al.* (11) subsequently measured the diffusion coefficient of various probes in two tumor models (host sites): the dorsal chamber and cranial window. As expected, they found that the effective diffusion coefficient varied inversely with molecular hydrodynamic radius. Furthermore, they observed that the large macromolecules (IgG, IgM, dextran 2,000,000 MW) diffused much faster in tumors grown in the cranial window compared to the dorsal chamber for the same tumor type. In agreement with the study of Netti *et al.*, immunohistochemistry showed that dorsal chamber tumors exhibit abundant fibrillar collagen type I while cranial window tumors showed only sparse collagen. These studies suggested that tumor collagen composition and organization significantly affect the penetration of macromolecules.

Further evidence that implicated tumor fibrillar collagen in diffusive hindrance was obtained from an *in vitro* collagen gel study (12). Collagen gels were prepared at concentrations similar to that found in various solid tumors and the diffusion coefficient of a range of tracers was measured by photobleaching. When the diffusion coefficients were adjusted to account for the tortuosity of the tumor interstitial space, they closely matched the diffusion coefficients in tumors of comparable collagen content. This study suggested that collagen can account for most of the diffusional hindrance in tumors. In total, these interstitial diffusion studies provide evidence that collagen content and structure play a significant role in regulating tumor interstitial diffusion and show that collagen fibers are excellent targets for matrix modification for improved transport.

Matrix modification to improve interstitial diffusion

To validate that collagen plays a key role in diffusive hindrance and to provide proof of principle that its modification can be used to improve interstitial transport, the diffusion coefficient of tracer molecules has been measured following application of various ECM degrading factors. First, dorsal chamber tumors were treated with either bacterial collagenase or hyaluronidase to assess their ability to alter interstitial diffusion (10). While bacterial collagenase treatment increased the diffusion coefficient of IgG by approximately two-fold in two tumor types, hyaluronidase had no effect.

Alexandrakis *et al.* (52) developed a method for measuring diffusion coefficients *in vivo* using fluorescence correlation spectroscopy (FCS) with a multiphoton microscope. This method has further shed light on the effect of matrix modification on interstitial diffusion. In the FCS experiment, the fluctuations in fluorescence intensity detected in the two-

photon focal volume – a result of the random movement of fluorescent particles in and out of the volume – are used to extract information about the diffusion of the molecules (53, 54). FCS measurements revealed both fast and slow diffusing components for a tracer injected into tumors, although this tracer exhibited only a single diffusion coefficient in free solution. This result provided evidence of the two-phase nature of diffusion in the tumor interstitium. Application of hyaluronidase to tumors decreased the fraction of rapidly diffusing molecules and decreased the diffusion coefficient of the slow diffusing molecules. Bacterial collagenase treatment increased the proportion of the fast diffusion component while not altering the diffusion coefficient of either component.

Recently, Brown *et al.* developed the novel technique of second harmonic generation (SHG) imaging to dynamically image and quantify fibrillar collagen *in vivo* (8). They used it to characterize changes in collagen induced by the treatment of tumors with the peptide relaxin and correlated these changes in collagen to interstitial diffusion. SHG is a scattering phenomenon exhibited by various anisotropic materials and has been shown to be induced by collagen (55-57). Relaxin is a peptide hormone produced mainly in tissues of the reproductive system and has been shown to have the ability to remodel the ECM (58-60). Relaxin can modify the matrix through several processes. Relaxin decreases the synthesis and secretion of collagen I molecules in various *in vitro* models (61, 62) and has also shown to have the ability to increase the expression of various matrix degrading molecules (61, 63-66). Brown *et al.* found that chronic treatment of a fibrous sarcoma with relaxin increased collagen turnover: while total SHG signal did not change over time, the length of existing fibers decreased. These changes led to ~50% and 100%

increases in the diffusion coefficients of IgG and $2x10^6$ molecular weight dextran, respectively.

These studies further support the hypothesis that interstitial fibrillar collagen is responsible for the limited diffusion of large macromolecules in fibrous tumors. Furthermore, they demonstrate that collagen degradation can be used as a technique to improve diffusive transport in tumors. This thesis aims to expand on these findings in two respects: (1) show that improved diffusion can be extended to therapeutics and will lead to improved efficacy of cancer treatment; (2) develop clinically relevant methods to degrade tumor fibrillar collagen by testing various human collagenases.

Matrix metalloproteinases (MMPs)

The human matrix metalloproteinases (MMPs) are a family of endopeptidases that can cleave nearly all ECM components, as well as other non-matrix proteins and cell surface molecules (67-69). They are involved in both normal tissue remodeling during development and maintenance, as well as in various diseases involving fibrosis or excessive tissue destruction. The MMP family includes both membrane-bound and free enzymes, and all bind Zn^{2+} at the catalytic site. Three of the secreted MMPs are capable of cleaving collagen type I: MMP-1 (interstitial collagenase, collagenase-1) (70, 71), MMP-8 (neutrophil collagenase, collagenase-2) (72) and MMP-13 (collagenase-3) (73).

The collagenases share a similar domain structure, consisting of an N-terminal signal peptide, propeptide domain, catalytic domain, hinge region and C-terminal hemopexin-like domain. The propeptide domain functions to keep the MMP in a latent zymogen

form: a cysteine sulfhydryl group in this domain acts as a fourth ligand for the catalytic site zinc and must be removed to allow a water molecule to bind and cleave peptide bonds of MMP substrates (74, 75). Activation occurs extracellularly and begins with truncation of the propeptide domain, either autoproteolytically or by other MMPs and proteases, followed by removal of the remaining propeptide fragment by the truncated zymogen, itself, to form the mature enzyme (76). The collagenases all cleave the individual chains of the triple-helical collagen I molecule at a specific peptide location, Gly_{775}-Leu/Ile_{776} (77-79), and appear to cleave all three chains together, with no preference for individual chains (76). The collagenase activity of these MMPs is inhibited by the secreted proteins tissue inhibitors of MMP (TIMPs) 1-4 in a stoichiometric fashion (79-84). It should be noted that while these MMPs are primarily characterized as type I collagenases, they are also able to cleave other extracellular matrix components including proteoglycans, glycoproteins and other fibrillar collagens (69).

With their ability to degrade nearly all ECM components and many cell surface proteins the MMPs have been implicated in various processes of cancer progression. Notably, certain MMPs have been found at elevated levels in various cancers and have been linked to the increased invasiveness and metastatic potential of cancer cells (85). They are involved in several processes of metastasis, including migration through the tumor stroma, invasion across the basement membrane and entrance into and extravasation from blood vessels or lymphatics. Important to this work, MMP-1, -8 and -13 show elevated expression in various cancers relative to surrounding non-neoplastic tissue (86-91) and have been correlated with increased invasiveness and metastatic potential (87, 89, 92-94). However, little evidence exists that these collagenases are directly involved in the

metastatic process. In fact, there is emerging evidence that MMP-8 may play an anti-metastatic role (95, 96).

Oncolytic viruses

Oncolytic viral therapy is the use of a replication competent virus to selectively kill cancer cells (Fig. 1.2). Antitumor efficacy is generally mediated by cell lysis or cytotoxicity of viral proteins, but can also arise from the induction of an immune response or expression of a cytotoxic transgene (97). The are generally two methods to generate tumor cell selectivity: selective infection and selective replication (98). To achieve tumor-selective infection, the surface of viral particles can be engineered to display proteins which bind specifically to receptors on the surface of tumor cells. Tumor cell selective replication is generally attained by either placing essential viral genes under the control of a tumor-specific promoter or by mutating or deleting viral genes that are are essential to viral replication in normal cells, but non-essential in neoplastic cells. The two most extensively investigated viruses for oncolytic therapy are adenovirus and HSV (98-100).

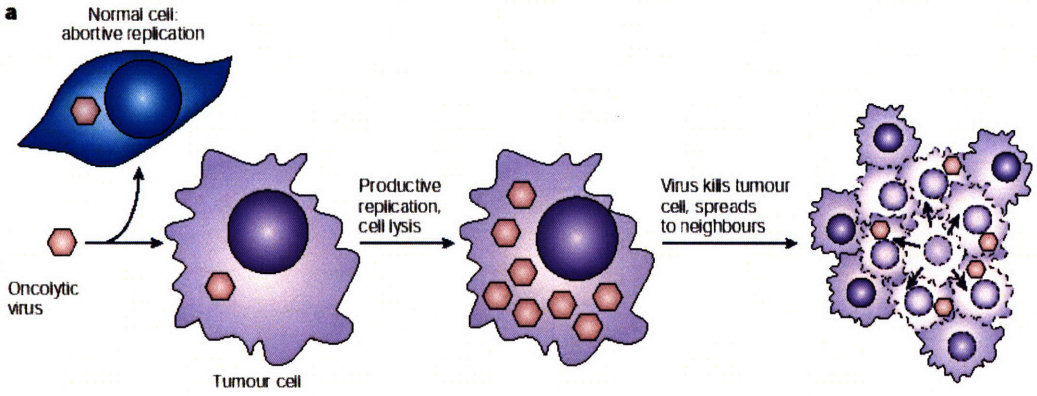

Figure 1.2. Oncolytic virus mechanism of action. The schematic shows the life cycle of a recombinant, oncolytic vector which has been mutated such that it selectively replicates in tumor cells but not normal cells. An oncolytic virus can infect a normal cell (blue) but will not be able to produce progeny virus. Conversely, when an oncolytic virus infects a tumor cell (purple), productive replication of progeny virus will occur. Infected cells will be lysed and progeny virus can go on to infect neighboring cells, continuing the cycle.

HSV is an enveloped, double stranded DNA virus which is non-integrating. Oncolytic HSV vectors have been developed both by incorporating tissue-specific promoters (101) and through the use of deletion mutations to inactivate proteins required for viral replication in normal cells (102). First generation deletion mutants focused on enzymes involved in nucleotide metabolism (such as ribonucleotide reductase (103, 104) and thymidine kinase (102, 105)) or the neurovirulence factor *γ34.5* (106, 107). These vectors provided proof of principle that safe and effective replication-competent HSV-1 vectors could be developed. Second generation vectors have focused on incorporating multiple

mutations to balance safety and efficacy. The multimutated vector G207 (MGH1) incorporates deletions of both copies of *γ34.5* and the inactivating insertion of the *E. coli LacZ* gene into the ribonucleotide reductase gene *ICP6* (108, 109). Recently, other HSV-1 vectors have been developed based on the same strategy. MGH2 is identical to MGH1 except that the *LacZ* insertion is replaced by the insertion of a transcription cassette containing the gene for enhanced green fluorescent protein (EGFP) and the prodrug activating genes *CYP2B1* and secreted human intestinal carboxylesterase (110). Terada *et al.* developed a method to generate HSV-1 vectors similar to G207/MGH1 but with the insertion of EGFP and any gene of interest (instead of *LacZ*) in *ICP6* (111).

G207 has been shown to be quite potent and safe in preclinical studies (109, 112-114). While developed for brain tumors, it has also been effective for other solid tumors including melanoma, breast and liver (115). The combined treatment of G207 and the chemotherapeutic cisplatin was effective for the treatment of head and neck squamous cell carcinoma in an animal model (116). Based on these encouraging preclinical findings, a phase I clinical trial was conducted with 21 glioma patients (117). All of the patients tolerated the treatment and showed no serious adverse effects. Eight patients showed reduction in tumor volume from 4 days to 1 month after treatment. G207 is currently in a phase I clinical trial of malignant brain tumors.

Although recent clinical trials have demonstrated the potential of adenovirus and HSV as oncolytic vectors in cancer therapy (118), the issue of poor distribution throughout the tumor remains (35, 119). As evidence of this, multiple injections with fractionation of the dose is often used to improve intratumor delivery, albeit with limited gains (120). While

vector distribution is often acknowledged as a significant factor in determining overall treatment efficacy, few studies specifically address this issue. This thesis examines the possibility of improving the transport and effectiveness of such vectors through modulation of the tumor extracellular matrix.

References

1. Jemal A, Siegel R, Ward E, Murray T, Xu J, Thun MJ. Cancer statistics, 2007. CA Cancer J Clin 2007 Jan-Feb;57(1):43-66.
2. Jain RK. Barriers to drug delivery in solid tumors. Sci Am 1994 Jul;271(1):58-65.
3. Jain RK. Delivery of molecular and cellular medicine to solid tumors. Adv Drug Deliv Rev 2001 Mar 1;46(1-3):149-68.
4. Day T. The permeability of interstitial connective tissue and the nature of the interfibrillary substance. J Physiol 1952;117:1-8.
5. Ogston AG, Sherman TF. Effects of hyaluronic acid upon diffusion of solutes and flow of solvent. J Physiol 1961 Apr;156:67-74.
6. Leu AJ, Berk DA, Lymboussaki A, Alitalo K, Jain RK. Absence of functional lymphatics within a murine sarcoma: a molecular and functional evaluation. Cancer Res 2000 Aug 15;60(16):4324-7.
7. Padera TP, Kadambi A, di Tomaso E, *et al.* Lymphatic metastasis in the absence of functional intratumor lymphatics. Science 2002 Jun 7;296(5574):1883-6.
8. Brown E, McKee T, diTomaso E, *et al.* Dynamic imaging of collagen and its modulation in tumors in vivo using second-harmonic generation. Nat Med 2003 Jun;9(6):796-800.
9. Davies Cde L, Berk DA, Pluen A, Jain RK. Comparison of IgG diffusion and extracellular matrix composition in rhabdomyosarcomas grown in mice versus in vitro as spheroids reveals the role of host stromal cells. Br J Cancer 2002 May 20;86(10):1639-44.
10. Netti PA, Berk DA, Swartz MA, Grodzinsky AJ, Jain RK. Role of extracellular matrix assembly in interstitial transport in solid tumors. Cancer Res 2000 May 1;60(9):2497-503.
11. Pluen A, Boucher Y, Ramanujan S, *et al.* Role of tumor-host interactions in interstitial diffusion of macromolecules: cranial vs. subcutaneous tumors. Proc Natl Acad Sci U S A 2001 Apr 10;98(8):4628-33.
12. Ramanujan S, Pluen A, McKee TD, Brown EB, Boucher Y, Jain RK. Diffusion and convection in collagen gels: implications for transport in the tumor interstitium. Biophys J 2002 Sep;83(3):1650-60.
13. Connolly J, Schnitt, S., Wang, H., Dvorak, A., and Dvorak, H. Principles of Cancer Pathology. In: Bast R, Kufe, D., Pollock, R., Weichselbaum, R., Holland, J., Frei, E., editor. Cancer Medicine. 5 ed. Hamilton: BC Decker Inc.; 2000.
14. Dvorak HF. Tumors: wounds that do not heal. Similarities between tumor stroma generation and wound healing. N Engl J Med 1986 Dec 25;315(26):1650-9.
15. Nagy JA, Brown LF, Senger DR, *et al.* Pathogenesis of tumor stroma generation: a critical role for leaky blood vessels and fibrin deposition. Biochim Biophys Acta 1989 Feb;948(3):305-26.
16. Brown LF, Lanir N, McDonagh J, Tognazzi K, Dvorak AM, Dvorak HF. Fibroblast migration in fibrin gel matrices. Am J Pathol 1993 Jan;142(1):273-83.
17. Greiling D, Clark RA. Fibronectin provides a conduit for fibroblast transmigration from collagenous stroma into fibrin clot provisional matrix. J Cell Sci 1997 Apr;110 (Pt 7):861-70.

18. Liotta LA, Rao CN. Role of the extracellular matrix in cancer. Ann N Y Acad Sci 1985;460:333-44.
19. Birk D, Silver, F., Trelstad, R. Matrix Assembly. In: Hay E, editor. Cell Biology of Extracellular Matrix. Second ed. New York: Plenum Press; 1991.
20. Olsen B. Collagen Biosynthesis. In: Hay E, editor. Cell Biology of Extracellular Matrix. New York: Plenum Press; 1991.
21. Birk DE, Trelstad RL. Extracellular compartments in tendon morphogenesis: collagen fibril, bundle, and macroaggregate formation. J Cell Biol 1986 Jul;103(1):231-40.
22. Trelstad RL, Hayashi K. Tendon collagen fibrillogenesis: intracellular subassemblies and cell surface changes associated with fibril growth. Dev Biol 1979 Aug;71(2):228-42.
23. Yeo T, Dvorak, H. Tumor Stroma. In: Colvin R, Bhan, A., McCluskey, R., editor. Diagnostic Immunopathology. Second ed. New York: Raven Press; 1995.
24. Barocas VH, Tranquillo RT. An anisotropic biphasic theory of tissue-equivalent mechanics: the interplay among cell traction, fibrillar network deformation, fibril alignment, and cell contact guidance. J Biomech Eng 1997 May;119(2):137-45.
25. Winlove CP, Parker KH. The physiological function of the extracellular matrix. In: Reed RK, Laine GA, Bert JL, Winlove P, McKale N, editors. Interstitium, Connective Tissue and Lymphatics. London: Portland Press; 1995. p. 137-65.
26. Iozzo RV. Matrix proteoglycans: from molecular design to cellular function. Annu Rev Biochem 1998;67:609-52.
27. Iozzo RV. Proteoglycans and neoplasia. Cancer Metastasis Rev 1988 Apr;7(1):39-50.
28. Liotta LA, Rao CN, Barsky SH. Tumor invasion and the extracellular matrix. Lab Invest 1983 Dec;49(6):636-49.
29. Bertrand P, Girard N, Delpech B, Duval C, d'Anjou J, Dauce JP. Hyaluronan (hyaluronic acid) and hyaluronectin in the extracellular matrix of human breast carcinomas: comparison between invasive and non-invasive areas. Int J Cancer 1992 Aug 19;52(1):1-6.
30. Ronnov-Jessen L, Petersen OW, Bissell MJ. Cellular changes involved in conversion of normal to malignant breast: importance of the stromal reaction. Physiol Rev 1996 Jan;76(1):69-125.
31. Alini M, Losa GA. Partial characterization of proteoglycans isolated from neoplastic and nonneoplastic human breast tissues. Cancer Res 1991 Mar 1;51(5):1443-7.
32. Yeo TK, Brown L, Dvorak HF. Alterations in proteoglycan synthesis common to healing wounds and tumors. Am J Pathol 1991 Jun;138(6):1437-50.
33. Jones PL, Gallagher BM, Sands H. Autoradiographic analysis of monoclonal antibody distribution in human colon and breast tumor xenografts. Cancer Immunol Immunother 1986;22(2):139-43.
34. Sands H, Jones PL, Shah SA, Palme D, Vessella RL, Gallagher BM. Correlation of vascular permeability and blood flow with monoclonal antibody uptake by human Clouser and renal cell xenografts. Cancer Res 1988 Jan 1;48(1):188-93.
35. Sauthoff H, Hu J, Maca C, *et al.* Intratumoral spread of wild-type adenovirus is limited after local injection of human xenograft tumors: virus persists and spreads systemically at late time points. Hum Gene Ther 2003 Mar 20;14(5):425-33.

36. van Etten B, ten Hagen TL, de Vries MR, Ambagtsheer G, Huet T, Eggermont AM. Prerequisites for effective adenovirus mediated gene therapy of colorectal liver metastases in the rat using an intracellular neutralizing antibody fragment to p21-Ras. Br J Cancer 2002 Feb 1;86(3):436-42.
37. Yuan F, Leunig M, Huang SK, Berk DA, Papahadjopoulos D, Jain RK. Microvascular permeability and interstitial penetration of sterically stabilized (stealth) liposomes in a human tumor xenograft. Cancer Res 1994 Jul 1;54(13):3352-6.
38. Boucher Y, Baxter LT, Jain RK. Interstitial pressure gradients in tissue-isolated and subcutaneous tumors: implications for therapy. Cancer Res 1990 Aug 1;50(15):4478-84.
39. Gerlowski LE, Jain RK. Microvascular permeability of normal and neoplastic tissues. Microvasc Res 1986 May;31(3):288-305.
40. Boucher Y, Jain RK. Microvascular pressure is the principal driving force for interstitial hypertension in solid tumors: implications for vascular collapse. Cancer Res 1992 Sep 15;52(18):5110-4.
41. Boucher Y, Kirkwood JM, Opacic D, Desantis M, Jain RK. Interstitial hypertension in superficial metastatic melanomas in humans. Cancer Res 1991 Dec 15;51(24):6691-4.
42. Comper WD, Laurent TC. Physiological function of connective tissue polysaccharides. Physiol Rev 1978 Jan;58(1):255-315.
43. Levick JR. Flow through interstitium and other fibrous matrices. Q J Exp Physiol 1987 Oct;72(4):409-37.
44. Reed RK, Rubin K. Connective tissue biology: integration and reductionism. London; Miami: Portland; 1998.
45. Burstein D, Gray ML, Hartman AL, Gipe R, Foy BD. Diffusion of small solutes in cartilage as measured by nuclear magnetic resonance (NMR) spectroscopy and imaging. J Orthop Res 1993 Jul;11(4):465-78.
46. Swabb EA, Wei J, Gullino PM. Diffusion and convection in normal and neoplastic tissues. Cancer Res 1974 Oct;34(10):2814-22.
47. Hedbys BO. Corneal resistance of the flow of water after enzymatic digestion. Exp Eye Res 1963 Apr;2:112-21.
48. Jackson GW, James DF. The hydrodynamic resistance of hyaluronic acid and its contribution to tissue permeability. Biorheology 1982;19(1/2):317-30.
49. Iozzo RV, Cohen I. Altered proteoglycan gene expression and the tumor stroma. Experientia 1993 May 15;49(5):447-55.
50. Berk DA, Yuan F, Leunig M, Jain RK. Fluorescence photobleaching with spatial Fourier analysis: measurement of diffusion in light-scattering media. Biophys J 1993 Dec;65(6):2428-36.
51. Chary SR, Jain RK. Direct measurement of interstitial convection and diffusion of albumin in normal and neoplastic tissues by fluorescence photobleaching. Proc Natl Acad Sci U S A 1989 Jul;86(14):5385-9.
52. Alexandrakis G, Brown EB, Tong RT, Campbell RB, Boucher Y, Jain RK. Two-photon fluorescence correlation microscopy reveals the two-phase nature of transport in tumors. Nature Medicine 2003(conditionally accepted).
53. Elson EL, Magde D. Fluorescence correlation spectroscopy. I. Conceptual basis and theory. Biopolymers 1974 Jan;13(1):1-27.

54. Magde D, Elson EL, Webb WW. Fluorescence correlation spectroscopy. II. An experimental realization. Biopolymers 1974 Jan;13(1):29-61.
55. Campagnola PJ, Millard AC, Terasaki M, Hoppe PE, Malone CJ, Mohler WA. Three-dimensional high-resolution second-harmonic generation imaging of endogenous structural proteins in biological tissues. Biophys J 2002 Jan;82(1 Pt 1):493-508.
56. Williams RM, Zipfel WR, Webb WW. Multiphoton microscopy in biological research. Curr Opin Chem Biol 2001 Oct;5(5):603-8.
57. Zoumi A, Yeh A, Tromberg BJ. Imaging cells and extracellular matrix in vivo by using second-harmonic generation and two-photon excited fluorescence. Proc Natl Acad Sci U S A 2002 Aug 20;99(17):11014-9.
58. Bani D. Relaxin: a pleiotropic hormone. Gen Pharmacol 1997 Jan;28(1):13-22.
59. Bathgate RA, Samuel CS, Burazin TC, Gundlach AL, Tregear GW. Relaxin: new peptides, receptors and novel actions. Trends Endocrinol Metab 2003 Jul;14(5):207-13.
60. Sherwood OD. Relaxin's physiological roles and other diverse actions. Endocr Rev 2004 Apr;25(2):205-34.
61. Unemori EN, Amento EP. Relaxin modulates synthesis and secretion of procollagenase and collagen by human dermal fibroblasts. J Biol Chem 1990 Jun 25;265(18):10681-5.
62. Unemori EN, Bauer EA, Amento EP. Relaxin alone and in conjunction with interferon-gamma decreases collagen synthesis by cultured human scleroderma fibroblasts. J Invest Dermatol 1992 Sep;99(3):337-42.
63. Binder C, Hagemann T, Husen B, Schulz M, Einspanier A. Relaxin enhances in-vitro invasiveness of breast cancer cell lines by up-regulation of matrix metalloproteases. Mol Hum Reprod 2002 Sep;8(9):789-96.
64. Lenhart JA, Ryan PL, Ohleth KM, Palmer SS, Bagnell CA. Relaxin increases secretion of matrix metalloproteinase-2 and matrix metalloproteinase-9 during uterine and cervical growth and remodeling in the pig. Endocrinology 2001 Sep;142(9):3941-9.
65. Qin X, Chua PK, Ohira RH, Bryant-Greenwood GD. An autocrine/paracrine role of human decidual relaxin. II. Stromelysin-1 (MMP-3) and tissue inhibitor of matrix metalloproteinase-1 (TIMP-1). Biol Reprod 1997 Apr;56(4):812-20.
66. Kapila S, Xie Y. Targeted induction of collagenase and stromelysin by relaxin in unprimed and beta-estradiol-primed diarthrodial joint fibrocartilaginous cells but not in synoviocytes. Lab Invest 1998 Aug;78(8):925-38.
67. Lauer-Fields JL, Juska D, Fields GB. Matrix metalloproteinases and collagen catabolism. Biopolymers 2002;66(1):19-32.
68. Nelson AR, Fingleton B, Rothenberg ML, Matrisian LM. Matrix metalloproteinases: biologic activity and clinical implications. J Clin Oncol 2000 Mar;18(5):1135-49.
69. Sternlicht MD, Werb Z. How matrix metalloproteinases regulate cell behavior. Annu Rev Cell Dev Biol 2001;17:463-516.
70. Stricklin GP, Bauer EA, Jeffrey JJ, Eisen AZ. Human skin collagenase: isolation of precursor and active forms from both fibroblast and organ cultures. Biochemistry 1977 Apr 19;16(8):1607-15.
71. Stricklin GP, Eisen AZ, Bauer EA, Jeffrey JJ. Human skin fibroblast collagenase: chemical properties of precursor and active forms. Biochemistry 1978 Jun 13;17(12):2331-7.

72. Hasty KA, Jeffrey JJ, Hibbs MS, Welgus HG. The collagen substrate specificity of human neutrophil collagenase. J Biol Chem 1987 Jul 25;262(21):10048-52.
73. Freije JM, Diez-Itza I, Balbin M, *et al.* Molecular cloning and expression of collagenase-3, a novel human matrix metalloproteinase produced by breast carcinomas. J Biol Chem 1994 Jun 17;269(24):16766-73.
74. Sanchez-Lopez R, Alexander CM, Behrendtsen O, Breathnach R, Werb Z. Role of zinc-binding- and hemopexin domain-encoded sequences in the substrate specificity of collagenase and stromelysin-2 as revealed by chimeric proteins. J Biol Chem 1993 Apr 5;268(10):7238-47.
75. Van Wart HE, Birkedal-Hansen H. The cysteine switch: a principle of regulation of metalloproteinase activity with potential applicability to the entire matrix metalloproteinase gene family. Proc Natl Acad Sci U S A 1990 Jul;87(14):5578-82.
76. Jeffery J. Interstitial Collagenases. In: Parks W, Mecham, R., editor. Matrix Metalloproteinases: Academic Press; 1998. p. 15-42.
77. Aimes RT, Quigley JP. Matrix metalloproteinase-2 is an interstitial collagenase. Inhibitor-free enzyme catalyzes the cleavage of collagen fibrils and soluble native type I collagen generating the specific 3/4- and 1/4-length fragments. J Biol Chem 1995 Mar 17;270(11):5872-6.
78. Eisen AZ, Jeffrey JJ, Gross J. Human skin collagenase. Isolation and mechanism of attack on the collagen molecule. Biochim Biophys Acta 1968 Mar 25;151(3):637-45.
79. Knauper V, Lopez-Otin C, Smith B, Knight G, Murphy G. Biochemical characterization of human collagenase-3. J Biol Chem 1996 Jan 19;271(3):1544-50.
80. Anand-Apte B, Bao L, Smith R, *et al.* A review of tissue inhibitor of metalloproteinases-3 (TIMP-3) and experimental analysis of its effect on primary tumor growth. Biochem Cell Biol 1996;74(6):853-62.
81. Bigg HF, Morrison CJ, Butler GS, *et al.* Tissue inhibitor of metalloproteinases-4 inhibits but does not support the activation of gelatinase A via efficient inhibition of membrane type 1-matrix metalloproteinase. Cancer Res 2001 May 1;61(9):3610-8.
82. Knauper V, Osthues A, DeClerck YA, Langley KE, Blaser J, Tschesche H. Fragmentation of human polymorphonuclear-leucocyte collagenase. Biochem J 1993 May 1;291 (Pt 3):847-54.
83. Liu YE, Wang M, Greene J, *et al.* Preparation and characterization of recombinant tissue inhibitor of metalloproteinase 4 (TIMP-4). J Biol Chem 1997 Aug 15;272(33):20479-83.
84. Ward RV, Hembry RM, Reynolds JJ, Murphy G. The purification of tissue inhibitor of metalloproteinases-2 from its 72 kDa progelatinase complex. Demonstration of the biochemical similarities of tissue inhibitor of metalloproteinases-2 and tissue inhibitor of metalloproteinases-1. Biochem J 1991 Aug 15;278 (Pt 1):179-87.
85. Egeblad M, Werb Z. New functions for the matrix metalloproteinases in cancer progression. Nat Rev Cancer 2002 Mar;2(3):161-74.
86. Baker EA, Bergin FG, Leaper DJ. Matrix metalloproteinases, their tissue inhibitors and colorectal cancer staging. Br J Surg 2000 Sep;87(9):1215-21.
87. Cazorla M, Hernandez L, Nadal A, *et al.* Collagenase-3 expression is associated with advanced local invasion in human squamous cell carcinomas of the larynx. J Pathol 1998 Oct;186(2):144-50.

88. Elnemr A, Yonemura Y, Bandou E, *et al.* Expression of collagenase-3 (matrix metalloproteinase-13) in human gastric cancer. Gastric Cancer 2003;6(1):30-8.
89. Nielsen BS, Rank F, Lopez JM, *et al.* Collagenase-3 expression in breast myofibroblasts as a molecular marker of transition of ductal carcinoma in situ lesions to invasive ductal carcinomas. Cancer Res 2001 Oct 1;61(19):7091-100.
90. Nomura H, Fujimoto N, Seiki M, Mai M, Okada Y. Enhanced production of matrix metalloproteinases and activation of matrix metalloproteinase 2 (gelatinase A) in human gastric carcinomas. Int J Cancer 1996 Feb 20;69(1):9-16.
91. Shimada T, Nakamura H, Yamashita K, *et al.* Enhanced production and activation of progelatinase A mediated by membrane-type 1 matrix metalloproteinase in human oral squamous cell carcinomas: implications for lymph node metastasis. Clin Exp Metastasis 2000;18(2):179-88.
92. Ala-Aho R, Johansson N, Baker AH, Kahari VM. Expression of collagenase-3 (MMP-13) enhances invasion of human fibrosarcoma HT-1080 cells. Int J Cancer 2002 Jan 20;97(3):283-9.
93. Inoue T, Yashiro M, Nishimura S, *et al.* Matrix metalloproteinase-1 expression is a prognostic factor for patients with advanced gastric cancer. Int J Mol Med 1999 Jul;4(1):73-7.
94. Shiozawa J, Ito M, Nakayama T, Nakashima M, Kohno S, Sekine I. Expression of matrix metalloproteinase-1 in human colorectal carcinoma. Mod Pathol 2000 Sep;13(9):925-33.
95. Agarwal D, Goodison S, Nicholson B, Tarin D, Urquidi V. Expression of matrix metalloproteinase 8 (MMP-8) and tyrosinase-related protein-1 (TYRP-1) correlates with the absence of metastasis in an isogenic human breast cancer model. Differentiation 2003 Mar;71(2):114-25.
96. Montel V, Kleeman J, Agarwal D, Spinella D, Kawai K, Tarin D. Altered metastatic behavior of human breast cancer cells after experimental manipulation of matrix metalloproteinase 8 gene expression. Cancer Res 2004 Mar 1;64(5):1687-94.
97. Mullen JT, Tanabe KK. Viral oncolysis. Oncologist 2002;7(2):106-19.
98. Chiocca EA. Oncolytic viruses. Nat Rev Cancer 2002 Dec;2(12):938-50.
99. Kirn D, Martuza RL, Zwiebel J. Replication-selective virotherapy for cancer: Biological principles, risk management and future directions. Nat Med 2001 Jul;7(7):781-7.
100. Nettelbeck DM, Curiel DT. Tumor-busting viruses. Sci Am 2003 Oct;289(4):68-75.
101. Miyatake S, Iyer A, Martuza RL, Rabkin SD. Transcriptional targeting of herpes simplex virus for cell-specific replication. J Virol 1997 Jul;71(7):5124-32.
102. Martuza RL, Malick A, Markert JM, Ruffner KL, Coen DM. Experimental therapy of human glioma by means of a genetically engineered virus mutant. Science 1991 May 10;252(5007):854-6.
103. Goldstein DJ, Weller SK. Herpes simplex virus type 1-induced ribonucleotide reductase activity is dispensable for virus growth and DNA synthesis: isolation and characterization of an ICP6 lacZ insertion mutant. J Virol 1988 Jan;62(1):196-205.
104. Mineta T, Rabkin SD, Martuza RL. Treatment of malignant gliomas using ganciclovir-hypersensitive, ribonucleotide reductase-deficient herpes simplex viral mutant. Cancer Res 1994 Aug 1;54(15):3963-6.

105. Coen DM, Kosz-Vnenchak M, Jacobson JG, *et al.* Thymidine kinase-negative herpes simplex virus mutants establish latency in mouse trigeminal ganglia but do not reactivate. Proc Natl Acad Sci U S A 1989 Jun;86(12):4736-40.
106. Chambers R, Gillespie GY, Soroceanu L, *et al.* Comparison of genetically engineered herpes simplex viruses for the treatment of brain tumors in a scid mouse model of human malignant glioma. Proc Natl Acad Sci U S A 1995 Feb 28;92(5):1411-5.
107. Markert JM, Malick A, Coen DM, Martuza RL. Reduction and elimination of encephalitis in an experimental glioma therapy model with attenuated herpes simplex mutants that retain susceptibility to acyclovir. Neurosurgery 1993 Apr;32(4):597-603.
108. Kramm CM, Chase M, Herrlinger U, *et al.* Therapeutic efficiency and safety of a second-generation replication-conditional HSV1 vector for brain tumor gene therapy. Hum Gene Ther 1997 Nov 20;8(17):2057-68.
109. Mineta T, Rabkin SD, Yazaki T, Hunter WD, Martuza RL. Attenuated multi-mutated herpes simplex virus-1 for the treatment of malignant gliomas. Nat Med 1995 Sep;1(9):938-43.
110. Tyminski E, Leroy S, Terada K, *et al.* Brain tumor oncolysis with replication-conditional herpes simplex virus type 1 expressing the prodrug-activating genes, CYP2B1 and secreted human intestinal carboxylesterase, in combination with cyclophosphamide and irinotecan. Cancer Res 2005 Aug 1;65(15):6850-7.
111. Terada K, Wakimoto H, Tyminski E, Chiocca EA, Saeki Y. Development of a rapid method to generate multiple oncolytic HSV vectors and their in vivo evaluation using syngeneic mouse tumor models. Gene Ther 2006 Apr;13(8):705-14.
112. Sundaresan P, Hunter WD, Martuza RL, Rabkin SD. Attenuated, replication-competent herpes simplex virus type 1 mutant G207: safety evaluation in mice. J Virol 2000 Apr;74(8):3832-41.
113. Toda M, Rabkin SD, Martuza RL. Treatment of human breast cancer in a brain metastatic model by G207, a replication-competent multimutated herpes simplex virus 1. Hum Gene Ther 1998 Oct 10;9(15):2177-85.
114. Varghese S, Newsome JT, Rabkin SD, *et al.* Preclinical safety evaluation of G207, a replication-competent herpes simplex virus type 1, inoculated intraprostatically in mice and nonhuman primates. Hum Gene Ther 2001 May 20;12(8):999-1010.
115. Toda M, Elbrigh MI, Fong Y, Rabkin SD. Oncolytic herpes simplex virus (G207) therapy: from basic to clinical. In: Maruta H, editor. Tumor-Suppressing Viruses, Genes, and Drugs. San Diego: Academic Press; 2002. p. 45-75.
116. Chahlavi A, Todo T, Martuza RL, Rabkin SD. Replication-competent herpes simplex virus vector G207 and cisplatin combination therapy for head and neck squamous cell carcinoma. Neoplasia 1999 Jun;1(2):162-9.
117. Markert JM, Medlock MD, Rabkin SD, *et al.* Conditionally replicating herpes simplex virus mutant, G207 for the treatment of malignant glioma: results of a phase I trial. Gene Ther 2000 May;7(10):867-74.
118. Liu TC, Galanis E, Kirn D. Clinical trial results with oncolytic virotherapy: a century of promise, a decade of progress. Nat Clin Pract Oncol 2007 Feb;4(2):101-17.
119. Ichikawa T, Chiocca EA. Comparative analyses of transgene delivery and expression in tumors inoculated with a replication-conditional or -defective viral vector. Cancer Res 2001 Jul 15;61(14):5336-9.

120. Nemunaitis J, Khuri F, Ganly I, *et al.* Phase II trial of intratumoral administration of ONYX-015, a replication-selective adenovirus, in patients with refractory head and neck cancer. J Clin Oncol 2001 Jan 15;19(2):289-98.

Chapter 2: Modeling of Herpes Simplex Virus Distribution in a Solid Tumor

Portions of the chapter have been taken from:

W. Mok and R.K. Jain, "Modeling of Herpes Simplex Virus Distribution in Solid Tumors: Implications for Cancer Therapy." In submission

Introduction

Viral vectors offer a promising approach to cancer treatment. Methods of antitumor efficacy can include cell lysis, cytotoxicity of viral proteins, induction of an immune response and expression of a cytotoxic transgene (1, 2). Oncolytic viral therapy – treatment with viruses that have been genetically modified to selectively replicate in cancer cells but not non-neoplastic cells – is a rapidly developing cancer gene therapy platform that can exhibit each of these anti-tumor properties (3, 4). Two of the most actively investigated viruses, adenovirus and herpes simplex virus (HSV), have demonstrated systemic safety and efficacy in various clinical applications (5, 6).

While viral gene therapy vectors show remarkable biological specificity and activity for the treatment of solid tumors, they suffer in comparison to conventional chemotherapeutics in one main respect: intratumor distribution. Viruses are orders of magnitude larger than small molecule chemotherapeutics (< 1 nm vs 50-200 nm) and encounter severe transport limitations in the tumor interstitium. The limited penetration of large vectors from the injection site or the vasculature has been well documented (7-9). The tumor extracellular matrix most likely plays an important role in the distribution of viral vectors within tumors (10, 11). In order to properly assess the therapeutic potential of a viral cancer gene therapy vector – as well as devise optimal delivery methods – a detailed understanding of the root causes of limited vector distribution is needed.

Mathematical modeling offers a useful method to explore this issue and guide experimental strategies to improve viral vector distribution and thus efficacy. Several models of oncolytic viral therapy exist in the literature (12-14). While highly informative,

these models focus on the role of various biological processes such as the immune response and the cytotoxicity, infectivity and burst size of the virus. In addition, they compare how different treatment/delivery schemes – manifested as initial intratumor viral distribution – affect the ability to control tumor growth with oncolytic viral therapy. The present investigation aims to address the more fundamental questions of how these initial distributions arise and what physicochemical characteristics of the virus are responsible. We consider the role of viral binding, diffusion and degradation and explore the potential improvements in distribution with various modifications to both the virus and tumor. Furthermore, while the previous models describe the behavior of adenoviral vectors, this study focuses on HSV, which also shows great potential in tumor treatment.

Experiments are performed in this study to determine the rate constants for viral degradation (via hydrolysis) and cell surface binding and the concentration of heparan sulfate on the surface of tumor cells. Values for the volume and concentration of virus following intratumor infusion and the effective diffusion coefficient of viral particles in the tumor are estimated from our previous work (10, 15) and work described in Chapter 3. Other parameters have been estimated from the literature. The model shows that intratumorally infused virus will spread minimally from the site of injection, a consequence of rapid cell surface binding and limited diffusion. However, various modifications to the tumor and virus can markedly improve the distribution of virus in the tumor.

Model Development

The tumor is modeled as a sphere of radius R. Diffusion-reaction equations describe the interstitial concentration of virus as a function of time and radial position. Diffusion in the interstitial compartment, binding of HSV particles to cells and degradation of both free and bound viral particles via hydrolysis are the processes described (Fig 2.1). Two species are considered: free interstitial virus and virus bound to cell surfaces.

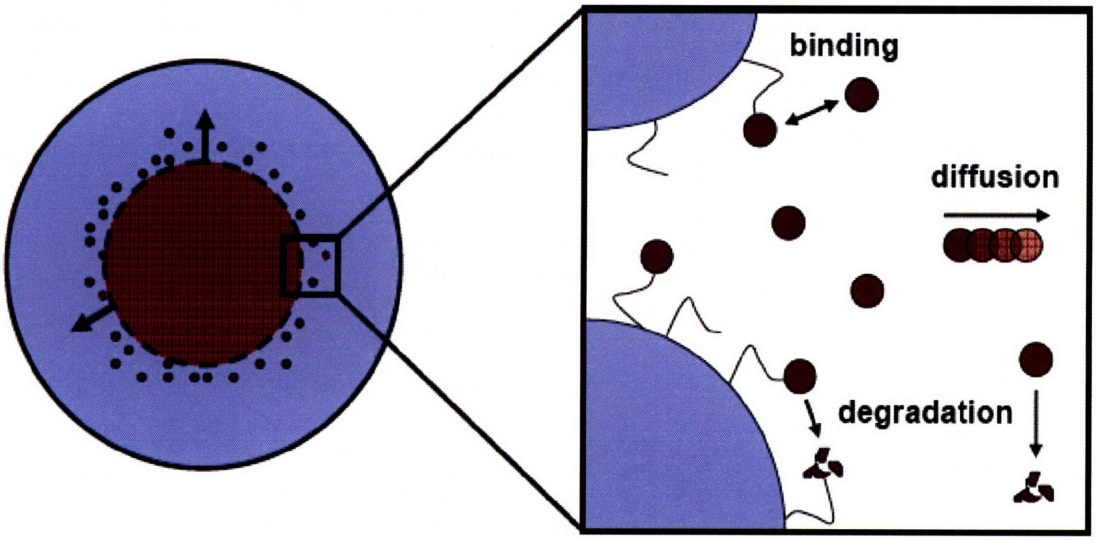

Figure 2.1. Schematic diagram of model. The tumor is modeled as a sphere. Initially virus is uniformly distributed in a spherical volume at the center of the tumor. Over time, virus spreads into the adjacent space. Three processes are considered: (1) association and dissociation of virus and cell surface heparan sulfate; (2) degradation of free and bound virus; (3) diffusion of free virus. At baseline conditions, HSV particles spread minimally from the initial injection volume due to rapid binding and slow diffusion. However, the spread of virus into the adjacent space can be enhanced by

either decreasing the binding affinity of HSV for heparan sulfate (*e.g.* via modifications to viral surface glycoproteins) or increasing diffusive transport (*e.g.* via modulation of the extracellular matrix). Furthermore, a high enough dose of virus can saturate receptors at the center of the tumor and promote diffusion outward.

HSV binding to the cell surfaces and subsequent internalization is not mediated by a simple single ligand-single receptor interaction. Rather it is a multi-step process which involves several viral envelope glycoproteins (16). Thus assumptions were made to facilitate mathematical modeling. Cell surface binding has been found to be primarily mediated by the interaction of the viral glycoproteins gB and gC with heparan sulfate (17-19). A comparison of binding affinities (20, 21) and separate mutant virion analyses (22, 23) suggest that gC binding to heparan sulfate is the primary mechanism for cell surface attachment of HSV. Thus we have modeled the binding of HSV to cells as an interaction between the glycoprotein gC and cell surface heparan sulfate. A second ligand-receptor interaction (gD-HVEM) facilitates internalization. Because the details of internalization are not well-understood, the internalization process was not included in the present model.

The concentration profile for free (interstitial) virus and bound virus are given by

$$\frac{\partial C_I}{\partial t} = \frac{D}{r^2}\frac{\partial}{\partial r}\left(r^2 \frac{\partial C_I}{\partial r}\right) - \frac{k_{on} C_I \left(C_{HS} - aC_B\right)}{\phi} + k_{off} C_B - k_d C_I \qquad (1)$$

$$\frac{\partial C_B}{\partial t} = \frac{k_{on} C_I \left(C_{HS} - aC_B\right)}{\phi} - k_{off} C_B - k_d C_B \qquad (2)$$

where C_I and C_B are the concentrations of free virus and bound virus, respectively (M); t is the time (s); r is the radial distance (cm); D is the effective diffusion coefficient of virus in the interstitial space (cm^2s^{-1}); k_{on} is the second order rate constant for binding of free virus ($M^{-1}s^{-1}$); k_{off} is the first order rate constant for dissociation of bound virus from the cell surface (s^{-1}); ϕ is the volume fraction available to virus in the tumor; C_{HS} is the concentration of cell surface receptors (M); a is the number of receptors sterically blocked by the binding of each viral particle; and k_d is the rate constant for degradation of the virus (s^{-1}), assumed to be the same for both bound and free virus.

The boundary conditions are specified by spherical symmetry at the center of the tumor and a virus sink at the edge of the tumor:

$$\frac{\partial C_I}{\partial r} = 0 \qquad \text{at } r = 0$$

$$C_I = 0 \qquad \text{at } r = R.$$

The initial conditions are

$$C_I = C_0 \qquad \text{for } r \le \rho$$

$$C_I = 0 \qquad \text{for } r > \rho$$

with no bound virus throughout the tumor. These conditions reflect a uniform initial concentration of virus in the center of the tumor following direct intratumor injection, a common approach in the treatment of solid tumors (24). The injection volume is spherical with a radius of ρ.

The differential equations were non-dimensionalized by incorporating the following variables

$$\eta = \frac{r}{R} \qquad s = \frac{Dt}{R^2} \qquad \theta_I = \frac{C_I}{C_0} \qquad \theta_B = \frac{C_B}{C_0}.$$

Terms were then grouped into three Damkohler numbers relating the rates of reaction and diffusion:

$$Da_{on} = \frac{k_{on} R^2 C_{HS}}{\phi D} \qquad Da_{off} = \frac{k_{off} R^2}{D} \qquad Da_d = \frac{k_d R^2}{D}.$$

Equations (1) and (2) were thus recast as

$$\frac{\partial \theta_I}{\partial s} = \frac{1}{\eta^2} \frac{\partial}{\partial \eta} \left(\eta^2 \frac{\partial \theta_I}{\partial \eta} \right) - Da_{on} \theta_I (1 - a' \theta_B) + Da_{off} \theta_B - Da_d \theta_I \qquad (3)$$

$$\frac{\partial \theta_B}{\partial s} = Da_{on} \theta_I (1 - a' \theta_B) - Da_{off} \theta_B - Da_d \theta_B \qquad (4)$$

where $a' \equiv \frac{aC_0}{C_{HS}}$.

The differential equations (3) and (4) were solved simultaneously using a numerical finite difference method in Matlab.

Parameter Estimation

Choice of Tumor and Initial Viral Distribution

The baseline parameter values for the model are given in Table 2.1. As we are interested in determining the transport limitations specifically in high collagen tumors, we used as our model tumor HSTS26T, a human soft tissue sarcoma which we have previously shown has elevated levels of collagen (11). The tumor radius was obtained from our previous studies (25, 26). The radius of initial viral distribution into a fibrous tumor was measured in our previous work (10). In that study the area of initial viral distribution was quantified by multi-photon imaging of fluorescently-labeled HSV vectors at the injection site.

Table 2.1: Baseline model parameters

Symbol	Definition	Value
D	Diffusion coefficient	5E-10 cm^2s^{-1}
k_{on}	Association rate constant	5E3 $M^{-1}s^{-1}$
k_{off}	Dissociation rate constant	8E-3 s^{-1}
k_d	Degradation rate constant	4.8E-5 s^{-1}
C_0	Initial virus concentration in injection volume	1.27E-9 M
R	Radius of tumor	5E-2 cm
ρ	Radius of initial viral injection	2.5E-2 cm
ϕ	Volume fraction of tumor accessible to virus	0.05
C_{HS}	Heparan sulfate concentration	1.74E-5 M
a	Heparan sulfate molecules per bound virus	1E3

Estimation of Transport Parameters

The effective diffusion coefficients of particles the size of HSV have not been measured in high collagen tumors. However, we previously measured the diffusion coefficient of particles up to ~40 nm diameter in fibrous melanoma xenografts and of ~150 nm diameter liposomes in tumors with relatively little collagen (15). By extrapolation, the effective diffusion coefficient of HSV particles in tumors with high collagen content is $5x10^{-10}$ cm^2s^{-1}. For validation we also estimated the diffusion coefficient based on the effective medium model for hindered diffusion of a solid sphere (27, 28). In separate studies we have previously found the Darcy permeability (K) of HSTS26T tumors to be 3 nm^2 (11) and 50 nm^2 (29). We should note that the Darcy permeability of collagen gels with similar collagen content to HSTS26T tumors (30 mg/ml interstitial matrix) was found to be 40 nm^2 after correction for the effect of cells (30). Assuming the diffusion coefficient of HSV particles in solution is equivalent to that of similarly sized liposomes, this leads to calculated diffusion coefficients of $2x10^{-9}$ cm^2s^{-1} ($K = 50$ nm^2) and $2x10^{-10}$ cm^2s^{-1} ($K = 3$ nm^2). Thus, our extrapolated value from the *in vivo* data seems reasonable.

Estimation of Kinetic Parameters

We estimated the rate constant for degradation of HSV particles in the tumor interstitium by measuring the rate of degradation in HSTS26T conditioned media and fitting to a first order kinetic model (Fig. 2.2). Briefly, replication competent HSV (MGH2) particles were incubated with 24 hour conditioned media from HSTS26T cells at several concentrations at 37°C and pH 7.4. At various time points the media was frozen in a dry ice/ethanol bath. The concentration of viable viral particles at each time point was

determined by titrating each sample with HSTS26T cells. The rate constant for degradation was estimated by fitting the data to a first order rate equation. Incubation was performed in duplicate and titration of both samples in triplicate, and the average values were used in the analysis. It appears that proteins secreted by tumor cells can degrade HSV since the half-time for degradation is ~4.25 hrs when incubated with conditioned media, as compared to ~24 hrs when incubated with PBS.

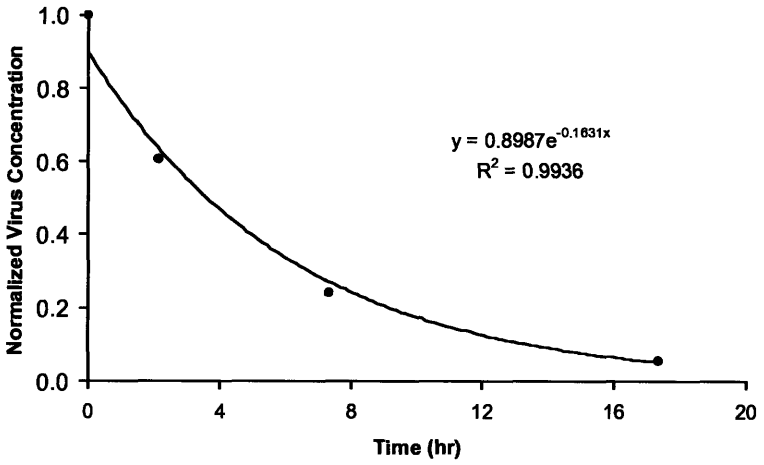

Figure 2.2. Estimation of degradation rate constant. HSV particles were incubated with 24 hour conditioned media from HSTS26T cells and the concentration of viable viral particles determined at various time points. The values were normalized to the initial concentration. The data was fit to a first order kinetic rate equation to determine the degradation rate constant.

The cell surface heparan sulfate concentration was determined experimentally for HSTS26T cells using a DMMB dye assay according to the manufacturer's protocol (Biocolor, Newtownabbey, Ireland). To determine the number of heparan sulfate

molecules blocked by the binding of a single viral particle to the cell surface, we first needed to determine the number of viral particles that can bind to a single cell. We modeled viral particles and cells as spheres of 150 nm and 10 μm diameter, respectively, and assumed simple cubic packing of virus on the cell surface. This analysis showed that that virus, rather than receptor, is limiting for HSV binding to cells (2.25×10^4 viruses/cell vs. 1.0×10^7 heparan sulfate molecules/cell). While simple cubic packing most likely cannot be achieved due to steric effects and the presence of other proteins on the cell surface, virus internalization occurs very rapidly ($t_{1/2}$ ~ minutes) (31) and frees space on the cell surface for other HSV particles to bind. As a conservative estimate, the calculated value for the number of viral particles that can bind a single cell was reduced by a factor of 2. The number of heparan sulfate molecules blocked by a single binding event was then estimated based on the total amount of heparan sulfate per cell.

The rate constant for dissociation of bound virus from cell surface heparan sulfate was estimated from a kinetic analysis of the binding of soluble gC to immobilized heparan sulfate using surface plasmon resonance (20). The kinetic data fit well with a 1:1 model (one molecule of gC binding to one molecule of heparan sulfate). The dissociation rate constant for this process was measured at 25°C. In order to adjust to the physiological temperature of 37°C, we estimated the effect of temperature on the binding rate constant using published kinetic analyses of a variety of other proteins (32-35). From these data we assumed an increase of ~1.0 in $\ln(k_{off}/T)$ for the temperature change of interest. While Rux *et al.* measured the kinetic rate constant for individual gC molecules, we applied them to HSV particles. Based on the spherical nature of the HSV particle, we assumed

that its attachment to the cell surface occurs at the pole, due to the interaction of a single gC molecule with heparan sulfate.

While Rux *et al.* also measured the association rate constant for binding of soluble gC to heparan sulfate (20), it was difficult to convert this value to a rate constant for HSV particles. It is not clear whether the affinity of viral particles scales with the number of gC molecules on its surface. To more accurately estimate the association rate constant we experimentally assessed the binding of HSV particles to HSTS26T cells in solution (Fig. 2.3). Briefly, replication competent HSV particles were incubated with HSTS26T cells in suspension with gentle agitation. At various time points, cells were pelleted by centrifugation and the supernatant immediately collected and frozen in a dry ice/ethanol bath. The concentration of viral particles at each time point was determined by titrating with HSTS26T cells. The rate constant for degradation was estimated by fitting the data to a second order rate equation.

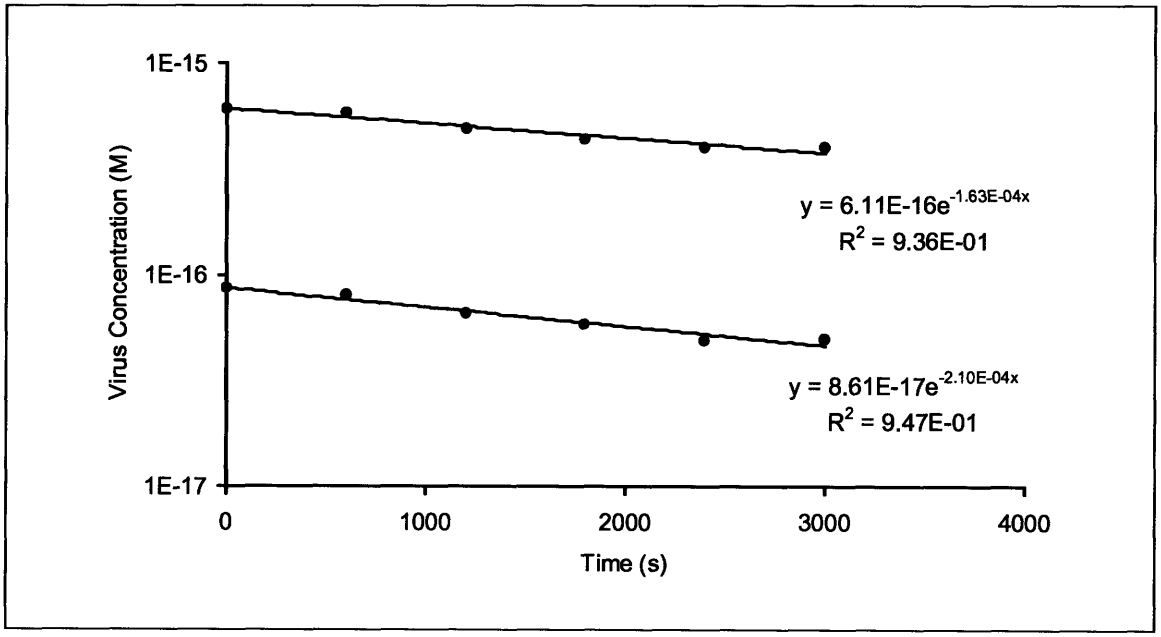

Figure 2.3. Estimation of association rate constant. HSV particles were incubated with HSTS26T cells in suspension with gentle agitation. The concentration of unbound virus was determined at various time points. The data was fit to a second order kinetic rate equation to estimate the rate constant for association. Viral degradation and dissociation were ignored in this model. In the fit equations, the exponential factor is given by the product of the association rate constant and the concentration of receptors.

Estimation of Volume Fraction and Viral Concentration

There exists no measurement of the volume fraction of HSV particles or other similarly sized particles in tumors. However, Krol *et al.* developed an *ex vivo* method to measure the volume fraction in tumors and determined the value for dextrans of various sizes (36). We estimated the volume fraction by using the value they measured for the largest dextran ($2x10^6$ MW) in subcutaneous MCA-R fibrosarcomas.

The initial intratumor viral concentration is taken from our experiments performed with direct injections of the oncolytic HSV vector MGH2 to treat a fibrous melanoma (10). The concentration of virus in the tumor can be estimated since both the viral dose, $1x10^6$ pfu (plaque forming units), and the volume of virus distribution – as determined by imaging of the fluorescently-labeled viral particles directly after injection – are known (see Chapter 3). It is important to note that pfu is not a direct measure of total number of viral particles. In the assay for determining pfu, plaque formation depends on multiple steps beyond simply binding and internalization of the viral particle. Thus, not every viable HSV particle (as defined in this model) will lead to plaque formation. The total

number of HSV particles can range from 3 to 100 times the pfu, as determined by PCR and PicoGreen staining analysis of wild type HSV (P. Grandi, personal communication). Clearly, this will be dependent on the experiment, cell line and virus preparation. As an approximation, we have estimated the total viral concentration from the pfu by using a factor of 50.

Baseline Simulation

Using the baseline values, the Damkohler numbers for association (Da_{on}), dissociation (Da_{off}) and degradation (Da_d) were calculated. These numbers provide a ratio of the time scale for diffusion relative to each of these three processes. All three Damkohler numbers are much greater than 1 ($Da_{on} = 5.6 \times 10^6$, $Da_{off} = 2.6 \times 10^4$, $Da_d = 1.5 \times 10^2$), signifying that the processes of binding and degradation occur much more rapidly than diffusion. The dimensionless free and bound virus concentration profiles shown in Figs. 2.4A,B reflect this. The concentrations have been normalized to the initial concentration of virus in the injection site and the radial dimension is normalized to the overall tumor radius (with 0 being the tumor center, 0.5 being the edge of the initial injection volume and 1 being the tumor edge). Overwhelmingly the virus remains bound to cell surfaces rather than free in the interstitial space, with nearly three orders of magnitude more virus bound than free at any time. Over time, the virus degrades (Fig. 2.5) and by 12 hours only ~13% of the initial amount is left in the tumor. Very little diffusion into the adjacent tumor space is observed, with only 4% of the remaining virus beyond the initial injection volume at 24 hrs. To confirm that the distinctive profile is a consequence of rapid binding and gradual degradation, the model simulation was also performed without degradation

(Fig. 2.4C) and without both degradation and binding (Fig. 2.4D). These concentration profiles are consistent with this understanding of the viral dynamics.

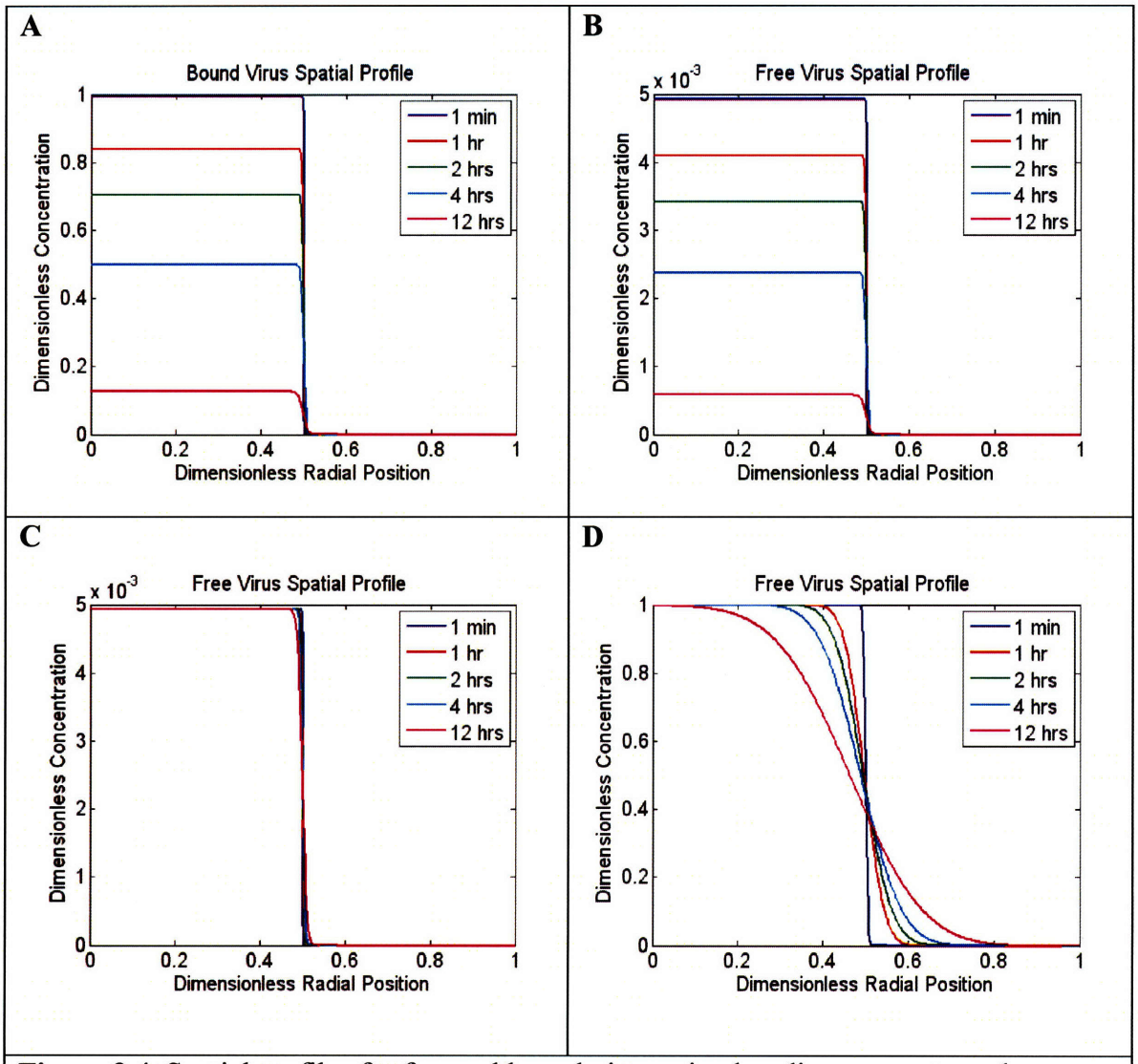

Figure 2.4. Spatial profiles for free and bound virus using baseline parameter values. Virus concentrations have been normalized to the initial free viral concentration throughout the injection site. The radial position has been normalized to the tumor radius. (A) Bound virus spatial profile. (B) Free virus spatial profile. (C) Free virus spatial profile from simulation without degradation term. (D) Free virus spatial profile from simulation without both degradation and binding terms.

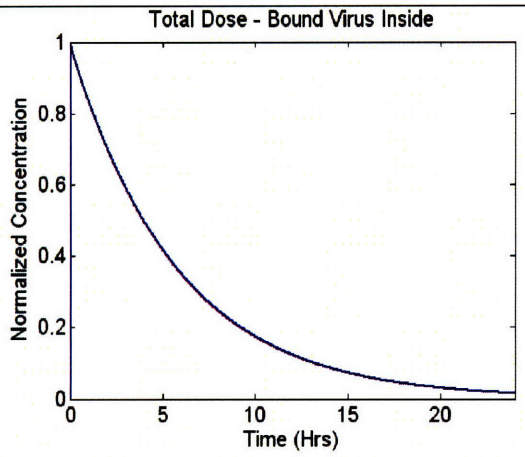

Figure 2.5. Total dose of bound virus in the initial injection volume over time. The dose has been normalized to the initial concentration in the injection volume.

Sensitivity Analysis

Next, we performed a sensitivity analysis to determine the relative importance of each parameter and to gauge the ability of various virus and tumor modifications to improve intratumor distribution and therapeutic efficacy (Table 2.2). To compare different simulations, various indices were considered 12 hours following the initial "injection". The total number of free and bound viral particles in both the initial distribution volume ("virus inside") as well as the adjacent, initially uninfected region ("virus outside") was calculated. The values normalized to the baseline simulation for each of the four species are also given, serving as a better measure of the relative change induced by each modification. We assessed the amount of viral spread from the initial injection site by calculating the volume of adjacent space which contains bound virus ("volume spread"). We chose as our threshold bound virus concentration 1% of the initial injection concentration (1.27×10^{-11} M). This concentration corresponds to ~500 bound viral

particles per cell, a number which likely leads to successful infection. The volume spread was calculated at each time point and the maximum value was chosen to best reflect the volume of the tumor that is infected with virus. A description of each of the simulations follows.

.2. Sensitivity analysis*#

ion	Virus Inside (# viral particles)		Virus Outside (# viral particles)		Virus Inside (Normalized)		Virus Outside (Normalized)		Spre Volu (Nor
	Free	**Bound**	**Free**	**Bound**	**Free**	**Bound**	**Free**	**Bound**	
	2.8E+04	6.1E+06	7.2E+02	1.6E+05	1.00	1.00	1.00	1.00	1.0
)	2.9E+03	6.3E+06	3.0E+01	6.5E+04	0.10	1.02	0.04	0.42	0.4
)	2.6E+05	5.6E+06	1.9E+04	4.2E+05	9.15	0.92	27.09	2.71	3.0
)0	1.6E+06	3.6E+06	3.6E+05	7.8E+05	57.62	0.58	497.68	4.98	7.4
	5.6E+01	1.2E+04	1.4E+00	3.1E+02	0.00	0.00	0.00	0.00	0.5
	1.2E+05	2.4E+07	2.9E+03	6.3E+05	4.09	3.98	4.06	4.02	1.7
	2.7E+04	5.8E+06	2.1E+03	4.5E+05	0.95	0.95	2.88	2.88	3.1
	3.1E+05	6.1E+07	8.9E+03	1.9E+06	10.83	9.95	12.31	11.97	1.9
	9.5E+06	4.8E+08	1.1E+06	1.4E+08	331.94	78.32	1493.53	906.18	8.6
	8.3E+04	6.0E+06	3.5E+03	2.5E+05	2.92	0.98	4.84	1.61	1.7
	9.6E+03	6.2E+06	1.5E+02	9.9E+04	0.34	1.01	0.21	0.64	0.7
ınd Da_{on} / 10	2.2E+05	4.8E+06	5.9E+04	1.3E+06	7.75	0.78	82.24	8.23	10.
ınd Da_{on} / 100	9.5E+05	2.1E+06	1.0E+06	2.3E+06	33.47	0.34	1449.71	14.53	26.

shown are for time = 12 hours following the beginning of the simulation, except for spread volume
for changes in Da_{off} are nearly equivalent to values for opposite and proportional changes in Da_{on}

Binding Kinetics

We first examined the effect that changes in virus binding characteristics would have on its distribution. Since virus binding dominates in the baseline simulation, we analyzed the extent to which a decrease in affinity to heparan sulfate would improve distribution. A ten-fold decrease in the affinity increases both the amount of bound virus in the adjacent space and the spread volume by nearly 3-fold (Fig. 2.6A). This change in the affinity constant was chosen to reflect possible changes to the virus, itself. Rux *et al.* found that deletion of residues 33-123 of gC results in an order of magnitude increase in its K_D (20). Furthermore, it has been shown that the gB-heparan sulfate interaction is the second strongest between HSV and cells, with a binding affinity that is an order of magnitude lower than for gC (20, 21). Thus a 10-fold decrease in the affinity constant approximates the change that would occur if gC is modified or deleted.

Beyond gC and gB, the interaction of other viral envelope glycoproteins with cell surfaces is less well studied. It has been found that the binding affinity of gD with its cell surface receptor is an order of magnitude lower than for gB-heparan sulfate, and two orders of magnitude lower than for gC-heparan sulfate (37). Thus we examined the effect of a two orders of magnitude decrease in the affinity, which would reflect changes to both gC and gB. This leads to a greater than 7-fold increase in the spread volume (Fig. 2.6A). As expected the amount of bound virus in the initial injection volume decreases as a greater fraction of virus is free and diffuses out of this volume. However, there is still $\sim 10^2$ bound viral particles per cell in this region, suggesting that we are not at the point of diminishing returns for overall cell infection.

Next we assessed the effect of a ten-fold increase in affinity. The spread volume decreased by more than a half, with a greater than two-fold decrease in the amount of bound virus in the adjacent region (Fig. 2.6A). When changes to the dissociation constant (*i.e.* Da_{off}) were analyzed, we found proportional and opposite effects when compared to changes in the association constant (*i.e.* Da_{on}). Thus, to avoid repetition these results are not displayed in Table 2.2. We should also note that a change in Da_{on} can reflect a change in either k_{on} or C_{HS}. Thus, binding affinity can be reduced by changing the virus, as mentioned above, or by finding tumors that contain less heparan sulfate receptors for cell surface binding.

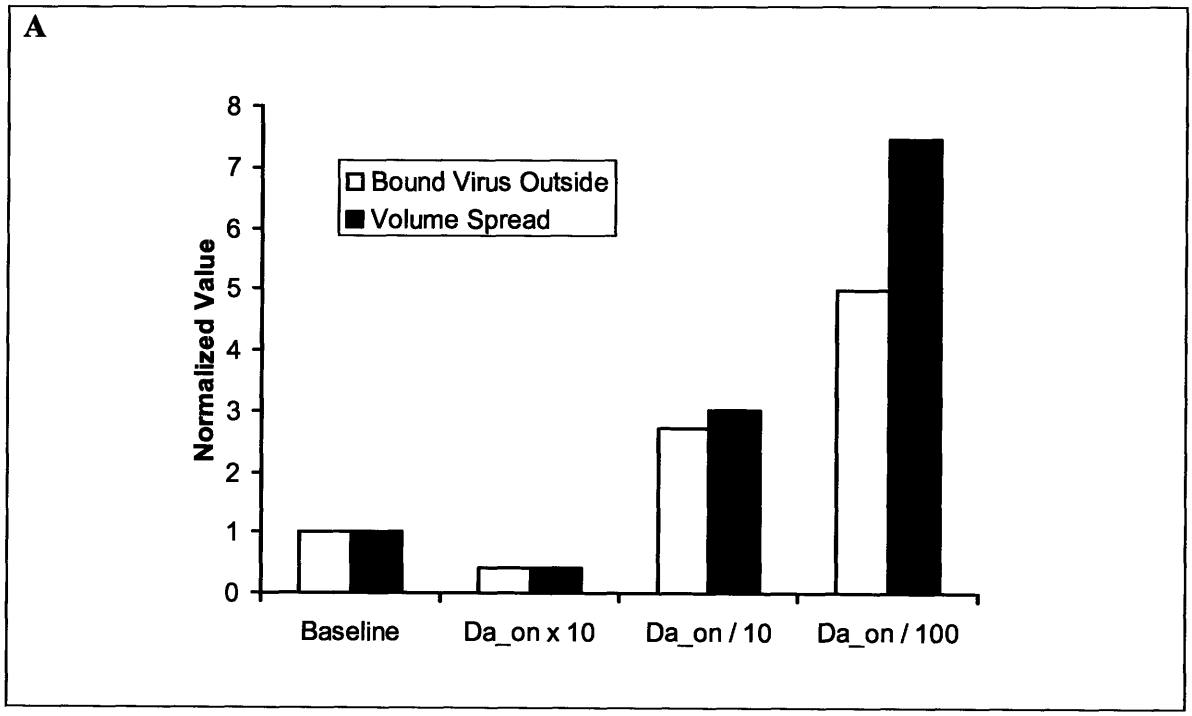

B

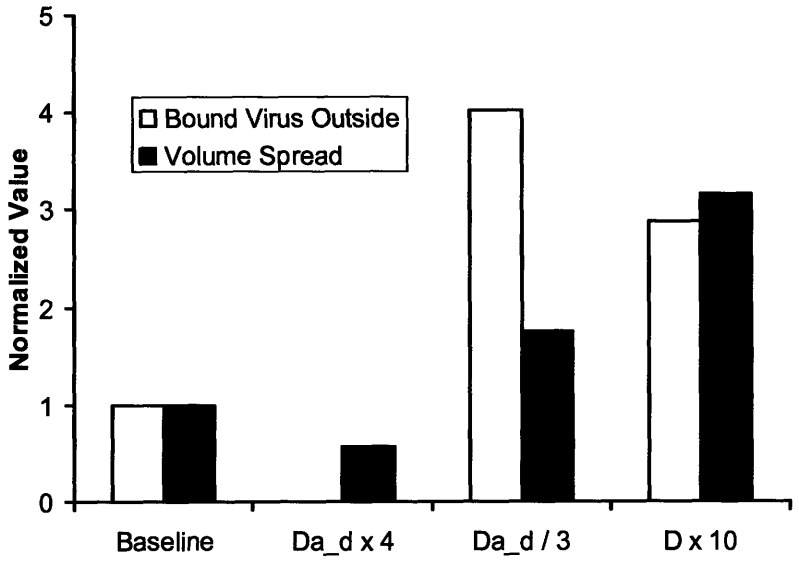

Figure 2.6. Effect of parameter modifications on bound virus concentration and spread volume. The values for the total concentration of bound virus outside the initial distribution volume and the spread volume are shown, normalized to the values in the baseline simulation. Values are for 12 hours after the beginning of the simulation for the amount of bound virus outside and are maximum values for volume spread. (A) Effect of changes in the binding kinetics on virus distribution. (B) Effect of changes in the degradation rate constant and diffusion coefficient on viral distribution.

Degradation

Our experiments showed that the $t_{1/2}$ for degradation of HSV particles at 37°C in tumor cell conditioned media is ~4 hrs, while $t_{1/2}$ ~ 24 hrs in PBS. However, these *in vitro* experiments may not completely capture the conditions *in vivo,* where the concentration of extracellular factors may be different. It is therefore important to analyze the

sensitivity of the model to this parameter. As this model does not take into account viral internalization – a process that occurs on the order of minutes – few insights can be drawn from changes in total bound virus induced by altering Da_d. Rather it is more useful to assess changes in the spread volume, which is affected by degradation since diffusion of free virus is a slow process. When the virus half life is decreased to 1 hr, nearly all free virus is degraded by 12 hrs. The maximum spread volume is only several microns from the injection volume, and the spread volume is half of the baseline value (Fig. 2.6B).

Conversely, increasing the virus half-life by a factor of 3 led to a 4-fold increase in the amount of virus in each compartment. Interestingly, the distribution was increased less than 2-fold (Fig. 2.6B), suggesting that while degradation occurs quickly, the limited spread of the virus is mainly a consequence of rapid binding.

Diffusion

Altering the diffusion coefficient can have an effect on the distribution of virus in the tumor. Our previous work has shown that the effective diffusion coefficient in a tumor correlates negatively with collagen content (11). In this model, we have chosen our effective diffusion coefficient to reflect transport in a collagen-rich fibrosarcoma. Thus we have chosen a particularly low value. Based on a comparison of the diffusion coefficient of various tracer molecules in tumors with high and low levels of collagen (15), we believe that a 10-fold increase in D more accurately reflects the conditions in less fibrous solid tumors. Furthermore, based on previous work we estimate that this increase in diffusion coefficient is possible for large particles such as HSV in high collagen tumors with the addition of collagen-modulating factors (11, 38). An order of

magnitude increase in the diffusion coefficient results in a 3-fold increase in both the amount of virus outside the initial injection volume and the spread volume (Fig. 2.6B). Thus, the model predicts that an oncolytic HSV vector would be more effective in treating a low collagen tumor than a high collagen one. It also suggests that matrix modification may be a useful method to improve viral vector distribution in those tumors with a significant amount of collagen and hindered diffusion.

Volume Fraction

The volume fraction of tumor accessible to virus has the potential to affect therapeutic response since it influences virus accumulation and distribution in the tumor. The variation in volume fraction for particles the size of HSV has not been determined in different tumors. However, the interstitial volume of tumors – which plays an important role in determining the available volume fraction – has been measured in various tumors and found to range from 10-60% (39-41). In a fibrosarcoma with an interstitial fluid space of ~50%, the accessible volume fraction for large macromolecules (molecular weight > 10^5) was found to be less than 0.1. Based on these data, to approximate various tumors we decided to run the simulation with a 3-fold increase ($\phi = 0.15$) and 3-fold decrease ($\phi = 0.017$) in the volume fraction. A 3-fold increase in the volume fraction results in a ~60% increase in the amount of bound virus outside the initial injection volume and the distance spread. In contrast, a 3-fold decrease reduces the spread volume by nearly a third (Table 2.2). These results show that variations in volume fraction between tumors may have an effect, but it may not be overwhelming. Relative to other parameters, viral distribution appears insensitive to this parameter.

Initial Dose

We analyzed the effect of input viral dose. A 10-fold increase in initial viral concentration resulted in nearly equivalent increases in viral concentrations in each of the compartments, and only a two-fold increase in the spread volume (Table 2.2). A slightly greater than proportional increase in the amount of virus outside the initial distribution volume was observed, suggesting that we are approaching the viral concentration necessary to saturate receptors. Indeed, for a 100-fold increase in the viral concentration, nearly 90% of the virus inside the injection site is unbound (Fig. 2.6A). The virus behaves like a moving front of bound virus, with degradation occurring over time. The amount of virus outside the initial injection volume has increased by three orders of magnitude compared to the baseline simulation and the volume spread has increased by more than 8-fold.

These results suggest that one simple way to improve viral distribution and perhaps efficacy is to increase the dose to saturate receptors and promote diffusion from the injection site. However, the model does not take into account loss of virus into the systemic circulation during infusion. Based on studies with adenoviral vectors, this may reduce the actual dose within the tumor by as much as an order of magnitude (42). Furthermore, in this work we have modeled relatively small tumors found in certain pre-clinical experimental models (1 mm diameter). Scaling up to human tumors would require an increase in dose of at least an order of magnitude. Taking these into consideration, at least a four orders of magnitude increase in dose would be necessary to achieve the improvements in distribution shown in Fig. 2.7A. This dose would be orders

of magnitude beyond what has been used in human clinical trials (6). Such a high dose would likely compromise the safety of an oncolytic HSV vector and would most certainly be impractical to obtain, given the relative difficulty of purifying HSV at high titers.

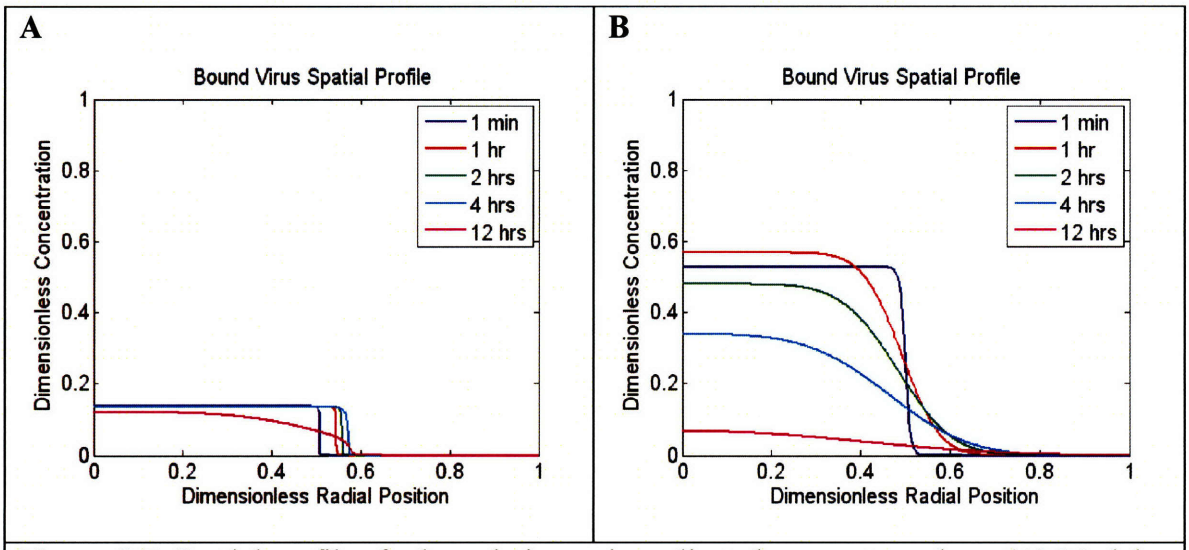

Figure 2.7. Spatial profiles for bound virus using adjusted parameter values. (A) Model simulation with the initial dose increased 100-fold, while all other parameters are kept at their baseline value. (B) Model simulation with the diffusion coefficient increased by a factor of 10, and Da_{on} decreased by a factor of 100, with all other parameters kept at their baseline value.

Implications and Limitations

Several limitations remain in the present model: (a) it does not take into account binding of the virus to extracellular matrix components (including heparan sulfate not on the cell surface) or other cell surface molecules and receptors; (b) it lacks a complete description of virus clearance, particularly via the systemic circulation, which has been found to be

quite significant for intratumorally injected virus; (c) it ignored downstream events such as bound virus internalization and replication; (d) it assumes a uniform distribution of virus in the center of the tumor following intratumor injection, ignoring the effects that matrix structures and infusion conditions can have on convective delivery during this process.

Nevertheless, the model has exposed some important characteristics of intratumor vius transport. The simulations show that rapid binding and impaired diffusion limit the distribution of virus in the tumor. After injection into the interstitial space, virus will quickly bind to cells. Even in the absence of binding, diffusion is a relatively slow process due to the large size of the virus. It has been observed experimentally that the spread of virus from the injection site can be quite limited (10). This model offers one possible explanation for this phenomenon for HSV. This finding has significant implications for the treatment of tumors with replication-competent HSV vectors, such as oncolytic vectors. Progeny virus that are released into the extracellular space following cell lysis will be subject to the same limited interstitial transport and will be able to infect cells only in close proximity. Using multiphoton imaging we have observed the propagation of oncolytic HSV in individual tumor xenografts and found that progeny virus typically infects only neighboring cells (10). The model results are consistent with this observation, although direct spread from cell to cell through junctions likely contributes, as well (43).

Since the initial virus distribution in the tumor is critical for an oncolytic virus to control tumor growth, this also points to the importance of the method of viral delivery. For a

direct intratumor injection, the rate and volume of infusion, tumor permeability and hydraulic conductivity and the number of injection sites will all be key parameters. Any choice of parameter values which improves the initial distribution may enhance treatment outcome. Indeed, a study has already shown that fractionated injection of an oncolytic HSV in multiple sites is advantageous to a single injection (44). Bobo *et al.* showed that the distribution of large molecules in the brain could be improved by prolonged infusion (45). They also showed that the volume of distribution increased linearly with the infusion volume. However, enhancing the distribution of therapeutics by optimizing infusion parameters may not be a viable option for many tumors. Boucher *et al.* found that even at low flow rates, albumin infused in the center of a fibrosarcoma distributed asymmetrically from the source (46). Fluid accumulated in necrotic regions and at the surface of the tumor, with channels of fluid connecting these regions. The extreme stiffness of these tumors – likely due to the composition and structure of the extracellular matrix – appeared to contribute to the difficulty in obtaining uniform and widespread delivery. Given this observation, an alternative method to enhance intratumoral infusion may be to increase the permeability and hydraulic conductivity of the tumor. In Chapter 5 we use the matrix degrading proteases matrix metalloproteinase-1 and -8 to modify the tumor extracellular matrix, increase hydraulic conductivity and enhance the distribution and efficacy of intratumorally injected oncolytic HSV vectors.

The model suggests that certain tumors may be more responsive to oncolytic HSV therapy than others, based on such factors as the concentration of heparan sulfate and the composition of the extracellular matrix (which determines the effective diffusion coefficient and accessible volume fraction). It also points to various methods of virus and

tumor modification which can enhance the efficacy of oncolytic HSV. Two such modifications are (a) a decrease in the binding affinity via alteration of the viral envelope and (b) an increase in the effective diffusion coefficient of virus through degradation of tumor collagen. A model simulation with both of these modifications shows significantly improved virus distribution (Fig. 2.7B). While modified HSV vectors with mutations in gC and gB have been developed (22, 23, 47), these changes have yet to be incorporated into oncolytic vectors. Whether these changes can improve viral spread and enhance efficacy is an exciting question that we hope will be answered shortly. A second approach to overcome rapid binding and enhance diffusion is to pre-block virus binding sites in the tissue, similar to the approach previously developed for antibodies (48). In theory, virus particles would diffuse farther but then compete for binding sites and eventually infect cells distant from the injection site. This method has the advantage of not altering the intrinsic affinity of the virus, which may have unforeseen consequences and decrease infection efficiency. As for modulation of tumor fibrillar collagen, we validate our predictions experimentally using bacterial collagenase in Chapter 3 (10). The challenge with this technique is finding clinically relevant ways to degrade the matrix while limiting the negative effects these changes may have on tumor cell invasion and metastasis.

References

1. Cross D, Burmester JK. Gene therapy for cancer treatment: past, present and future. Clin Med Res 2006;4: 218-27.
2. Mullen JT, Tanabe KK. Viral oncolysis. Oncologist 2002;7: 106-19.
3. Chiocca EA. Oncolytic viruses. Nat Rev Cancer 2002;2: 938-50.
4. Kirn D, Martuza RL, Zwiebel J. Replication-selective virotherapy for cancer: Biological principles, risk management and future directions. Nat Med 2001;7: 781-7.
5. Aghi M, Martuza RL. Oncolytic viral therapies - the clinical experience. Oncogene 2005;24: 7802-16.
6. Liu TC, Galanis E, Kirn D. Clinical trial results with oncolytic virotherapy: a century of promise, a decade of progress. Nat Clin Pract Oncol 2007;4: 101-17.
7. Sauthoff H, Hu J, Maca C, *et al.* Intratumoral spread of wild-type adenovirus is limited after local injection of human xenograft tumors: virus persists and spreads systemically at late time points. Hum Gene Ther 2003;14: 425-33.
8. van Etten B, ten Hagen TL, de Vries MR, Ambagtsheer G, Huet T, Eggermont AM. Prerequisites for effective adenovirus mediated gene therapy of colorectal liver metastases in the rat using an intracellular neutralizing antibody fragment to p21-Ras. Br J Cancer 2002;86: 436-42.
9. Yuan F, Leunig M, Huang SK, Berk DA, Papahadjopoulos D, Jain RK. Microvascular permeability and interstitial penetration of sterically stabilized (stealth) liposomes in a human tumor xenograft. Cancer Res 1994;54: 3352-6.
10. McKee TD, Grandi P, Mok W, *et al.* Degradation of fibrillar collagen in a human melanoma xenograft improves the efficacy of an oncolytic herpes simplex virus vector. Cancer Res 2006;66: 2509-13.
11. Netti PA, Berk DA, Swartz MA, Grodzinsky AJ, Jain RK. Role of extracellular matrix assembly in interstitial transport in solid tumors. Cancer Res 2000;60: 2497-503.
12. Tao Y, Guo Q. The competitive dynamics between tumor cells, a replication-competent virus and an immune response. J Math Biol 2005;51: 37-74.
13. Wein LM, Wu JT, Kirn DH. Validation and analysis of a mathematical model of a replication-competent oncolytic virus for cancer treatment: implications for virus design and delivery. Cancer Res 2003;63: 1317-24.
14. Wodarz D. Viruses as antitumor weapons: defining conditions for tumor remission. Cancer Res 2001;61: 3501-7.
15. Pluen A, Boucher Y, Ramanujan S, *et al.* Role of tumor-host interactions in interstitial diffusion of macromolecules: cranial vs. subcutaneous tumors. Proc Natl Acad Sci U S A 2001;98: 4628-33.
16. Shukla D, Spear PG. Herpesviruses and heparan sulfate: an intimate relationship in aid of viral entry. J Clin Invest 2001;108: 503-10.
17. Herold BC, Visalli RJ, Susmarski N, Brandt CR, Spear PG. Glycoprotein C-independent binding of herpes simplex virus to cells requires cell surface heparan sulphate and glycoprotein B. J Gen Virol 1994;75 (Pt 6): 1211-22.
18. Shieh MT, WuDunn D, Montgomery RI, Esko JD, Spear PG. Cell surface receptors for herpes simplex virus are heparan sulfate proteoglycans. J Cell Biol 1992;116: 1273-81.

19. WuDunn D, Spear PG. Initial interaction of herpes simplex virus with cells is binding to heparan sulfate. J Virol 1989;63: 52-8.
20. Rux AH, Lou H, Lambris JD, Friedman HM, Eisenberg RJ, Cohen GH. Kinetic analysis of glycoprotein C of herpes simplex virus types 1 and 2 binding to heparin, heparan sulfate, and complement component C3b. Virology 2002;294: 324-32.
21. Williams RK, Straus SE. Specificity and affinity of binding of herpes simplex virus type 2 glycoprotein B to glycosaminoglycans. J Virol 1997;71: 1375-80.
22. Herold BC, WuDunn D, Soltys N, Spear PG. Glycoprotein C of herpes simplex virus type 1 plays a principal role in the adsorption of virus to cells and in infectivity. J Virol 1991;65: 1090-8.
23. Laquerre S, Argnani R, Anderson DB, Zucchini S, Manservigi R, Glorioso JC. Heparan sulfate proteoglycan binding by herpes simplex virus type 1 glycoproteins B and C, which differ in their contributions to virus attachment, penetration, and cell-to-cell spread. J Virol 1998;72: 6119-30.
24. Nemunaitis J, Khuri F, Ganly I, *et al.* Phase II trial of intratumoral administration of ONYX-015, a replication-selective adenovirus, in patients with refractory head and neck cancer. J Clin Oncol 2001;19: 289-98.
25. Baxter LT, Jain RK. Transport of fluid and macromolecules in tumors. I. Role of interstitial pressure and convection. Microvasc Res 1989;37: 77-104.
26. Gerlowski LE, Jain RK. Microvascular permeability of normal and neoplastic tissues. Microvasc Res 1986;31: 288-305.
27. Phillips RJ, Deen WM, Brady JF. Hindered transport in fibrous membranes and gels. AIChE J 1989;35: 1761-9.
28. Solomentsev YE, Anderson JL. Rotation of a sphere in Brinkman fluids. Phys Fluids 1996;8: 1119-21.
29. Griffon-Etienne G, Boucher Y, Brekken C, Suit HD, Jain RK. Taxane-induced apoptosis decompresses blood vessels and lowers interstitial fluid pressure in solid tumors: clinical implications. Cancer Res 1999;59: 3776-82.
30. Ramanujan S, Pluen A, McKee TD, Brown EB, Boucher Y, Jain RK. Diffusion and convection in collagen gels: implications for transport in the tumor interstitium. Biophys J 2002;83: 1650-60.
31. Wanas E, Efler S, Ghosh K, Ghosh HP. Mutations in the conserved carboxy-terminal hydrophobic region of glycoprotein gB affect infectivity of herpes simplex virus. J Gen Virol 1999;80 (Pt 12): 3189-98.
32. Day YS, Baird CL, Rich RL, Myszka DG. Direct comparison of binding equilibrium, thermodynamic, and rate constants determined by surface- and solution-based biophysical methods. Protein Sci 2002;11: 1017-25.
33. Deinum J, Gustavsson L, Gyzander E, Kullman-Magnusson M, Edstrom A, Karlsson R. A thermodynamic characterization of the binding of thrombin inhibitors to human thrombin, combining biosensor technology, stopped-flow spectrophotometry, and microcalorimetry. Anal Biochem 2002;300: 152-62.
34. Oddie GW, Gruen LC, Odgers GA, King LG, Kortt AA. Identification and minimization of nonideal binding effects in BIAcore analysis: ferritin/anti-ferritin Fab' interaction as a model system. Anal Biochem 1997;244: 301-11.
35. Roos H, Karlsson R, Nilshans H, Persson A. Thermodynamic analysis of protein interactions with biosensor technology. J Mol Recognit 1998;11: 204-10.

36. Krol A, Maresca J, Dewhirst MW, Yuan F. Available volume fraction of macromolecules in the extravascular space of a fibrosarcoma: implications for drug delivery. Cancer Res 1999;59: 4136-41.
37. Willis SH, Rux AH, Peng C, *et al.* Examination of the kinetics of herpes simplex virus glycoprotein D binding to the herpesvirus entry mediator, using surface plasmon resonance. J Virol 1998;72: 5937-47.
38. Brown E, McKee T, diTomaso E, *et al.* Dynamic imaging of collagen and its modulation in tumors in vivo using second-harmonic generation. Nat Med 2003;9: 796-800.
39. Bakay L. The extracellular space in brain tumours. I. Morphological considerations. Brain 1970;93: 693-8.
40. Gullino PM, Grantham FH, Smith SH. The Interstitial Water Space Of Tumors. Cancer Res 1965;25: 727-31.
41. O'Connor SW, Bale WF. Accessibility of circulating immunoglobulin G to the extravascular compartment of solid rat tumors. Cancer Res 1984;44: 3719-23.
42. Wang Y, Hu JK, Krol A, Li YP, Li CY, Yuan F. Systemic dissemination of viral vectors during intratumoral injection. Mol Cancer Ther 2003;2: 1233-42.
43. Dingwell KS, Brunetti CR, Hendricks RL, *et al.* Herpes simplex virus glycoproteins E and I facilitate cell-to-cell spread in vivo and across junctions of cultured cells. J Virol 1994;68: 834-45.
44. Currier MA, Adams LC, Mahller YY, Cripe TP. Widespread intratumoral virus distribution with fractionated injection enables local control of large human rhabdomyosarcoma xenografts by oncolytic herpes simplex viruses. Cancer Gene Ther 2005;12: 407-16.
45. Bobo RH, Laske DW, Akbasak A, Morrison PF, Dedrick RL, Oldfield EH. Convection-enhanced delivery of macromolecules in the brain. Proc Natl Acad Sci U S A 1994;91: 2076-80.
46. Boucher Y, Brekken C, Netti PA, Baxter LT, Jain RK. Intratumoral infusion of fluid: estimation of hydraulic conductivity and implications for the delivery of therapeutic agents. Br J Cancer 1998;78: 1442-8.
47. Cai WZ, Person S, Warner SC, Zhou JH, DeLuca NA. Linker-insertion nonsense and restriction-site deletion mutations of the gB glycoprotein gene of herpes simplex virus type 1. J Virol 1987;61: 714-21.
48. Jain RK. Delivery of molecular and cellular medicine to solid tumors. Adv Drug Deliv Rev 2001;46: 149-68.

Chapter 3: Enhancement of Viral Vector Delivery with Bacterial Collagenase

Portions of the chapter have been taken from:

McKee, T. D.*, Grandi, P.*, **Mok, W.***, Alexandrakis, G., Insin, N., Zimmer, J. P., Bawendi, M. G., Boucher, Y., Breakefield, X. O., and Jain, R. K., "Degradation of fibrillar collagen in a human melanoma xenograft improves the efficacy of an oncolytic herpes simplex virus vector." *Cancer Research, 66:* 2509-2513, 2006. ***authors contributed equally**

Introduction

Oncolytic vectors, mutant viruses that replicate preferentially in tumor cells, have shown promise in various preclinical tumor models (1, 2). Oncolytic viral therapy employs a novel method of tumor destruction mediated by viral replication and selective lysis of cancer cells (3, 4). The creation of more virus by infected tumor cells and resultant infectious spread improves over passive forms of therapeutic delivery (5, 6). Early phase human trials of G207, an oncolytic herpes simplex virus (HSV) vector, for treatment of recurrent malignant glioblastomas have demonstrated both safety and efficacy (7). However, the inability to efficiently propagate and infect cells distant from the injection site limits the capacity of oncolytic viruses to achieve consistent therapeutic responses (8). In this study, we show that fibrillar collagen, the major barrier to macromolecular transport in the tumor interstitium (9-11), also limits viral distribution within tumors. Direct degradation of the fibrillar collagen network improves viral distribution, leading to improved oncolytic viral therapy.

Materials and Methods

Viral vectors

The HSV-1 recombinant viruses used in this study were the replication defective mutant Gal4 (ICP4$^-$, *lacZ*$^+$; from Neal DeLuca, University of Pittsburgh (12)) and MGH2 (ICP6$^-$, γ34.5$^-$, eGFP$^+$; from E. Antonio Chiocca and Yoshi Saeki, The Ohio State University (13)). MGH2 is a replication conditional virus attenuated by the deletion of two

nonessential viral gene, ICP6 and γ34.5 (14). Virus replication is impaired in non-dividing cells but not tumor cells.

Gal4 and MGH2 stocks were propagated in E5 and E26 cells (from Neal DeLuca (15)), respectively, which supply the HSV-1 ICP4 protein (E5) or HSV ICP4 and ICP27 proteins (E26) *in trans*. To obtain GFP-labelled HSV particles, E5 and E26 cells were transfected with a plasmid encoding the fusion protein VP16-GFP (pVP16-GFP (16)) and infected with Gal4 and MGH2, respectively. After purification and concentration the titer of each virus preparation was quantified by counting *lacZ*-positive cells for Gal4 and GFP-positive cells for MGH2.

Dorsal skinfold window preparation

Human melanoma Mu89 cells were grown in dorsal skinfold chambers in SCID mice as described previously (9). All animal experiments were done with the approval of the Institutional Animal Care and Use Committee.

Injection and imaging of labeled vectors and tracers

For dorsal chamber tumor studies, HSV vectors labeled with VP16-GFP were mixed with either 0.2 μg/μl bacterial collagenase (Sigma, C0773, St Louis, MO) or PBS, to a final titer of $1x10^6$ t.u./μl. For microsphere experiments, quantum dot (QD)-encoded silica microspheres were synthesized according to a previously developed procedure (17). For all injections, 1 μl of solution was infused into the tumor at constant pressure (~1 □l/10 min) using a glass micropipette connected to a syringe pump. Images were obtained using a custom-built multiphoton laser scanning microscope (18) using a 20X/0.5NA objective

lens. Excitation was at 880 nm, with simultaneous detection of SHG (9) via a 435DF30 emission filter, and GFP via a high-pass 475 dichroic and a 525DF100 emission filter. Cascade Blue dextran was visualized by exciting at 780 nm and imaging the same region (for Cascade Blue dextran and GFP), followed by image registration. Microspheres (containing 642 nm maximum emission QDs) were imaged with a 610DF70 emission filter. Three dimensional image stacks containing 20 images of 5 μm thickness were obtained wherever fluorescence intensity from the injected particles was detected. A maximum intensity z-projection of each colored stack generated a 2D image. Images of consecutive adjacent regions in the x and y directions were combined into a montage, generating a single image of the entire injection site.

Image analysis

The pixel intensities of collagen (red pixels) and injected particles (viral vectors, green pixels; dextran, blue pixels) were spatially compared along lines drawn perpendicular to the periphery of virus containing regions. Analysis was performed in 5 distinct image stacks and at different depths, for a total of 20 lines measured within each tumor. The mean pixel intensities were plotted as a function of the relative distance from the observed interface with fibrillar collagen. All lines were registered such that the largest change in SHG intensity was maintained at the origin of the graph.

For quantification of viral vector distribution following injection, the entire area of viral distribution was outlined on the images. The border of the viral focus was determined as the location at which the intensity dropped to 10% of the mean intensity at the center of

injection. The calculation of the area was performed with imaging software (ImageJ, U. S. National Institutes of Health, Bethesda, MD, http://rsb.info.nih.gov/ij/).

Flank tumor growth delay

Mu89 cells were implanted subcutaneously in the flank of SCID mice and allowed to reach 100 mm^3 average volume. Mice were then randomized into 4 groups (6-7 animals per group) and given 10 µl intratumoral injections of either PBS; 1.0 µg collagenase; $1x10^6$ t.u. MGH2; or a mixture $1x10^6$ t.u. MGH2 and 1.0 µg collagenase. A second injection was performed two days later. Tumor volume was measured every 2-3 days and calculated as volume = $\pi AB^2/6$, where A and B are maximum and minimum diameters, respectively. Mice died from natural progression of disease or were euthanized when (a) tumor mass exceeded a size of 2,000 mm^3 or (b) premorbid behavior was noted. For tumors failing to reach ten times initial volume due to morbidity, the time to last measurement substituted as a conservative approximation of growth.

Metastasis assay

Tumors were grown subcutaneously in the leg of SCID mice. At a size of ~100 mm^3 they were treated with an intratumor injection with either 10 µl of PBS or 10 µl of PBS with 1.0 µg collagenase, followed by a similar injection two days later. Tumors were allowed to grow to 500 mm^3, at which point the tumor-bearing leg was amputated. Any bleeding was controlled and the wound closed with wound clips. Six weeks following primary tumor resection, the mice was euthanized by an intraperitoneal injection of sodium

pentobarbital (200 mg/kg). A full gross autopsy was performed to locate visible metastatic nodules and the lungs were examined histologically for micrometastases.

Immunohistochemistry protocol for herpes simplex virus

1. Dry slides overnight at RT
2. Incubate in ice cold acetone at -20°C for 10 minutes
3. Wash with PBS 3x for 3 minutes
4. Block for 1 hr at RT with 10% normal goat serums, 1% BSA, 0.1% triton solution
5. Incubate with primary antibody (polyclonal rabbit anti-HSV type I, Dako, Glostrup, Denmark) at a dilution of 1:100 overnight at 4°C
6. Wash with PBS 3x for 3 minutes
7. Incubate with secondary antibody (Cy3 anti-rabbit) at a dilution of 1:200, 30 min RT
8. Wash with PBS 3x for 3 minutes
9. Mount sections with Vectashield mounting media with DAPI (Vector Laboratories, Burlingame, CA)

Statistical analysis

Data are expressed as mean ± SEM. Statistical significance between groups was determined by an unpaired Student t-test. Statistical analysis was performed using StatView 4.51 software (SAS Institute, Inc., Cary, NC). Differences were considered statistically significant for $P < 0.05$.

Results

Distribution of virion particles is hindered by collagen rich regions

To quantify virus distribution, one microliter containing $1x10^6$ viral transducing units (t.u.) of VP16-GFP labeled non-replicative HSV-1 virions (Gal4) was directly injected into Mu89 human melanomas grown in dorsal skin windows in SCID mice. *In vivo* multiphoton imaging of viral particles was performed approximately 30 minutes following injection with simultaneous second harmonic generation (SHG) imaging of fibrillar collagen. Viral particles distributed primarily within collagen-free areas of the tumor, with limited penetration into collagen-rich regions (Fig. 3.1A). To quantify viral penetration, pixel counts of collagen (SHG) and virus (GFP) were measured along lines perpendicular to the periphery of virus containing regions (one example line is shown in Fig. 3.1A). Averaging over 20 lines per injection revealed an inverse correlation between collagen and viral particles, such that an increase in the amount of fibrillar collagen present corresponded to a sharp decrease in virus signal (Fig. 3.1B). While collagen is known to hinder macromolecular transport (10, 11), nearly complete exclusion to this extent has not been previously observed. To directly compare viral distribution with another macromolecular tracer, Cascade Blue-conjugated $2x10^6$ molecular weight dextran tracer molecules ($R_H \sim 20$ nm) were co-injected with HSV vectors. Whereas the dextran penetrated into collagen rich regions, viral particles were excluded (Fig. 3.1A,B). In the collagen containing regions, the mean dextran intensity is significantly greater than the mean virus intensity when both are normalized to the maximum signal from each channel ($P < 0.001$). To further clarify the role of particle size in collagen exclusion,

quantum dot-loaded microspheres similar in size to HSV particles (~ 150 nm diameter) were directly injected into Mu89 tumors. As with HSV particles, these microspheres were excluded from collagen rich tumor areas (Fig. 3.1E). The microsphere distribution area was similar to that of HSV vectors (Fig. 3.1D).

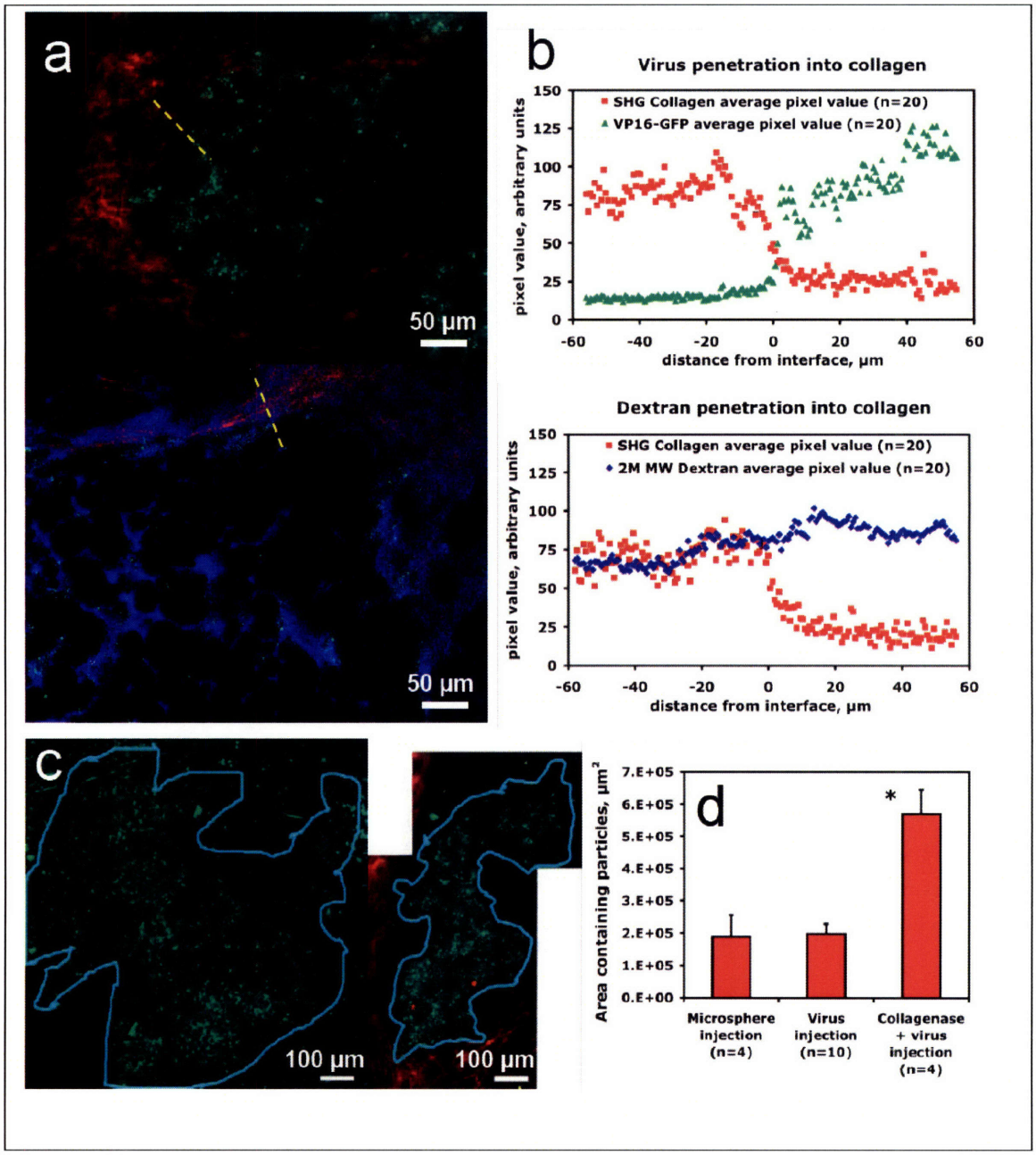

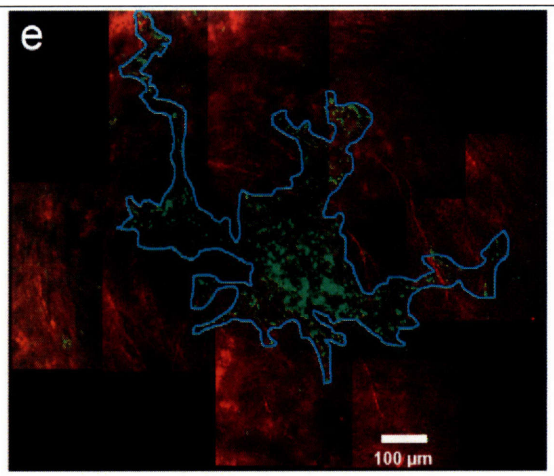

Figure 3.1. Viral vector distribution following intratumoral injection. (A) Multiphoton images of Mu89 melanomas 30 minutes after intratumoral injection of VP16-GFP labeled Gal4 vectors (green), either alone (upper image) or with Cascade blue-conjugated dextran (blue, lower image). Second harmonic generation (SHG) signal denotes fibrillar collagen (red pseudocolor). HSV vectors localized in extracellular spaces around individual tumor cells and were excluded by areas of intense SHG signal. In contrast, the smaller dextran tracer penetrated regions rich in fibrillar collagen. (B) Relative localization of collagen and injected particles determined by pixel analysis. Spatial comparison of pixel intensities was performed for collagen (red pixels) and either viral particles (green pixels; upper plot) or dextran (blue pixels; lower plot). Analysis was performed along lines drawn perpendicular to the border of SHG signal, and mean values plotted. A representative image and line are shown for each case (A, yellow lines). Collagen and viral localization in the tumor are anti-correlative. (C) Multiphoton images of viral vector distribution following co-injection with collagenase (left) compared with injection of virus alone (right). Each image is a montage of several multiphoton images. The area of distribution is outlined in blue in

each case. (D) Comparison of the area of viral vector and microsphere distribution following intratumoral injection. Areas measured from a maximum intensity projection of 10 images taken ~30 minutes following injection. Collagenase and virus co-injection resulted in a nearly 3-fold increase in the area of viral distribution compared with microspheres and HSV particles alone ($P < 0.05$). (E) Multiphoton images of microsphere distribution following intratumor injection. Microspheres shown in green and SHG in red pseudocolor.

Disruption of the collagen network improves virus distribution and gene expression

To test whether disruption of collagen could improve viral penetration into tumors, viral vectors were co-injected with bacterial collagenase (0.2 μg/μl). Collagenase increased the area of viral distribution by nearly 3-fold compared to control injections (Fig. 3.1D). Rather than distributing into restricted regions bounded by fibrillar collagen, vectors spread more uniformly from the injection site upon collagenase treatment (Fig. 3.1C).

Collagenase enhances the efficacy of oncolytic viral therapy

The oncolytic virus MGH2 has the same backbone as G207 (14), but carries the GFP reporter gene instead of *lacZ*. MGH2 replicates in Mu89 melanoma cells in culture, resulting in GFP expression and cell lysis within 24-48 hours. $1x10^6$ t.u. of MGH2 were injected into Mu89 tumors as before. Low resolution fluorescence microscopy one day following injection showed that the area of infection was localized to only a small proportion (~15%) of the entire tumor mass, corresponding to the site of injection (Fig.

3.2A middle). Even 11 days following the initial injection of MGH2, viral vectors could not penetrate sufficiently to infect the entire tumor mass (Fig. 3.2A bottom). No significant treatment response was observed in any of the tumors injected with MGH2 alone or with bacterial collagenase alone (Fig. 3.2A,C bottom).

To confirm that collagen was the cause of this limited tumor cell infection, high resolution multiphoton imaging of viral vectors, transduced cells and fibrillar collagen was also performed (Fig. 3.3). Imaging of the GFP-labeled MGH2 particles immediately after injection showed that, as before, virus spread is limited by fibrillar collagen (Fig. 3.3 left). Imaging of infected tumors cells (which express large amounts of GFP) three days later shows that the area of infection corresponds to the initial area of virus distribution and is surrounded by fibrillar collagen (Fig. 3.3 middle). It appears that virus was not able to diffuse and infect cells beyond the initial injection volume. At 8 days post-injection, GFP expression is severely diminished as the initially infected cells have died and neighboring cells beyond the collagen have not been infected (Fig. 3.3 right).

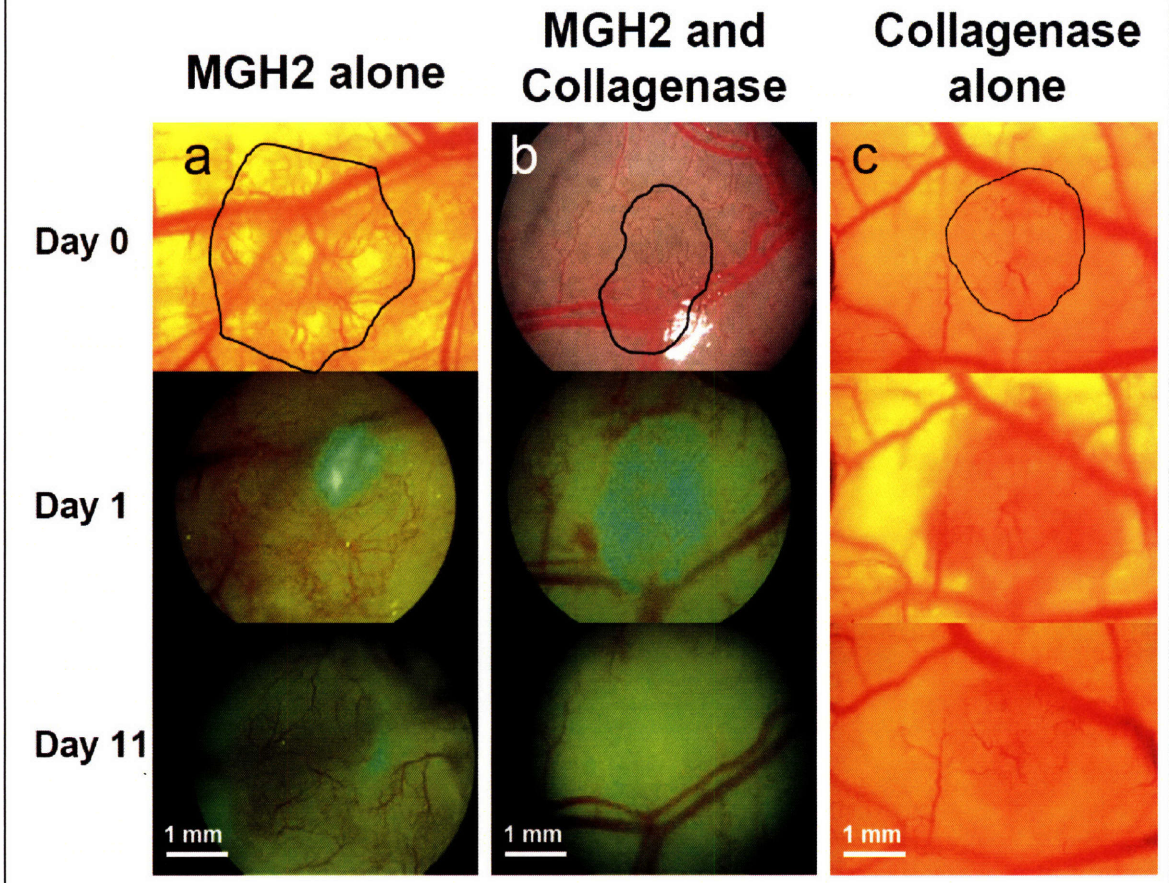

Figure 3.2. Effect of collagenase on oncolytic viral therapy. Low resolution microscopic images of dorsal chamber Mu89 melanomas treated with the oncolytic vector MGH2 in combination with PBS (A) or MGH2 in combination with collagenase (B). Collagenase treatment alone is shown for comparison (C). N=4 for all three treatment groups. Representative brightfield images of tumors prior to injection (tumors outlined in black, top panels). Representative fluorescent microscopic images of tumors 1 day (middle panels) and 11 days (bottom panels) after injection. Infection of tumor cells was detected by expression of the reporter gene GFP (encoded by the virus). Co-injection of MGH2 and collagenase resulted in a greater distribution of infected cells (B, middle panel), relative to injection of MGH2 alone (A, middle panel). At 11 days, regression of

the tumor (as evidenced by absence of tumor vasculature) was achieved with MGH2 and collagenase co-injection (B, bottom panel), while no significant change in volume was observed with MGH2 treatment alone (A, bottom panel). Collagenase treated tumors recover from any induced hemorrhage by day 11 (C, lower panel).

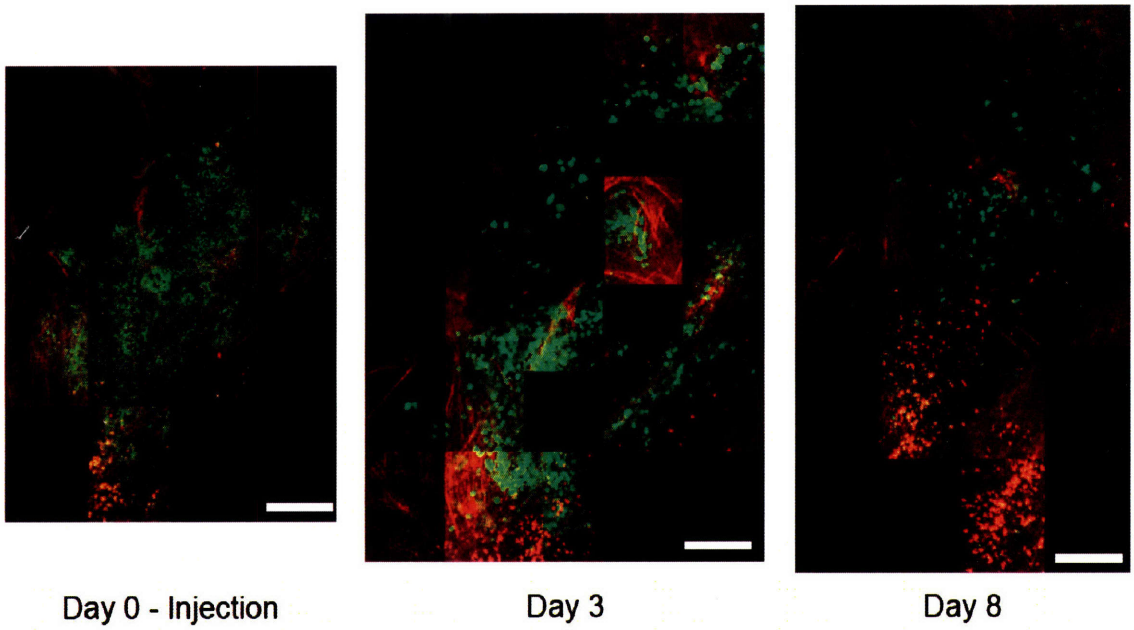

Figure 3.3. Viral distribution and tumor cell transduction following intratumor injection of oncolytic virus MGH2. Representative high resolution multiphoton images of injected MGH2 and infected tumor cells (both green) and second harmonic generation (red pseudocolor). *Left*: images taken of GFP-labeled MGH2 30 minutes following intratumor injection. *Middle and Right*: images taken of MGH2-infected cells (expressing GFP) 3 and 8 days following injection in the same tumor. Fibrillar collagen surrounds the injected virus and infected cells. Scale bar is 250 μm.

In contrast, when the same amount of oncolytic virus was co-injected with collagenase (0.2 μg/μl), the initial viral distribution was greater relative to virus alone, translating into an improved area of tumor cell infection (Fig. 3.2B middle). Therapeutic response was observed in all four collagenase co-treated tumors, with a significant decrease in tumor size in two cases (Fig. 2B bottom).

We then tested if the co-injection of collagenase and MGH2 would increase the therapeutic efficacy of MGH2 over longer time intervals. When Mu89 tumors growing in the flank of SCID mice reached 100 mm^3, they were injected intratumorally with either 1 μg collagenase, $1x10^6$ t.u. of MGH2, or both collagenase and MGH2, followed by similar injections two days later. Control tumors were injected with PBS alone. The time for the tumor to reach ten times the initial volume (mean ± SEM) was compared for each group (Fig. 4). Both collagenase treatment alone (19 ± 1 days) and MGH2 injection alone (27 ± 3 days) had no significant effect on tumor growth compared to PBS control (24 ± 3 days) ($P > 0.05$, both cases). With MGH2 treatment alone, one tumor showed marked regression, but recurred after 10 days. Co-injection of MGH2 with collagenase (50 ± 9 days) significantly delayed the growth of tumors compared to all other treatment groups ($P < 0.05$ for all cases). Two out of seven tumors failed to grow to 200 mm^3 even 60 days after treatment; a third experienced apparently complete regression, although it recurred 20 days later.

A

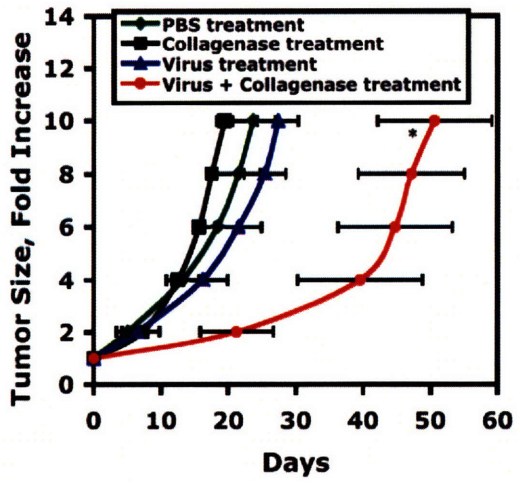

B

Treatment	Time to 10-fold increase in tumor size	Number of mice with significant tumor regression
PBS	23 ± 3 days	0/6
Collagenase	19 ± 1 days	0/6
MGH2	27 ± 3 days	1/6
MGH2 and Collagenase	50 ± 8 days	3/7

Figure 3.4. Effect of collagenase on MGH2-induced tumor growth delay. Tumors were grown subcutaneously in the hind flank of SCID mice. When tumors reached ~100 mm^3, animals were divided into four groups (n = 6-7) and treated twice (day 0 and day 2) with 10 µl of PBS (green), collagenase (0.1 µg/µl) (black), MGH2 ($1x10^6$ t.u.) in PBS (blue), or MGH2 ($1x10^6$ t.u.) and collagenase (0.1 µg/µl) in PBS (red). (A) Tumor volumes were measured every 2-3 days and the time to reach a given volume was expressed as mean ± SEM for each group. (B) The time to reach ten times the initial volume was compared. There was no significant difference between PBS (23 ± 3 days) and either collagenase treatment alone (19 ± 1 days) or MGH2 alone (27 ± 3 days) ($P > 0.05$ for both cases). However, MGH2 and collagenase co-treatment induced a significant tumor growth delay (50 ± 8 days) relative to all other groups ($P < 0.05$ for all cases).

Improved efficacy is due to initial improved distribution of viral particles

To investigate the mechanism of improved efficacy, tumors were treated as before with MGH2, either alone or with collagenase, and analyzed two days after the second

injection. Tissue sections were stained for structural virion proteins, counterstained for nuclei (DAPI), and imaged for GFP expression using confocal microscopy to determine viral distribution. As expected, HSV antigen was present within and surrounding cells expressing GFP. In MGH2-treated tumors, virion particles and infected cells distributed in a localized fashion reminiscient of the needle track (Fig. 5A). In contrast, for MGH2 and collagenase treatment, a diffuse distribution of infected cells was observed throughout the entire tumor section, spanning an area of up to 3 x 7 mm (Fig. 5B). Later timepoints showed continued viral spread, but only within collagen free areas.

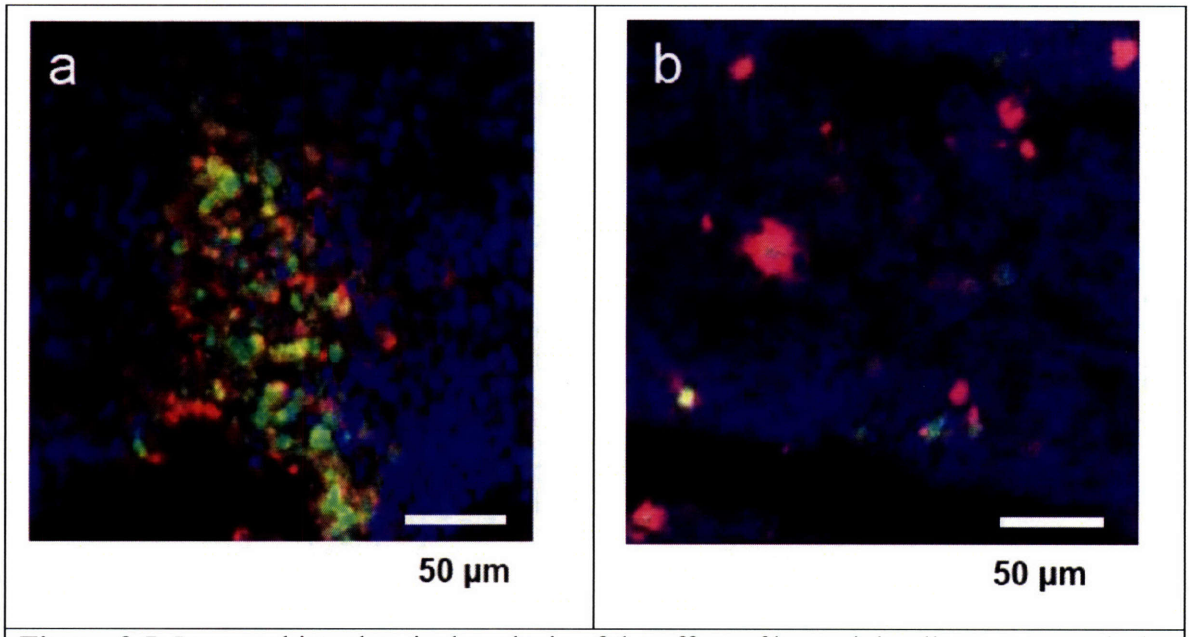

Figure 3.5. Immunohistochemical analysis of the effect of bacterial collagenase on viral infection. Representative tissue sections of subcutaneous Mu89 tumors two days following injection with either (A) MGH2 alone or (B) MGH2 and collagenase were labeled with anti-HSV antibodies. GFP expression from MGH2-infected cells (green), HSV proteins detected with Cy3-conjugated secondary antibodies (red) and nuclear stain DAPI (blue) are shown.

Bacterial collagenase does not affect metastatic behavior

Matrix modification has long been linked to tumor cell invasion and metastasis. Thus, in order to assess if improving the efficacy of oncolytic viruses by collagen degradation is a viable technique for the treatment of patients, we performed a metastasis assay. Mu89 tumors were grown subcutaneously in the leg of SCID mice and treated with collagenase as before. Following tumor growth to 5 times the initial size, the primary tumor was resected. An autopsy was performed 6 weeks later to identify metastatic nodules. There was no increase in metastasis observed with collagenase treatment (Table 3.1). Due to the low incidence of metastasis in this study, the assay was repeated for two other tumors: human soft tissue sarcoma HSTS26T and spontaneous murine osteosarcoma PO107. In both cases no lymph node and lung metastasis was observed in either treatment group. Thus, it appears that bacterial collagenase treatment at this concentration does not enhance metastatic behavior.

Table 3.1. Effect of bacterial collagenase on lymph node and lung metastasis

Treatment	No. of mice[a]	No. of animals with lymph node metastasis[b]	No. of animals with lung metastasis
PBS	4	1/4	0/4
Bacterial Collagenase	4	1/4	0/4

[a] in both treatment groups, primary tumor regrowth was occurred in one animal
[b] in both treatment groups, lymph node metastasis was observed in the animal in which primary tumor regrowth occurred

Discussion

The development of strategies to improve both the initial vector distribution within tumors and the ability of these vectors to propagate through the entire tumor mass is critical to the success of oncolytic viral therapy (2). Previous reports show that protease pretreatment can increase the therapeutic efficacy of a non-replicative viral vector (19). However, the mechanism of improved efficacy was undefined due to the use of nonspecific digestive enzymes – normally used to dissociate tissues – which degrade multiple extracellular matrix components. Thus, we wished to determine whether fibrillar collagen – previously shown to be a major barrier to macromolecular diffusion in tumors (10, 11) – is the matrix component which limits viral distribution in certain tumors.

Our results demonstrate the important role that fibrillar collagen can play in regulating the initial distribution of viral vectors in certain fibrous tumors. Whereas the smaller tracer particles distributed relatively uniformly within the tumor, the vast majority of larger HSV virions were located only in collagen-poor areas. Furthermore, silica microspheres similar in size to viral particles – but lacking their ability to bind to cell and matrix proteins – were excluded from collagen. This suggests that the effective pore size cutoff of the collagen network is smaller than the size of these viral particles. This may have a significant impact since many tumors in humans show extensive stromal infiltration with extracellular matrix and collagen deposition (20).

Fibrillar collagen is also important in the propagation of oncolytic viral vectors through the tumor. Oncolytic vectors are thought to overcome some of the delivery issues faced by non-replicating viral vectors through their ability to propagate on site in tumors

(thereby amplifying the input dose) and spread from tumor cell to tumor cell. We found that the collagen network, in addition to restricting the initial distribution, limited the maximal spread of MGH2 infection within the tumor. Tumor cell infection remained confined to a small area and the tumor continued to grow. Co-injection of MGH2 with collagenase resulted in a broad, uniform distribution of viral particles and infected cells, with substantial tumor regression and enhanced efficacy. This dispersed distribution of virus can improve therapeutic outcome in several ways: 1) the broad initial virion distribution improves the chance that viral vectors can penetrate all regions of the tumor; 2) the occurrence of multiple infections of the same tumor cell decreases, while the number of distinct tumor cell infections increases; and 3) once the virus replicates and lyses the cell it has infected, it has access to a greater number of previously uninfected neighboring cells. All together, these processes can lead to increased oncolytic activity, as shown schematically in Fig. 3.6.

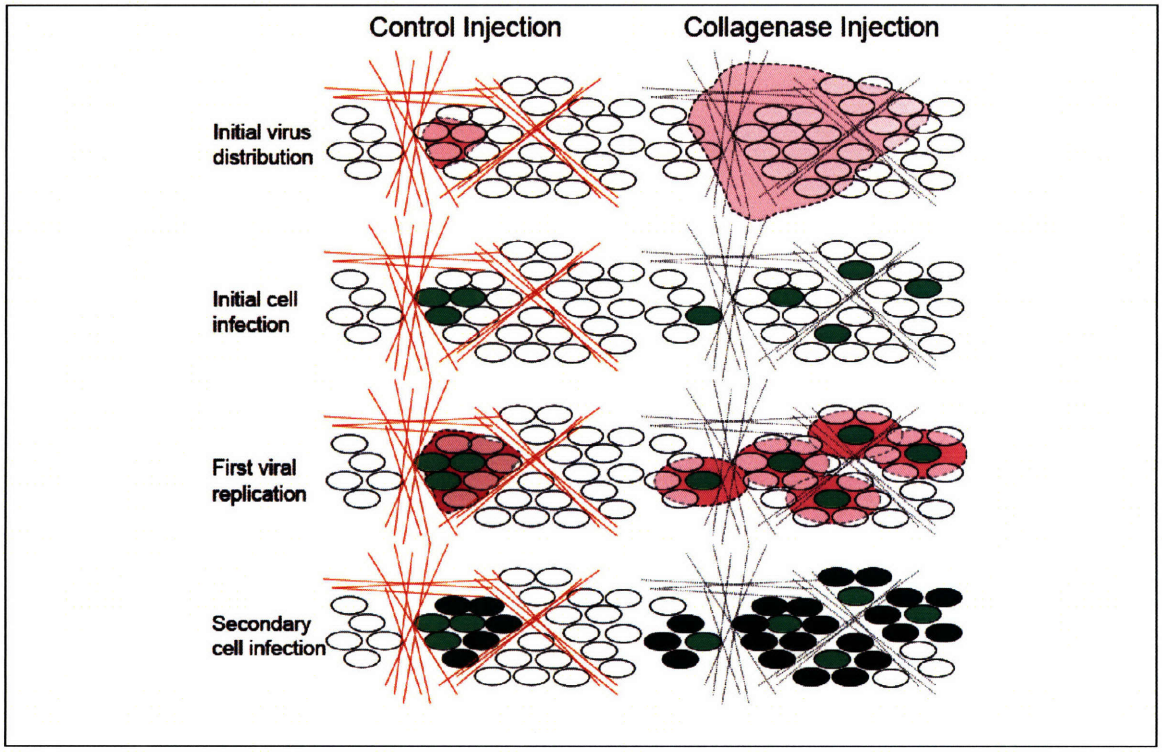

Figure 3.6. Schematic model of improvement in oncolytic viral distribution and tumor cell infection with collagenase treatment. Following direct intratumor injection, viral spread (pink area) is limited by fibrillar collagen (red lines) and results in a cluster of infected cells (light green). The collagen network also restricts the distribution of subsequent viral progeny and tumor cell infection beyond the initial injection site is not achieved. In contrast, co-injection of virus with collagenase results in a more diffuse distribution of viral particles and a greater number of initially infected cells (light green). Viral particles released by these cells have greater access to neighboring uninfected cells. This process results in more widespread secondary infection (dark green) and ultimately greater therapeutic efficacy.

Researchers have developed other methods to try to overcome the limited distribution of oncolytic vectors in tumors (21). Some use multiple injections, either on successive days or with fractionation of the dose at multiple sites (22). However, in the absence of extracellular matrix modification, viral distribution at each individual injection site would still be limited by collagen. Indeed, a phase II trial with an oncolytic adenoviral vector showed limited improvement in efficacy even with daily injections that included fractionation (23). Alternatively, combination therapy with either radiation or chemotherapy is often employed to improve oncolytic activity (24). Collagenase treatment is compatible with combination therapy and could further improve efficacy. This may be a complementary therapy for combination with radiation, which can induce fibrosis and lead to an increase in interstitial collagen content (25).

We noted that intratumoral haemorrhage occurred in many tumors treated with collagenase. While bleeding from collagenase treatment alone did not affect tumor growth, this phenomenon demonstrates the complex interactions between the extracellular matrix and cells within the tumor, including both tumor and host endothelial cells. We observed no increase in metastasis when tumors were treated with bacterial collagenase (Table 3.1) and a previous study has shown that direct injections of collagenase/dispase and trypsin did not affect metastasis (19). Despite these encouraging results, it is still possible that collagenases may have a negative effect on tumor cell invasion and metastasis, perhaps at different doses. The development of this matrix-modulating technique for clinical applications may require the use of specific matrix proteases, such as MMP-8, which degrades collagen and has been shown to decrease metastasis (26).

In conclusion, we determined that even with the on-site generation of viral particles provided by the replication-competent nature of an oncolytic HSV vector, fibrillar collagen still prevents viral spread throughout the tumor in a melanoma model. Collagen network disruption increases initial vector distribution and subsequent propagation through the tumor mass, significantly improving therapeutic outcome. This result has implications for other viral particles, gene delivery strategies and nano-technology based delivery systems, as all face the problem of insufficient delivery to the target cells. Furthermore, any method decreasing tumor collagen content may have similar effects. These findings suggest ways to increase the potency of gene therapy in certain types of cancer and other diseases.

References

1. Chiocca, E. A. Oncolytic viruses. Nat Rev Cancer, *2:* 938-950, 2002.
2. Everts, B. and van der Poel, H. G. Replication-selective oncolytic viruses in the treatment of cancer. Cancer Gene Ther, *12:* 141-161, 2005.
3. Kirn, D., Martuza, R. L., and Zwiebel, J. Replication-selective virotherapy for cancer: Biological principles, risk management and future directions. Nat Med, *7:* 781-787, 2001.
4. Martuza, R. L., Malick, A., Markert, J. M., Ruffner, K. L., and Coen, D. M. Experimental therapy of human glioma by means of a genetically engineered virus mutant. Science, *252:* 854-856, 1991.
5. Ichikawa, T. and Chiocca, E. A. Comparative analyses of transgene delivery and expression in tumors inoculated with a replication-conditional or -defective viral vector. Cancer Res, *61:* 5336-5339, 2001.
6. Lee, C. T., Park, K. H., Yanagisawa, K., Adachi, Y., Ohm, J. E., Nadaf, S., Dikov, M. M., Curiel, D. T., and Carbone, D. P. Combination therapy with conditionally replicating adenovirus and replication defective adenovirus. Cancer Res, *64:* 6660-6665, 2004.
7. Markert, J. M., Parker, J. N., Gillespie, G. Y., and Whitley, R. J. Genetically engineered human herpes simplex virus in the treatment of brain tumours. Herpes, *8:* 17-22, 2001.
8. Harrison, D., Sauthoff, H., Heitner, S., Jagirdar, J., Rom, W. N., and Hay, J. G. Wild-type adenovirus decreases tumor xenograft growth, but despite viral persistence complete tumor responses are rarely achieved--deletion of the viral E1b-19-kD gene increases the viral oncolytic effect. Hum Gene Ther, *12:* 1323-1332, 2001.
9. Brown, E., McKee, T., diTomaso, E., Pluen, A., Seed, B., Boucher, Y., and Jain, R. K. Dynamic imaging of collagen and its modulation in tumors in vivo using second-harmonic generation. Nat Med, *9:* 796-800, 2003.
10. Netti, P. A., Berk, D. A., Swartz, M. A., Grodzinsky, A. J., and Jain, R. K. Role of extracellular matrix assembly in interstitial transport in solid tumors. Cancer Res, *60:* 2497-2503, 2000.
11. Pluen, A., Boucher, Y., Ramanujan, S., McKee, T. D., Gohongi, T., di Tomaso, E., Brown, E. B., Izumi, Y., Campbell, R. B., Berk, D. A., and Jain, R. K. Role of tumor-host interactions in interstitial diffusion of macromolecules: cranial vs. subcutaneous tumors. Proc Natl Acad Sci U S A, *98:* 4628-4633, 2001.
12. Chiocca, E. A., Choi, B. B., Cai, W. Z., DeLuca, N. A., Schaffer, P. A., DiFiglia, M., Breakefield, X. O., and Martuza, R. L. Transfer and expression of the lacZ gene in rat brain neurons mediated by herpes simplex virus mutants. New Biol, *2:* 739-746, 1990.
13. Tyminski, E., Leroy, S., Terada, K., Finkelstein, D. M., Hyatt, J. L., Danks, M. K., Potter, P. M., Saeki, Y., and Chiocca, E. A. Brain tumor oncolysis with replication-conditional herpes simplex virus type 1 expressing the prodrug-activating genes, CYP2B1 and secreted human intestinal carboxylesterase, in combination with cyclophosphamide and irinotecan. Cancer Res, *65:* 6850-6857, 2005.

14. Kramm, C. M., Chase, M., Herrlinger, U., Jacobs, A., Pechan, P. A., Rainov, N. G., Sena-Esteves, M., Aghi, M., Barnett, F. H., Chiocca, E. A., and Breakefield, X. O. Therapeutic efficiency and safety of a second-generation replication-conditional HSV1 vector for brain tumor gene therapy. Hum Gene Ther, *8:* 2057-2068, 1997.
15. Samaniego, L. A., Webb, A. L., and DeLuca, N. A. Functional interactions between herpes simplex virus immediate-early proteins during infection: gene expression as a consequence of ICP27 and different domains of ICP4. J Virol, *69:* 5705-5715, 1995.
16. Bearer, E. L., Breakefield, X. O., Schuback, D., Reese, T. S., and LaVail, J. H. Retrograde axonal transport of herpes simplex virus: evidence for a single mechanism and a role for tegument. Proc Natl Acad Sci U S A, *97:* 8146-8150, 2000.
17. Chan, Y., Zimmer, J. P., Stroh, M., Steckel, J. S., Jain, R. K., and Bawendi, M. G. Incorporation of Luminescent Nanocrystals into Monodisperse Core-Shell Silica Microspheres. Advanced Materials, *16:* 2092-2097, 2004.
18. Brown, E. B., Campbell, R. B., Tsuzuki, Y., Xu, L., Carmeliet, P., Fukumura, D., and Jain, R. K. In vivo measurement of gene expression, angiogenesis and physiological function in tumors using multiphoton laser scanning microscopy. Nat Med, *7:* 864-868, 2001.
19. Kuriyama, N., Kuriyama, H., Julin, C. M., Lamborn, K. R., and Israel, M. A. Protease pretreatment increases the efficacy of adenovirus-mediated gene therapy for the treatment of an experimental glioblastoma model. Cancer Res, *61:* 1805-1809, 2001.
20. Elenbaas, B. and Weinberg, R. A. Heterotypic signaling between epithelial tumor cells and fibroblasts in carcinoma formation. Exp Cell Res, *264:* 169-184, 2001.
21. Jia, W. and Zhou, Q. Viral vectors for cancer gene therapy: viral dissemination and tumor targeting. Curr Gene Ther, *5:* 133-142, 2005.
22. Currier, M. A., Adams, L. C., Mahller, Y. Y., and Cripe, T. P. Widespread intratumoral virus distribution with fractionated injection enables local control of large human rhabdomyosarcoma xenografts by oncolytic herpes simplex viruses. Cancer Gene Ther, *12:* 407-416, 2005.
23. Nemunaitis, J., Khuri, F., Ganly, I., Arseneau, J., Posner, M., Vokes, E., Kuhn, J., McCarty, T., Landers, S., Blackburn, A., Romel, L., Randlev, B., Kaye, S., and Kirn, D. Phase II trial of intratumoral administration of ONYX-015, a replication-selective adenovirus, in patients with refractory head and neck cancer. J Clin Oncol, *19:* 289-298, 2001.
24. Kim, S. H., Wong, R. J., Kooby, D. A., Carew, J. F., Adusumilli, P. S., Patel, S. G., Shah, J. P., and Fong, Y. Combination of mutated herpes simplex virus type 1 (G207 virus) with radiation for the treatment of squamous cell carcinoma of the head and neck. Eur J Cancer, *41:* 313-322, 2005.
25. Znati, C. A., Rosenstein, M., McKee, T. D., Brown, E., Turner, D., Bloomer, W. D., Watkins, S., Jain, R. K., and Boucher, Y. Irradiation reduces interstitial fluid transport and increases the collagen content in tumors. Clin Cancer Res, *9:* 5508-5513, 2003.

26. Montel, V., Kleeman, J., Agarwal, D., Spinella, D., Kawai, K., and Tarin, D. Altered metastatic behavior of human breast cancer cells after experimental manipulation of matrix metalloproteinase 8 gene expression. Cancer Res, *64:* 1687-1694, 2004.

Chapter 4: Degradation of Tumor Collagen with Recombinant Human Enzymes

Introduction

While the application of bacterial collagenase to degrade tumor collagen and improve the transport of therapeutics has been advanced as a proof of principle concept (1), moving this technique into the clinic will require the use of a human enzyme or an agent which can upregulate the expression of a such an enzyme in tumors. Our lab has previously worked with the peptide hormone relaxin, which is primarily produced during pregnancy to stimulate collagen remodeling in the reproductive tract, but has recently been found to have pleiotropic effects (2-4). We found that chronic relaxin treatment accelerated collagen turnover and increased diffusive transport (5). The mechanism by which relaxin modifies collagen is still unclear. It has been found in different systems to affect both collagen production (6-8) and degradation (9, 10). Relaxin most likely initiates a signaling cascade which reduces collagen deposition by fibroblast and upregulates collagenase expression or induces their activation. However, recent reports suggest that relaxin may enhance tumor cell invasiveness and metastasis (9, 11, 12), which would clearly limit its therapeutic potential. Alternative to this approach is to treat tumors with a human collagenase. This is the most direct extension of the matrix degradation method used in the bacterial collagenase study.

Catabolism of extracellular matrix components is generally carried out by members of the matrix metalloproteinase (MMP) family of enzymes. These endopeptidases cleave nearly all extracellular matrix components and are thought to be important in matrix remodeling during development as well as homeostasis (13, 14). Unsurprisingly, these enzymes have also been found to play a role in various diseases involving matrix modification, such as

arthritis, fibrosis and cancer metastasis (15, 16). Three soluble MMPs have been found to have the ability to cleave type I collagen: MMP-1, -8 and -13 (17-19). While all three enzymes cleave collagen at a single site into approximately ¼ and ¾-length fragments, their collagenase activity is most likely not identical. The activity of these three MMPs against fibrillar collagen type I has not been directly compared; however, although each enzyme exhibits activity against collagen types I, II and III, they vary in their relative rates of activity for these substrates (20-23). In addition to these three MMPs, one other enzyme has been found to be able to cleave collagen type I: cathepsin K. This enzyme is responsible for collagen degradation in osteoclasts during bone resorption (24, 25). In contrast to the MMPs, cathepsin K degrades collagen type I at multiple sites (26). In this study we directly compare these four collagenases using an *in vitro* collagen fiber degradation assay. We assess the ability of the most promising candidates to degrade collagen in tumors, enhance interstitial transport and improve the efficacy of a macromolecular therapeutic.

Materials and Methods

Dorsal skinfold chamber

All animal experiments were done with the approval of the Institutional Animal Care and Use Committee (MGH SRAC protocol 2004N000063). Human soft tissue sarcoma HSTS26T cells were grown in dorsal skinfold chambers in SCID mice as described previously (27). The entire preparation was done under anesthesia (100 mg ketamine hydrochloride/10 mg of xylazine per kg body weight intramuscularly) in aseptic conditions inside the animal colony. Briefly, the back of the mouse was shaved and hair

removed using hair removal cream. Two symmetrical titanium frames were stitched on to fix the extended double layer of dorsal skin between the frames. Roughly 15 mm diameter of skin was removed from one side, leaving the opposite side of the skin, striated muscle and subcutaneous tissue intact. The fascia was carefully removed and a cover glass was mounted into the frame. The animals were allowed to recover for at least one day prior to tumor implantation. Tumors were allowed to grow for at least two weeks prior to experimentation.

Enzymes

MMP-1 cDNA was purchased from ATCC. MMP-8 cDNA was a kind gift from David Tarin (University of California, San Diego). MMP-13 cDNA was a kind gift from Carlos Lopez Otin (University of Oviedo). Cathepsin K cDNA was purchased from Invitrogen (Carlsbad, CA). The cDNA for all full length enzymes were subcloned into the mammalian expression vector peak13 (kind gift from Brian Seed, Massachusetts General Hospital). HSTS26T cells were transiently transfected with each collagenase expression vector using Lipofectamine 2000 (Invitrogen, Carlsbad, CA) according to the manufacturer's protocol. Twelve hours following transfection, the cells were washed and incubated with serum free media. Twenty-four hour conditioned media was collected for the collagenase activity assay. Recombinant bacterial collagenase was purchased from Sigma (St. Louis, MO). Recombinant MMP-1 and -8 were purchased from Millipore (Billerica, MA).

Activation of enzymes

Conditioned media containing MMP-1, -8 and -13 expressed from HSTS26T cells were activated with p-aminophenylmercuric acetate (APMA, Sigma, St. Louis, MO). APMA was dissolved in DMSO at a stock concentration of 20 mM and used to activate MMPs at a final concentration of 2 mM. Samples were incubated at 37°C for 1 hr and western blot analysis proceeded immediately afterward.

Recombinant MMPs used for *in vivo* tumor superfusion were activated with trypsin. A 1:10 volume of 1 mg/ml trypsin (Worthington, Lakewood, NJ) was added to the sample and incubated at 37°C for 7 minutes. A 1:10 volume of 5 mg/ml soybean trypsin inhibitor (Worthington, Lakewood, NJ) was then added to the sample to inactivate the trypsin. Samples were used immediately in experiments. Bacterial collagenase did not require activation.

Collagenase activity assay

MMP activity was determined using an *in vitro* collagenolytic activity assay modified from the method of Johnson-Wint (28, 29). Briefly, type I collagen was purified from rat tail by solubilization with acetic acid and subsequently acetylated with [^{14}C] acetic anhydride. Fibrils were allowed to form from the radiolabeled collagen and were dried onto wells of a 96-well plate, forming a thin film. Conditioned media samples were added to wells and incubated at 37°C for 2.5 hours. The supernatants containing soluble radiolabeled collagen (from cleavage) were transferred to scintillation vials and counted in a Beckman model LS-3801 scintillation counter. Bacterial collagenase was used as a

control to cleave all the radiolabeled collagen in select wells. One unit of activity corresponds to degradation of 10% of the collagen in 2.5 hrs at 37°C.

Second harmonic generation imaging

Imaging of second harmonic generation (SHG) in dorsal chamber tumors was performed with a custom-built multiphoton laser scanning microscope (30) using a 20X/0.5NA objective lens. Excitation was at 880 nm and SHG was detected via a 435DF30 emission filter with a high pass 475 dichroic. Three dimensional image stacks were obtained of the top 130 μm from the surface of the tumor (27 images of 5 μm thickness). Six to ten image stacks were obtained to create a montage covering the entire tumor or a significant portion of it. The total SHG signal intensity in each stack was measured by image analysis (ImageJ) and the mean intensity for each individual tumor calculated.

Multiphoton fluorescence recovery after photobleaching

The diffusion coefficient of $2x10^6$ molecular weight dextran was measured in dorsal chamber tumors using multiphoton fluorescence recover after photobleaching (MPFRAP). A custom-built multiphoton microscope (30) was adapted for MPFRAP based on a previous design (31). One half microliter of FITC-labeled dextran (Sigma, St. Louis, MO) was injected at a concentration of 2 mg/ml at a depth of 200 μm below the surface of the tumor. Injections were performed using glass micropipettes that were pulled to obtain a 20 μm inner diameter tip (27). Injections were performed at nearly constant flow rate over 2-3 minutes.

MPFRAP was performed approximately 30 minutes after injection. The laser was set at 800 nm and a 40X/0.75 NA objective lens was used with a 525/100 filter between 405 and 605 high pass dichroics. The multiphoton laser was focused on locations in the extracellular space 40-70 μm below the surface of the tumor. During each bleach/recovery cycle, the sample was bleached with a 160 μs pulse train of light, followed by an ~40 ms recovery monitored in 40 μs time bins. The length of the bleach and the time bins for monitoring recovery were chosen to avoid significant error due to diffusion during these two time periods. Based on the analysis of Brown *et al.* (31), the systematic error in the detected fluorescence intensity due to diffusion during the bleach pulse and over the course of recovery is $\sim 1.05(\Delta t/\tau_D)$ where Δt is the length of the bleach pulse or monitoring time bin and τ_D is the time constant for diffusive recovery. The characteristic fluorescence recovery time of 2×10^6 molecular weight dextran *in vivo* was found to be ~10 ms. Thus, a bleaching pulse length of 160 μs is short enough to avoid significant diffusion during the bleach pulse (error of ~1.68%) and a monitoring time bin of 40 μs is short enough to accurately monitor the recovery (error of ~0.42%).

The monitoring power was chosen such that photobleaching did not occur. The bleaching power was chosen such that excitation saturation did not occur. Each bleach/recovery cycle was repeated 500 to 1000 times for a given spot/measurement. Approximately 10 to 20 measurements were taken for each individual tumor. Data acquisition typically lasted 2 hrs. The recovery curves were fit to the following equation, derived in Brown *et al.* (31), which gives the time-dependent detected fluorescence signal due to diffusion into the focal volume:

$$F(t) = F_0 \sum_{n=0}^{\infty} \frac{m^{3/2}(-\beta)^n}{n!} \frac{1}{(m+bn+(bnmt/\tau_D)} \frac{1}{\sqrt{m+bn+(bnmt/R\tau_D)}}.$$

$F(t)$ is the time-dependent fluorescence signal, F_0 is the prebleach equilibrium fluorescence signal, m is the number of photons required to generate a fluorescence photon, β is the bleach depth parameter, b is the number of photons absorbed in a bleaching event, t is the time, R is the square ratio of the $1/e^2$ beam dimensions (w_z^2/w_r^2) and τ_D is the characteristic radial diffusion time of the fluorophore, defined as $w_r^2/8D$, where D is the diffusion coefficient. The beam dimensions for for the objective lens at a wavelength of 840 nm was calculated theoretically, with $w_z = 1.837 \times 10^{-6}$ m and $w_r^2 = 3.221 \times 10^{-7}$ m.

Oncolytic virus

The oncolytic HSV-1 vector MGH2 (ICP6$^-$, γ34.5$^-$, eGFP$^+$) was obtained from E. Antonio Chiocca and Yoshi Saeki (The Ohio State University). MGH2 stocks were propagated in E11 cells (gift from Yoshi Saeki). Infected cells were pelleted, resuspended in 1 ml of HBSS and subjected to 3 freeze/thaw cycles in a dry ice/ethanol bath with 1 minute of vortexing in between. Lysed cells were spun down at 3500 rpm for 15 minutes. The supernatants were filtered through a cell strainer and a 0.45 μm syringe filter. The filtered supernatant was layered over 5 ml of 25% sucrose (in PBS) in a 38.5 ml centrifuge tube. This was topped off with HBSS and spun down at 20,000 rpm for 3 hours at 4°C. The supernatant was aspirated and the viral pellet was covered with 200 μl HBSS and incubated overnight at 4°C. The virus was resuspended the following day and stored at -80°C. The virus was titered using HSTS26T cells.

Flank tumor growth delay

HSTS26T tumors were implanted subcutaneously in the leg of SCID mice and allowed to reach 60 mm^3 average volume. Mice were then randomized into 3 groups (6-7 animals per group) and given 10 µl intratumoral injections of either 2.5 x 10^5 t.u. of MGH2 in trypsin/trypsin inhibitor solution; 2.5 x 10^5 t.u. of MGH2 with 1.0 µg activated recombinant MMP-1; or 2.5 x 10^5 t.u. of MGH2 with 1.0 µg activated recombinant MMP-8. A second similar injection was performed two days later. All injections were 15 µl total volume. Tumor volume was measured every 3-4 days and calculated as volume = $\pi AB^2/6$, where A and B are maximum and minimum diameters, respectively.

Results

Screening human collagenases

Several human enzymes have been identified in the literature as having the ability to cleave collagen type I based on *in vitro* assays: MMP-1, MMP-8, MMP-13 and cathepsin K. In order to assess which would be most promising for our specific application – degradation of fibrillar collagen in a solid tumor – we first directly compared each enzyme in an *in vitro* assay. Each enzyme was expressed in human soft tissue sarcoma HSTS26T cells and collected in the conditioned media. Expression was confirmed by western blot. Each enzyme was activated and then incubated with reconstituted collagen fibrils that had been [^{14}C] radiolabeled. The amount of degradation was assessed by measuring the amount of cleaved collagen in the supernatant after 2.5 hrs at 37°C. MMP-1 and MMP-8 showed significant collagenase activity relative to the control (Fig. 4.1). In

contrast, MMP-13 and cathepsin K showed no collagenase activity. Previous studies have shown that the collagenase activity of cathepsin K is highly pH-dependent, with maximal activity in slightly acidic conditions (25). Other studies have shown that the activity of cathepsin K is enhanced by the formation of a complex with chondroitin sulfate (32, 33). Therefore, the collagenase activity assays for cathepsin K were repeated at a range of pH (4.0 – 8.0), in the presence and absence of chondroiton sulfate and with various methods of activation. However, significant activity was not observed in any sample. Based on these findings, we moved forward with MMP-1 and -8 as potential collagen-degrading enzymes.

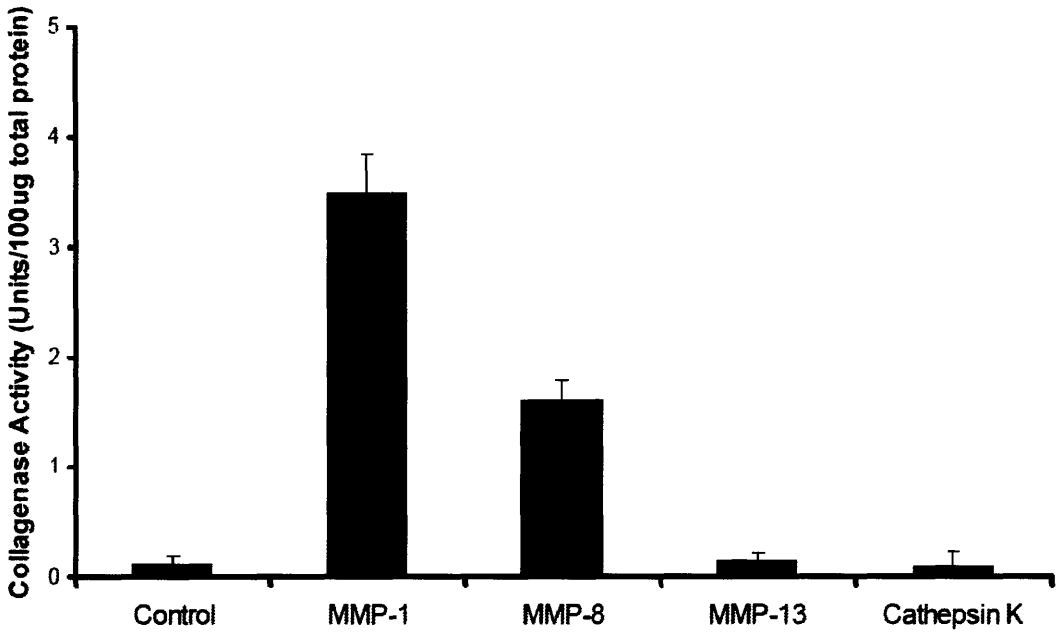

Figure 4.1. Collagenase activity of various human enzymes. Human collagenases were expressed in HSTS26T cells and collected in the conditioned media. Samples were activated with the appropriate agent and incubated with radiolabeled collagen fibrils. The amount of collagenase activity was assessed by measurement of cleaved molecules in the

supernatant. MMP-1 and -8 show significant collagenase activity ($P < 0.05$) while MMP-13 and cathepsin K showed no difference compared to the control. Mean values and standard errors shown.

Collagen degradation in vivo with MMP-1 and MMP-8

Next we sought to determine the extent of collagen degradation *in vivo*. Purified recombinant MMP-1 and MMP-8 were activated with trypsin and superfused on the surface of HSTS26T tumors grown orthotopically in the dorsal chamber of SCID mice. Fibrillar collagen I was monitored with multiphoton imaging of second harmonic generation (SHG). SHG signal emanates from a highly fibrillar subfraction of collagen has been found to correlate with total collagen content *in vivo* (5). Total SHG intensity in tumors was measured before treatment and 12, 36 and 84 hours after superfusion of MMPs (Fig. 4.2). Over a period of ~ 4 days, the fibrillar collagen content in untreated tumors did not significantly change. SHG intensity decreased significantly by 12 hours following MMP-1 superfusion but not MMP-8. The change in collagen content with MMP-1 was maintained at 84 hrs post-treatment.

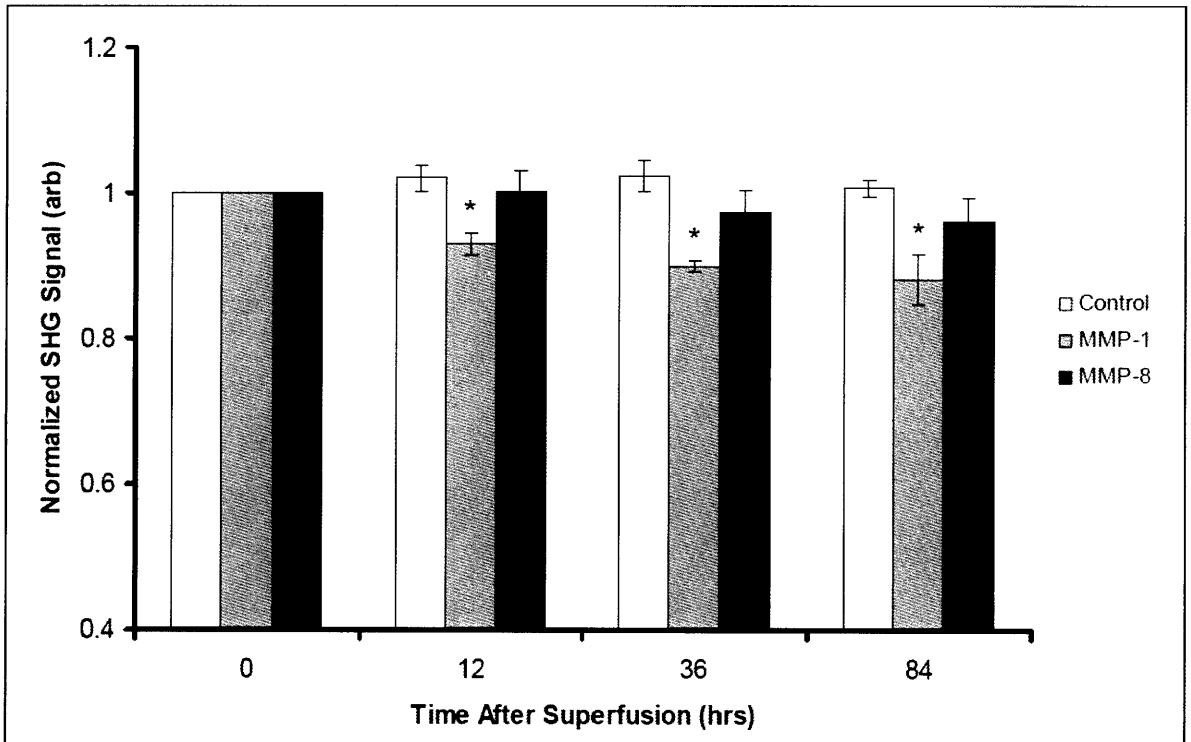

Figure 4.2. Effect of human collagenase superfusion on second harmonic generation intensity over a long time period. 10 μl of activated MMP-1 and -8 (0.1 μg/μl) were superfused on HSTS26T tumors grown in the dorsal skinfold chamber of SCID mice. SHG throughout the tumor was imaged at various time points before and after superfusion. Mean normalized intensities and standard errors are shown. At 12, 36 and 84 hours, MMP-1, but not MMP-8, induces a significant decrease relative to control tumors ($P < 0.05$).

Since the degradation of collagen with MMP-1 treatment has already occurred by 12 hours, we sought to examine the kinetics of this degradation by measuring collagen content during the first several hours following superfusion. Since the half life of MMPs in tumors is most likely on the order of hours, this is a relevant time scale for observation. The previous experiment was repeated, but SHG imaging was performed over the first 2

hours following MMP superfusion. The same region of the tumor was imaged every 5 minutes (Fig. 4.3). As expected, no change in collagen was observed in control tumors and with recombinant MMP-8 application. MMP-1 superfusion caused a small but significant change in collagen.

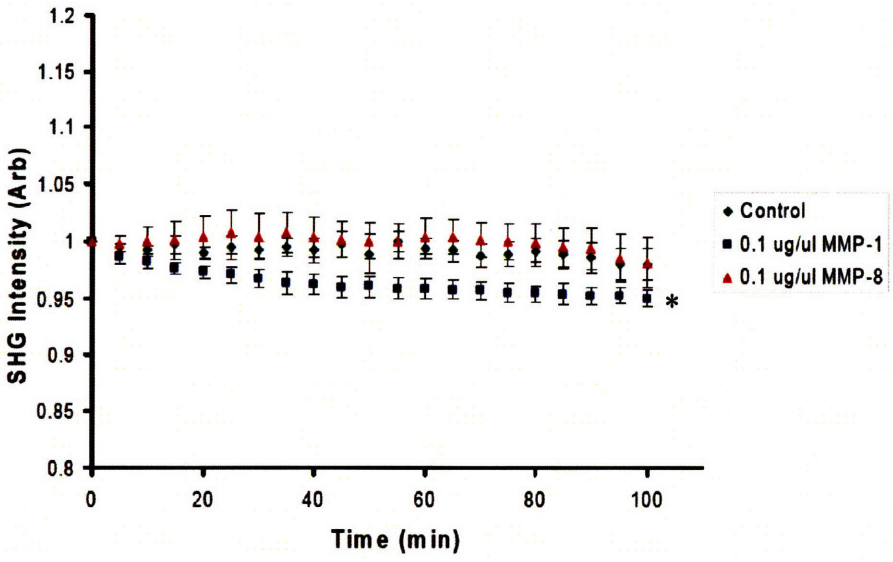

Figure 4.3. Effect of human collagenase superfusion on tumor second harmonic generation intensity over a short time period. 10 μl of active MMPs was superfused on HSTS26T tumors grown in the dorsal skinfold chamber of SCID mice. A 250 μm x 200 μm x 130 μm area of the tumor was imaged every 5 minutes for ~100 minutes and the SHG intensity in a maximum intensity z-projection was measured. The normalized mean intensities and standard errors are shown. At 100 minutes, MMP-1 results in a small but significant decrease in collagen relative to control ($P < 0.05$) while MMP-8 does not.

Bacterial collagenase had previously been shown to degrade collagen, improve diffusion and enhance the distribution and efficacy of an intratumorally injected therapeutic (5, 34-36). Thus, it serves as a reference for gauging the extent of collagen degradation necessary to improve the transport and efficacy of therapeutics. With this in mind we assessed the ability of bacterial collagenase to degrade collagen in an identical assay. A nearly equimolar amount of bacterial collagenase led to a significant decrease in collagen within 100 minutes (Fig. 4.4). The effect was significantly more dramatic than with MMP-1 and was dose dependent. We should note that while purified bacterial collagenase is relatively easy to obtain in large quantities, recombinant MMPs are much more difficult. For this reason testing the dose response of MMP-1 and -8 was not feasible.

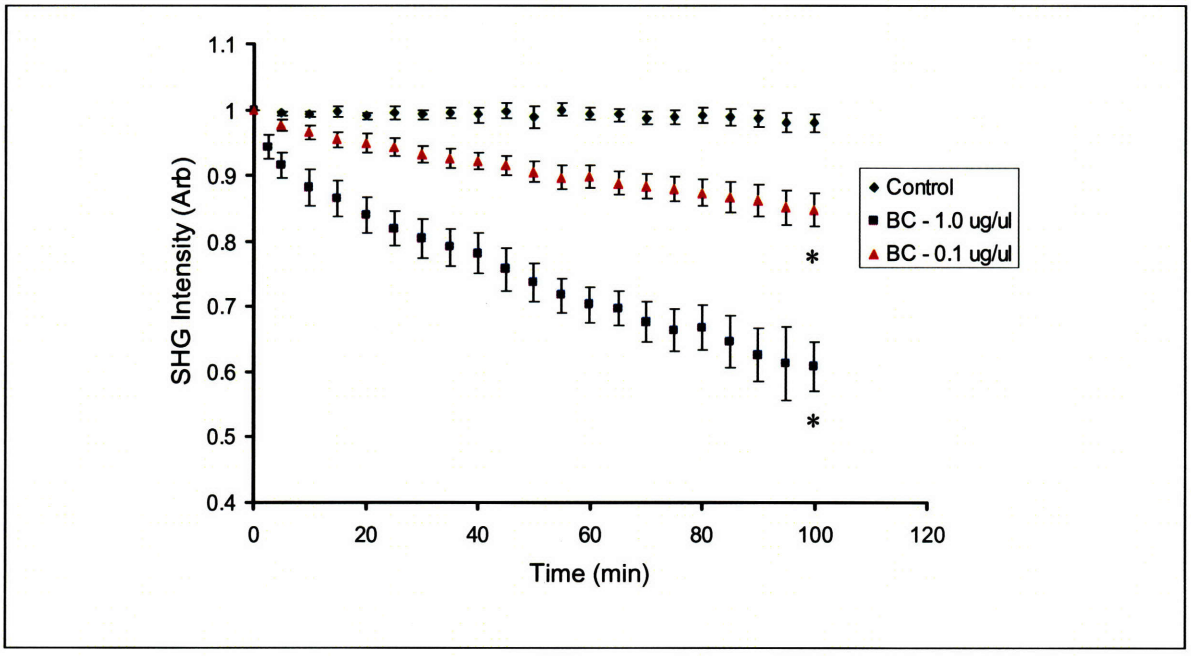

Figure 4.4. Effect of bacterial collagenase superfusion on tumor SHG intensity over a short time period. 10 μl of bacterial collagenase was superfused on HSTS26T tumors grown in the dorsal skinfold chamber of SCID mice. SHG signal was imaged as before. The normalized mean intensities and standard errors are shown. At 100 minutes, both concentrations of bacterial collagenase resulted in a significant decrease in collagen relative to control ($P < 0.05$ in both cases).

Effect of recombinant MMPs on interstitial diffusion

While theses result show that the effect of MMP-1 and MMP-8 on tumor collagen at this dose are subtle at best, the possibility exists that such subtle changes may lead to significant improvements in interstitial transport. Indeed, chronic relaxin treatment of tumors did not alter total SHG signal, but did alter the length of collagen fibers and consequently the diffusion of tracer particles (5). To determine what effect these recombinant MMPs have on tumor interstitial transport we measured the diffusion coefficient of $1x10^6$ molecular weight dextran with multiphoton fluorescence recovery after photobleaching (MPFRAP). These dextran tracer particles have an estimated hydrodynamic diameter of ~40 nm, making them relevant for the study of the transport of macromolecules such as antibodies (12 nm diameter) and viral vectors (20-150 nm diameter). We found that the diffusion coefficient is unchanged in MMP-1 and MMP-8 treated tumors (Fig. 4.5). As expected from the dramatic effects on tumor collagen, treatment with bacterial collagenase leads to a significant increase in the diffusion coefficient ($P < 0.05$). Thus, it appears that while application of 0.1 μg/μl recombinant

MMP-1 to tumors can modify the tumor collagen, the effect is not dramatic enough to significantly alter diffusive transport.

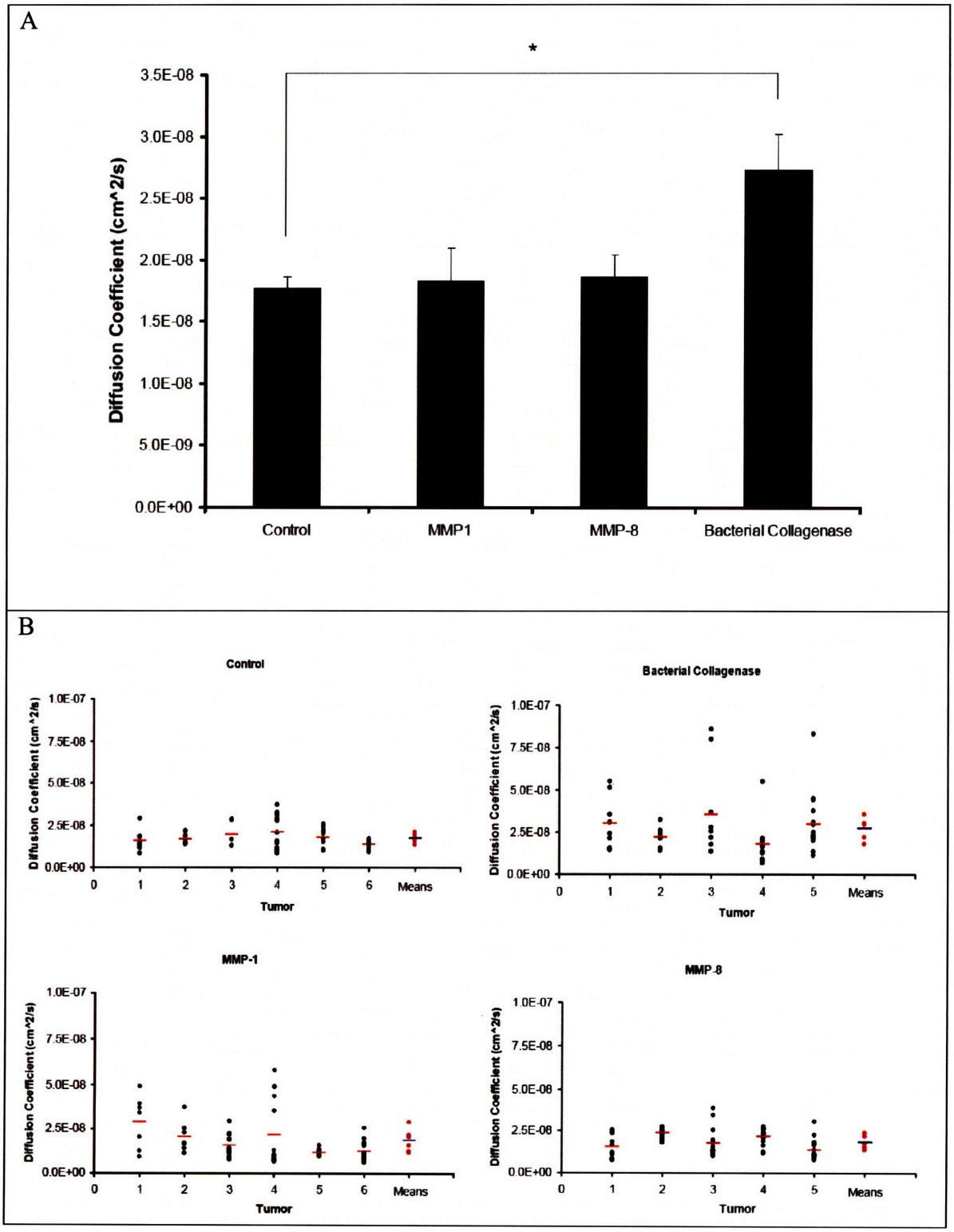

Figure 4.5. Effect of collagenase superfusion on diffusion. The effective diffusion coefficient of $1x10^6$ molecular weight dextran in HSTS26T tumors grown in the dorsal chamber was measured by MPFRAP. (A) Mean diffusion coefficients with standard errors. N = 5-6 for each treatment. Bacterial collagenase treatment causes a significant increase in the diffusion coefficient relative to control ($P < 0.05$). MMP-1 and MMP-8 application does not alter the effective diffusion coefficient. (B) Individual diffusion coefficient measurements for each tumor (black dots), mean for each tumor (red lines and dots) and mean for each treatment (blue lines).

Effect of MMPs on oncolytic HSV treatment of tumors

Finally, we also checked if co-injection of MMP-1 or MMP-8 can enhance the efficacy of the oncolytic HSV vector MGH2 as bacterial collagenase can. While collagen content was not dramatically decreased and the diffusion of tracer particles was not affected, perhaps some other alteration occurred that could improve viral distribution. Ultimately we are interested in developing methods to improve oncolytic viral therapy. To that end, HSTS26T tumors were grown subcutaneously in the leg of SCID mice. At ~60 mm^3 they were treated with an injection of either $2.5x10^6$ t.u. of MGH2 alone, MGH2 with 1.0 μg MMP-1 or MGH2 with 1.0 μg MMP-8. A similar injection was repeated two days later. The tumor volume was monitored over several weeks. MMP-1 and MMP-8 co-injection did not enhance the efficacy of MGH2 therapy (Fig. 4.6).

A

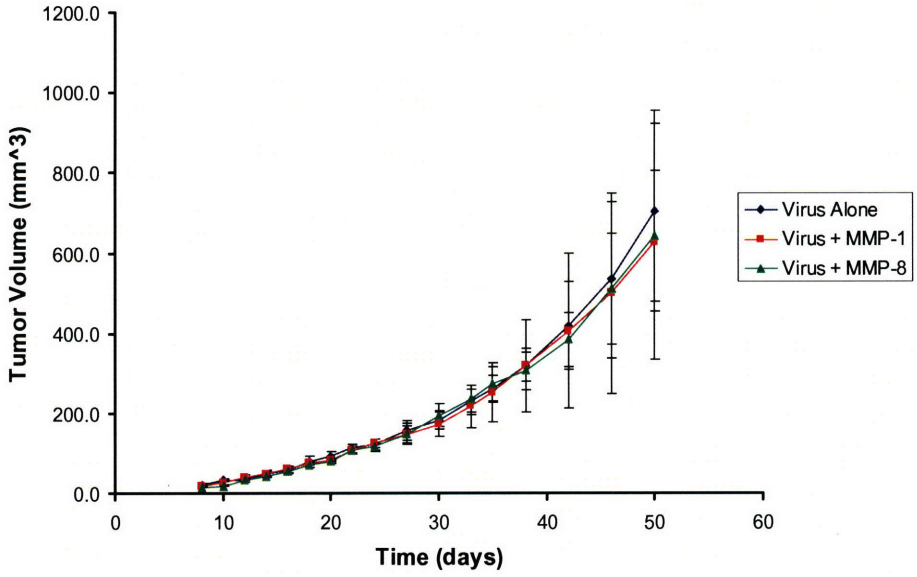

B

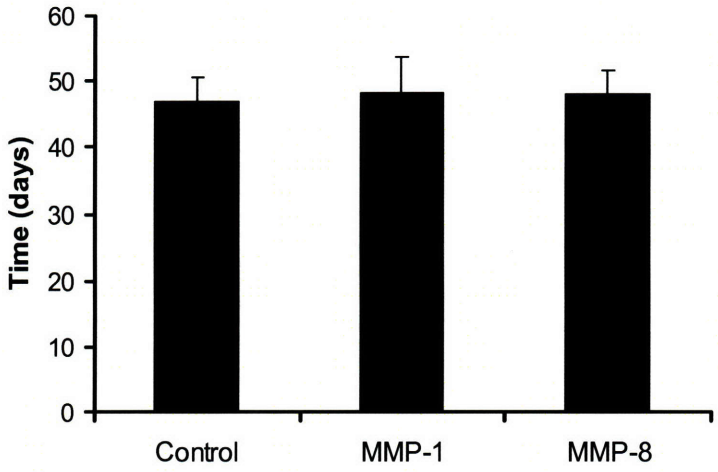

Figure 4.6. Effect of recombinant MMP-1 and MMP-8 on oncolytic HSV treatment. HSTS26T tumors were grown subcutaneously in the leg of SCID mice and treated with two intratumor injections of either $2.5x10^6$ t.u. of MGH2 alone or in combination with 1.0 μg recombinant MMP-1 or MMP-8. (A) Mean tumor volume of treated and control tumors with standard errors. (B) Growth delay induced by oncolytic HSV treatment,

given as the time for the tumor to grow to ten times the size at treatment. There is no significant difference in the growth delay between tumors treated with virus alone or with recombinant MMPs.

Discussion

We have found that while all four human enzymes we screened are reported to have activity against collagen type I, only MMP-1 and -8 showed significant activity in our fibril assay. It is still uncertain why MMP-13 exhibited almost no collagenase activity relative to the other MMPs. MMP-13 is enzymatically similar to the other two enzymes: it has a similar domain structure and cleaves collagen type I at the same peptide bond (Gly_{775}-Ile_{776}). While MMP-13 does not share much sequence homology to MMP-1 (18), neither does MMP-8 (19). One possibility for why no activity was observed is that the true substrate for MMP-13 *in vivo* is type II collagen, rather than type I. MMP-13 has significantly greater activity against collagen type II relative to type I (21) and is better at degrading collagen type II than either MMP-1 or MMP-8 (37, 38). Furthermore, MMP-13 has been found to play a role in collagen II degradation in osteoarthritis and rheumatoid arthritis (39-41). A second possibility is that the mechanism of MMP-13 activation differs from its counterparts. Indeed it has been shown that MMP-13 can be activated by a proteolytic cascade that includes MMP-14 and MMP-2 (42), while MMP-1 and -8 have not been found to be activated in such a manner. APMA was chosen as the *in vitro* activating agent for all three enzymes since it has been used in numerous

biochemical assays for each. Perhaps this agent is sufficient for activating MMP-1 and -8 but does not maximally activate MMP-13.

The low activity of cathepsin K is less surprising. While it has been found that cathepsin K is a very potent collagenase – on par with bacterial collagenase – these activity assays were performed at pH 5.5, the pH in osteoclasts where cathepsin K degrades collagen in physiological settings (26). As discussed above, the collagenase activity of cathepsin K varies with pH and is optimal in acidic conditions (25). This can be partially explained by the fact that autolysis occurs readily and the stability of cathepsin K at 37°C is low at neutral pH: in one half hour nearly 90% of activity is lost. Thus, while we adjusted the pH of samples to 6.0 and below in our activity assays – and found no activity – the enzyme may have autodegraded while in the media, which can be neutral or slightly basic. Indeed, our western blots of the conditioned media samples showed multiple bands, suggesting that some of the enzyme had gone through autodegradation. In addition, studies have shown that while chondroiton sulfate and keratin sulfate can enhance collagenase activity by forming a complex with cathepsin K, the other GAGs such as dermatin sulfate and heparan sulfate can effectively inhibit activity by binding and preventing the interaction of the enzyme with the "productive" GAGs (33). We may have observed no activity in the presence of chondroiton sulfate in our assays due to the binding of cathepsin K to other GAGs while in the media. In total, this suggests that it may still be possible to use cathepsin K to degrade collagen in tumors even while little activity was observed in our assays with conditioned media. Tumors can be slightly acidic and contain various soluble GAGs. Purified, recombinant cathepsin K can even be complexed with chondroiton sulfate before being applied to tumors. However, the

intricate nature of activation, inhibition and degradation of this enzyme suggests that their use as collagenases *in vivo* may require substantial optimization.

In our *in vivo* assays, MMP-1 and MMP-8 were not able to replicate our previous findings with bacterial collagenase. Total collagen levels in tumors – as assessed by SHG signal – decreased only slightly with recombinant MMP-1 application and not at all with MMP-8. Neither MMP affected diffusion or the efficacy of an oncolytic HSV vector. One possible reason may be the nature of collagen cleavage for each type of enzyme. Bacterial collagenase is not a single enzyme, but rather a collection of seven distinct enzymes (43-45). It is believed that there are two main gene products – the true collagenases – and that the lower molecular weight enzymes are proteolytic cleavage products of these full length enzymes (46). Importantly, these lower molecular weight enzymes have gelatinase activity and bacterial collagenase can cleave collagen at multiple sites into small peptides. When we have degraded collagen molecules with bacterial collagenase, we find that collagen is converted into peptide fragments that are all smaller than 10 kDa. In contrast, MMP-1 and -8 cleaves collagen at a single site into two relatively large fragments (47, 48). While both MMPs contain some gelatinase activity, it is one to two orders of magnitude less than the collagenase activity (21). Thus in and of itself, MMP-1 and -8 may not be able to solubilize fibrillar collagen as bacterial collagenase does. Perhaps the breakdown of collagen into small peptides facilitates its clearance from the interstitium and is key to the improvements in transport seen with bacterial collagenase.

An alternative hypothesis is that the dose used in these studies is insufficient to effect the changes in collagen needed to improve interstitial diffusion. In our *in vitro* collagenase activity assay, the activity of MMPs is less than that of bacterial collagenase on a per molar basis. This suggests that increasing the dose may be necessary to see an equivalent improvement in collagen degradation and diffusive transport *in vivo*. Due to the difficulty in producing and purifying human proteins, increasing the dose of recombinant proteins from that used in this study is prohibitively expensive. Expression of these collagenases in the tumor cells, themselves, by stable transfection offers another option that would effectively increase the dose and have several other advantages. First, this would provide chronic rather than acute delivery of the enzymes to the tumor; collagenase would be delivered throughout the course of tumor progression. Second, this ensures that the collagenase is delivered to all parts of the tumor, since it will be expressed by all tumor cells. Finally, this would provide proof of principle for genetic delivery of a human collagenase in a therapeutic setting, such as with an oncolytic viral vector.

References

1. McKee TD, Grandi P, Mok W, *et al.* Degradation of fibrillar collagen in a human melanoma xenograft improves the efficacy of an oncolytic herpes simplex virus vector. Cancer Res 2006 Mar 1;66(5):2509-13.
2. Bani D. Relaxin: a pleiotropic hormone. Gen Pharmacol 1997 Jan;28(1):13-22.
3. Sherwood OD. Relaxin's physiological roles and other diverse actions. Endocr Rev 2004 Apr;25(2):205-34.
4. Silvertown JD, Summerlee AJ, Klonisch T. Relaxin-like peptides in cancer. Int J Cancer 2003 Nov 20;107(4):513-9.
5. Brown E, McKee T, diTomaso E, *et al.* Dynamic imaging of collagen and its modulation in tumors in vivo using second-harmonic generation. Nat Med 2003 Jun;9(6):796-800.
6. Samuel CS, Unemori EN, Mookerjee I, *et al.* Relaxin modulates cardiac fibroblast proliferation, differentiation, and collagen production and reverses cardiac fibrosis in vivo. Endocrinology 2004 Sep;145(9):4125-33.
7. Unemori EN, Amento EP. Relaxin modulates synthesis and secretion of procollagenase and collagen by human dermal fibroblasts. J Biol Chem 1990 Jun 25;265(18):10681-5.
8. Unemori EN, Beck LS, Lee WP, *et al.* Human relaxin decreases collagen accumulation in vivo in two rodent models of fibrosis. J Invest Dermatol 1993 Sep;101(3):280-5.
9. Binder C, Hagemann T, Husen B, Schulz M, Einspanier A. Relaxin enhances in-vitro invasiveness of breast cancer cell lines by up-regulation of matrix metalloproteases. Mol Hum Reprod 2002 Sep;8(9):789-96.
10. Unemori EN, Pickford LB, Salles AL, *et al.* Relaxin induces an extracellular matrix-degrading phenotype in human lung fibroblasts in vitro and inhibits lung fibrosis in a murine model in vivo. J Clin Invest 1996 Dec 15;98(12):2739-45.
11. Feng S, Agoulnik IU, Bogatcheva NV, *et al.* Relaxin promotes prostate cancer progression. Clin Cancer Res 2007 Mar 15;13(6):1695-702.
12. Kamat AA, Feng S, Agoulnik IU, *et al.* The role of relaxin in endometrial cancer. Cancer Biol Ther 2006 Jan;5(1):71-7.
13. Sternlicht MD, Werb Z. How matrix metalloproteinases regulate cell behavior. Annu Rev Cell Dev Biol 2001;17:463-516.
14. Woessner JF, Nagase H. Matrix Metalloproteinases and TIMPs. New York, NY: Oxford University Press; 2000.
15. Birkedal-Hansen H, Moore WG, Bodden MK, *et al.* Matrix metalloproteinases: a review. Crit Rev Oral Biol Med 1993;4(2):197-250.
16. Egeblad M, Werb Z. New functions for the matrix metalloproteinases in cancer progression. Nat Rev Cancer 2002 Mar;2(3):161-74.
17. Eisen AZ, Jeffrey JJ, Gross J. Human skin collagenase. Isolation and mechanism of attack on the collagen molecule. Biochim Biophys Acta 1968 Mar 25;151(3):637-45.
18. Freije JM, Diez-Itza I, Balbin M, *et al.* Molecular cloning and expression of collagenase-3, a novel human matrix metalloproteinase produced by breast carcinomas. J Biol Chem 1994 Jun 17;269(24):16766-73.

19. Hasty KA, Pourmotabbed TF, Goldberg GI, *et al.* Human neutrophil collagenase. A distinct gene product with homology to other matrix metalloproteinases. J Biol Chem 1990 Jul 15;265(20):11421-4.
20. Horwitz AL, Hance AJ, Crystal RG. Granulocyte collagenase: selective digestion of type I relative to type III collagen. Proc Natl Acad Sci U S A 1977 Mar;74(3):897-901.
21. Knauper V, Lopez-Otin C, Smith B, Knight G, Murphy G. Biochemical characterization of human collagenase-3. J Biol Chem 1996 Jan 19;271(3):1544-50.
22. Murphy G, McAlpine CG, Poll CT, Reynolds JJ. Purification and characterization of a bone metalloproteinase that degrades gelatin and types IV and V collagen. Biochim Biophys Acta 1985 Sep 20;831(1):49-58.
23. Welgus HG, Jeffrey JJ, Eisen AZ. The collagen substrate specificity of human skin fibroblast collagenase. J Biol Chem 1981 Sep 25;256(18):9511-5.
24. Bossard MJ, Tomaszek TA, Thompson SK, *et al.* Proteolytic activity of human osteoclast cathepsin K. Expression, purification, activation, and substrate identification. J Biol Chem 1996 May 24;271(21):12517-24.
25. Bromme D, Okamoto K, Wang BB, Biroc S. Human cathepsin O2, a matrix protein-degrading cysteine protease expressed in osteoclasts. Functional expression of human cathepsin O2 in Spodoptera frugiperda and characterization of the enzyme. J Biol Chem 1996 Jan 26;271(4):2126-32.
26. Garnero P, Borel O, Byrjalsen I, *et al.* The collagenolytic activity of cathepsin K is unique among mammalian proteinases. J Biol Chem 1998 Nov 27;273(48):32347-52.
27. Leunig M, Yuan F, Menger MD, *et al.* Angiogenesis, microvascular architecture, microhemodynamics, and interstitial fluid pressure during early growth of human adenocarcinoma LS174T in SCID mice. Cancer Res 1992 Dec 1;52(23):6553-60.
28. Johnson-Wint B. A quantitative collagen film collagenase assay for large numbers of samples. Anal Biochem 1980 May 1;104(1):175-81.
29. Moses MA, Sudhalter J, Langer R. Identification of an inhibitor of neovascularization from cartilage. Science 1990 Jun 15;248(4961):1408-10.
30. Brown EB, Campbell RB, Tsuzuki Y, *et al.* In vivo measurement of gene expression, angiogenesis and physiological function in tumors using multiphoton laser scanning microscopy. Nat Med 2001 Jul;7(7):864-8.
31. Brown EB, Wu ES, Zipfel W, Webb WW. Measurement of molecular diffusion in solution by multiphoton fluorescence photobleaching recovery. Biophys J 1999 Nov;77(5):2837-49.
32. Li Z, Hou WS, Escalante-Torres CR, Gelb BD, Bromme D. Collagenase activity of cathepsin K depends on complex formation with chondroitin sulfate. J Biol Chem 2002 Aug 9;277(32):28669-76.
33. Li Z, Yasuda Y, Li W, *et al.* Regulation of collagenase activities of human cathepsins by glycosaminoglycans. J Biol Chem 2004 Feb 13;279(7):5470-9.
34. Alexandrakis G, Brown EB, Tong RT, *et al.* Two-photon fluorescence correlation microscopy reveals the two-phase nature of transport in tumors. Nat Med 2004 Feb;10(2):203-7.
35. Netti PA, Berk DA, Swartz MA, Grodzinsky AJ, Jain RK. Role of extracellular matrix assembly in interstitial transport in solid tumors. Cancer Res 2000 May 1;60(9):2497-503.

36. Pluen A, Boucher Y, Ramanujan S, *et al.* Role of tumor-host interactions in interstitial diffusion of macromolecules: cranial vs. subcutaneous tumors. Proc Natl Acad Sci U S A 2001 Apr 10;98(8):4628-33.
37. Billinghurst RC, Dahlberg L, Ionescu M, *et al.* Enhanced cleavage of type II collagen by collagenases in osteoarthritic articular cartilage. J Clin Invest 1997 Apr 1;99(7):1534-45.
38. Mitchell PG, Magna HA, Reeves LM, *et al.* Cloning, expression, and type II collagenolytic activity of matrix metalloproteinase-13 from human osteoarthritic cartilage. J Clin Invest 1996 Feb 1;97(3):761-8.
39. Freemont AJ, Byers RJ, Taiwo YO, Hoyland JA. In situ zymographic localisation of type II collagen degrading activity in osteoarthritic human articular cartilage. Ann Rheum Dis 1999 Jun;58(6):357-65.
40. Konttinen YT, Ainola M, Valleala H, *et al.* Analysis of 16 different matrix metalloproteinases (MMP-1 to MMP-20) in the synovial membrane: different profiles in trauma and rheumatoid arthritis. Ann Rheum Dis 1999 Nov;58(11):691-7.
41. Lindy O, Konttinen YT, Sorsa T, *et al.* Matrix metalloproteinase 13 (collagenase 3) in human rheumatoid synovium. Arthritis Rheum 1997 Aug;40(8):1391-9.
42. Knauper V, Will H, Lopez-Otin C, *et al.* Cellular mechanisms for human procollagenase-3 (MMP-13) activation. Evidence that MT1-MMP (MMP-14) and gelatinase a (MMP-2) are able to generate active enzyme. J Biol Chem 1996 Jul 19;271(29):17124-31.
43. Bond MD, Van Wart HE. Relationship between the individual collagenases of Clostridium histolyticum: evidence for evolution by gene duplication. Biochemistry 1984 Jun 19;23(13):3092-9.
44. Bond MD, Van Wart HE. Characterization of the individual collagenases from Clostridium histolyticum. Biochemistry 1984 Jun 19;23(13):3085-91.
45. Bond MD, Van Wart HE. Purification and separation of individual collagenases of Clostridium histolyticum using red dye ligand chromatography. Biochemistry 1984 Jun 19;23(13):3077-85.
46. Yoshida E, Noda H. Isolation and characterization of collagenases I and II from Clostridium histolyticum. Biochim Biophys Acta 1965 Sep 20;105(3):562-74.
47. Gross J, Harper E, Harris ED, *et al.* Animal collagenases: specificity of action, and structures of the substrate cleavage site. Biochem Biophys Res Commun 1974 Nov 27;61(2):605-12.
48. Hasty KA, Wu H, Byrne M, *et al.* Susceptibility of type I collagen containing mutated alpha 1(1) chains to cleavage by human neutrophil collagenase. Matrix 1993 May;13(3):181-6.

Chapter 5: Effect of MMP-1 and MMP-8 Expression in Tumors

Portions of the chapter have been taken from:

W. Mok, Y. Boucher and R.K. Jain, "Matrix Metalloproteinase-1 and -8 Improve the Distribution and Efficacy of an Oncolytic Virus." In press, *Cancer Research*

Introduction

There are several methods by which collagenases can be delivered to the tumor to achieve matrix degradation and improve interstitial transport. In the previous two chapters, purified, recombinant collagenases have been directly applied to, or injected into, tumors. While this has been a successful strategy with bacterial collagenase (1), our work with human collagenases in the preceding chapter highlights one of the limitations of this method: recombinant enzymes can be difficult and expensive to purify in large amounts. This drawback prevented us from testing higher doses of MMP-1 and -8 – both of which are less potent collagenases than bacterial collagenase – and perhaps realizing more dramatic effects on tumor collagen and improvement in transport.

An alternative strategy to delivering the protein is to deliver its genetic precursor, the cDNA. Delivery of genetic material via non-viral vectors such as liposomes is well suited for cancer therapy since its large scale production is cost-effective and it has shown biological success both *in vitro* and *in vivo* (2). The other main class of genetic delivery vehicles includes viral vectors. This thesis focuses on improving the transport of oncolytic viral vectors. These viral vectors are unique in that they can serve as both genetic delivery vectors and as therapeutics, themselves, since they lyse cancer cells (3). Recombinant oncolytic viruses can be developed which contain an expression cassette for a human collagenase. In theory, tumor cells infected by such an oncolytic vector will produce the collagenase, as well as viral proteins. This collagenase will be secreted from the infected cell and released upon cell lysis. The enzymes can diffuse throughout the interstitium and degrade collagen, potentially improving the spread of the progeny virus.

One main advantage of this approach over the use of recombinant enzymes is that tumor cells infected by progeny virus continue to express the transgene. Thus, this method provides chronic, rather than acute, delivery of collagenase to the tumor.

In order to provide proof of principle that genetic delivery of human collagenases to tumors is a suitable method to alter their interstitial matrix, an experimental model is developed whereby tumor cells are stably transfected with either MMP-1 or MMP-8 and tumors are grown in mice. This model represents the best case scenario for gene transfer of MMPs, as all tumor cells will be expressing the enzyme throughout the entire course of tumor development.

MMP-1 and -8 have the ability to degrade multiple fibrillar collagens – not just type I collagen – as well as various glycoproteins and proteoglycans (4). Thus, they have the potential to significantly alter the composition and structure of the tumor extracellular matrix, especially when delivered chronically such as via overexpression in cells. Therefore, in the present chapter we characterize the effect of MMP expression on the main structural components of the extracellular matrix (*i.e.* collagen I, hyaluronic acid and sulfated GAGs). Since these matrix components are known to regulate both diffusive and convective transport in tissue, we measure both the effective diffusion coefficient of tracer particles and the hydraulic conductivity of these tumors. Both diffusion and convection can limit the transport and distribution of cancer therapeutics. As described earlier, our lab has shown that the tumor ECM can significantly hinder the interstitial diffusion of macromolecules (5, 6). In Chapter 3, we provided evidence that ECM structures can impede the convection of viral particles into the tumor during infusion (1).

Here we characterize the effect of MMP-1 and -8 expression on the tumor ECM composition, diffusive and convective transport and the efficacy of oncolytic viral therapy.

Materials and Methods

Dorsal skinfold chamber

All animal experiments were done with the approval of the Institutional Animal Care and Use Committee (MGH SRAC protocol 2004N000063). Human soft tissue sarcoma HSTS26T cells and transfected clones were grown in dorsal skinfold chambers in SCID mice as described previously (7). The entire preparation was done under anesthesia (100 mg ketamine hydrochloride/10 mg of xylazine per kg body weight intramuscularly) in aseptic conditions inside the animal colony. Briefly, the back of the mouse was shaved and hair removed using hair removal cream. Two symmetrical titanium frames were stitched on to fix the extended double layer of dorsal skin between the frames. Roughly 15 mm diameter of skin was removed from one side, leaving the opposite side of the skin, striated muscle and subcutaneous tissue intact. The fascia was carefully removed and a cover glass was mounted into the frame. The animals were allowed to recover for at least one day prior to tumor implantation. Tumors were allowed to grow for at least two weeks prior to experimentation.

Plasmid construction and stable transfections

A retroviral transfection system was used to generate stable MMP-1 and MMP-8 transfectants. The cDNA coding for human MMP-1 was purchased from ATCC and the

cDNA coding for human MMP-8 was a gift from David Tarin (University of California, San Diego). The full length cDNAs were subcloned into the retroviral vector pBMN-I-GFP (Garry Nolan, Stanford University). The vector contains an IRES allowing for expression of enhanced green fluorescence protein (EGFP).

Retroviral vectors for the stable transfections were packaged according to the following protocol, described previously (8). 80-90% confluent T75 flasks of 293ET packaging cells were transiently transfected with each BMN vector (15 μg) in combination with plasmids expressing vesicular stomatitis virus glycoprotein (VSVG, 5 μg) and gag/pol (7 μg). After overnight incubation, the 293ET cells were washed three times with PBS and then 10 mL of fresh media was added. The following day the conditioned media containing retrovirus was collected and fresh media added to the flask. The conditioned media was spun down to remove any cell debris and passed through a 0.45 μM filter (Whatman, Brentford, UK). Subconfluent HSTS26T cells were incubated with the conditioned media containing retrovirus. The conditioned media from the 293ET packaging cells were collected the following two days and transduction repeated. Clones with stable transduction were isolated using fluorescence activated cell sorting. Expression of MMPs was confirmed with western blot.

Protein isolation

Tumors were grown subcutaneously in the leg of SCID mice. At an appropriate size, tumors were harvested and immediately snap frozen in liquid nitrogen and stored at -80°C. Tissue was homogenized in 100 μL RIPA buffer. Samples were kept on ice for 30 minutes and then spun down at 14,000 g for 20 minutes to pellet the cell debris. The

supernatant containing tissue protein was collected. Protein concentration was measured using the Bradford assay (BioRad Laboratories, Hercules, CA) according to the manufacturer's instructions. Pre-diluted BSA (Pierce Biotechnology, Rockford, IL) was used as a protein standard. Protein samples were stored at -80°C prior to use in activity assays and western blots.

Western blot

Loading buffer containing β-mercaptoethanol was added to the protein samples and they were boiled at 100°C for 5 minutes. Samples were loaded into a 10% Bis-Tris gel (Invitrogen, Carlsbad, CA) and run at 150V for ~ 1 hr. The proteins were transferred to a nitrocellulose membrane. The transfer was performed at 30V for 1 hr at room temperature. The membrane was washed with TBST for 10 minutes. The membrane was placed in 20 mL of blocking buffer (TBST with 5% milk) and incubated at room temperature for 3 hrs with gently shaking. The membrane was incubated with primary antibody at 4°C overnight with gentle shaking. Polyclonal antibodies AB806 and AB8115 (Millipore, Billerica, MA) were used at a dilution of 1:2,500 for detection of MMP-1 and MMP-8, respectively. Polyclonal antibody EL 2900 (for cleaved collagen I) was a gift from Eunice Lee (Shriners Hospital for Children, Canada) and was used at a concentration of 4 μg/ml (1:500). The following day, the membrane was washed 3x for 10 minutes with TBST with vigorous shaking. The membrane was then incubated for 1 hr at room temperature with an HRP-conjugated secondary antibody (Amersham, Buckinghamshire, UK). The membrane was washed again with TBST with vigorous shaking and proteins detected using the ECL or ECL Plus kit (Amersham,

Buckinghamshire, UK). Membranes were stripped by incubating with stripping buffer (Pierce Biotechnology, Rockford, IL) at 37°C and beta actin detected with a polyclonal antibody (Santa Cruz Biotechnology, Santa Cruz, CA).

Collagenase activity assay

MMP activity was determined using an *in vitro* collagenolytic activity assay modified from the method of Johnson-Wint (9, 10). Briefly, type I collagen was purified from rat tail by solubilization with acetic acid and subsequently acetylated with [^{14}C] acetic anhydride. Fibrils were allowed to form from the radiolabeled collagen and were dried onto wells of a 96-well plate, forming a thin film. Tumor lysate samples were added to wells and incubated at 37°C for 2.5 hours. To activate the MMPs, a 1:10 volume of 1 mg/ml trypsin (Worthington, Lakewood, NJ) was added to the sample and incubated at 37°C for 7 minutes. A 1:10 volume of 5 mg/ml soybean trypsin inhibitor (Worthington, Lakewood, NJ) was then added to the sample to inactivate the trypsin. Samples were immediately added to wells containing collagen. The supernatants containing soluble radiolabeled collagen (from cleavage) were transferred to scintillation vials and counted in a Beckman model LS-3801 scintillation counter. Bacterial collagense was used as a control to cleave all the radiolabeled collagen in select wells. Bovine corneal collagense was used as the enzyme control in inhibitor assays. One unit of activity corresponds to degradation of 10% of the collagen in 2.5 hrs at 37°C.

SHG imaging and quantification

Imaging of second harmonic generation (SHG) in dorsal chamber tumors was performed with a custom-built multiphoton laser scanning microscope (11) using a 20X/0.5NA objective lens. Excitation was at 880 nm and SHG was detected via a 435DF30 emission filter with a high pass 475 dichroic. Three dimensional image stacks were obtained of the top 130 μm from the surface of the tumor (27 images of 5 μm thickness). Six to ten image stacks were obtained to create a montage covering the entire tumor or a significant portion of it. The total SHG signal intensity in each stack was measured by image analysis (ImageJ) and the mean intensity for each individual tumor calculated.

Histology

Tumor tissue was harvested, fixed in 4% paraformaldehyde for 3 hrs and incubated in PBS overnight. Tissue was embedded in either paraffin or optimal cutting temperature compound (Tissue-Tek). 20 μm thickness sections were cut.

Collagen I staining of frozen sections and quantification was performed as described previously (6). Rabbit polyclonal antibody against collagen I (LF-67) was obtained from Larry Fisher (National Institute of Dental Research) and used at a dilution of 1:200. A Cy3-conjugated secondary antibody (Jackson Immunoresearch, West Grove, PA) was used. Cell nuclei were stained with DAPI. For quantification of the fraction of tissue occupied by collagen I staining, images were taken with a multiphoton microscope (11). Using 800 nm light with a 20X/0.5 numerical aperture lens, image stacks (10 images) were obtained of the stained sections. A 625/75 filter was used for Cy3 imaging and

435/40 for DAPI, with a 570 dichroic. A maximum intensity projection of the image stacks was taken to generate a single image, thereby ensuring that each pixel value represents the best colocalization of the excitation volume with the slice. Ten images were taken per section in random locations and 7 sections were analyzed for each group. Using a series of threshold pixel values the fraction of tissue section containing nuclear, non-specific and specific collagen staining was determined.

HSV-1 and HA binding protein (HABP) staining was performed on paraffin sections. Tissue sections were deparaffinized and hydrated. Sections were permeabilized with 3% hydrogen peroxide for 5 minutes, washed three times in PBS with 3% BSA and blocked for 1 hr with 3% BSA/PBS. The tissue was incubated with a polyclonal anti-HSV-1 antibody (Dako, Glostrup, Denmark) at a dilution of 1:8000 for 30 minutes at room temperature. For HA staining tissues were incubated with biotinylated HA binding protein (EMD Chemical, Madison, WI) at a dilution of 1:150. Sections were incubated with peroxidase-conjugated streptavidin and DAB chromogen was used as substrate (Dako, Glostrup, Denmark). For quantification of HA staining, 8 random images were taken per section with a 20X objective lens with an inverted microscope (Olympus, Center Valley, PA). Image analysis was performed using a macro developed in Adobe Photoshop. The brown pseudocolor was selected and thresholded using the color selection function and the mean brown pixel count for each section was measured. For HSV staining, individual images were taken with a 10X objective lens to create a montage of the entire tumor. The contrast was insufficient for image analysis using the macro. Instead, a square grid with 100 μm length grid boxes was overlayed on the images

and grid boxes containing brown staining were counted. In both cases, 6-7 tissues sections were analyzed per tumor type.

Construction of recombinant HSV vectors

Recombinant oncolytic HSV-1 vectors expressing MMP-1 and MMP-8 were generated using the HSVQuik system (12) (Fig. 5.1). A brief description of the protocol follows, while a more detailed version can be found in the manuscript. The MMP-1 and MMP-8 cDNA were subcloned into the pcDNA3.1 mammalian expression vector (Invitrogen, Carlsbad, CA). The expression cassette containing the CMV promoter, MMP cDNA and polyA was amplified by PCR and subcloned into the pTransfer shuttle plasmid. The pTransfer multiple cloning site is flanked by *FRT* and *loxP* sites to mediate homologous recombination. pTransfer-MMP-x plasmids were electroporated together with an FLP-expressing helper plasmid into bacteria carrying fHSVQuik-1 BAC plasmid. The fHSVQuik-1 BAC was cloned from the MGH1 genome, which contains deletions in both copies of the *γ34.5* gene and a *lacZ* insertion at the *UL39* locus. It contains two recombination sequences: *FRT* sites to facilitate insertion of transgene cassettes into the *UL39* locus and *loxP* sites for later removal of prokaryotic plasmid sequences from the vector genome. It also contains the EGFP coding sequence to visualize infected cells and an RFP expression cassette in the middle of the BAC backbone to monitor the presence of the BAC sequences in the vector genome. Approximately 100 ng of each pTransfer plasmid and the FLP-expressing helper plasmid were used. An electrical pulse was applied using the Gene Pulser II device with a setting of 1.8 kV, 200 Ω, 25 μF. Cointegrants of the pTransfer-MMP-x and fHsvQuik-1 fused at the *FRT* sites (fHsvQ1-

MMP-x) were obtained by selection with chloramphenicaol and ampicillin (both 15 μg/ml). BAC DNA was prepared by conventional alkaline method and candidate clones were screened with HindIII restriction digest patterns.

The fHsvQ1-MMP-x has the transgene cassette inserted at the *UL39* locus and two unidirectional *loxP* sites now flanking all of the prokaryotic plasmid backbones and the RFP marker gene. fHsvQ1-MMP-x (2 μg) and a Cre-expressing helper plasmid (0.5 μg) were cotransfected into Vero cells using LipfectAMINE reagent (Invitrogen, Carlsbad, CA). Transfected cells were harvested and freeze/thawed to recover packaged recombinant virus. Vero cells were infected with serially diluted samples of the vector supernatant and individual recombinant HSV vectors were propagated. The expression of GFP but not RFP was confirmed. MMP expression by infected Vero cells was confirmed by western blot.

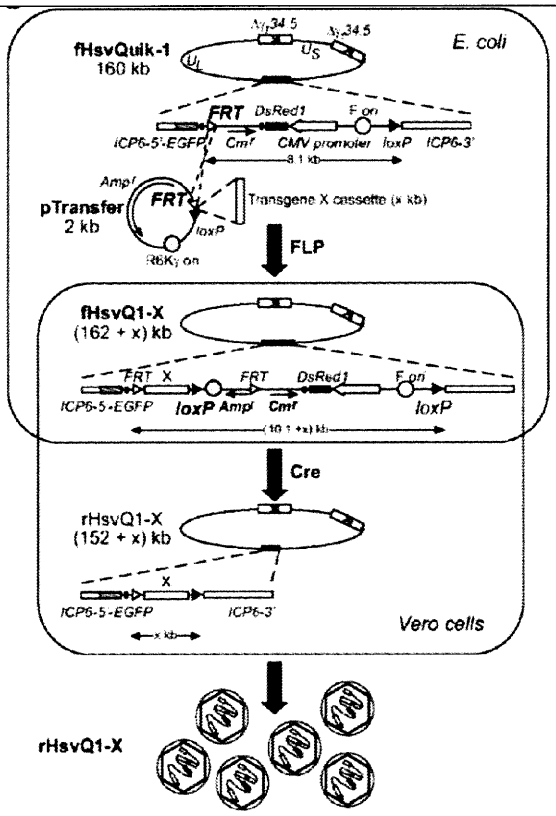

Figure 5.1. Schematic strategy for generation of recombinant oncolytic HSV vectors. fHsvQuik-1 is a BAC plasmid developed from the genome of MGH1, an oncolytic HSV vector containing deletions in both copies of the *γ34.5* gene and a *lacZ* insertion at the *UL39* locus. Co-electroporation of fHsvQuik-1 with pTransfer vectors containing the gene of interest and an FLP-expressing plasmid result in insertion of the gene of interest in the *UL39* locus, generating fHsvQ1-x. Co-transfection of Vero cells with fHsvQ1-x and a Cre-expressing plasmid results in removal of the prokaryotic plasmid backbones and packaging of recombinant virus (rHsvQ1-x).

Tumor growth delay

HSTS26T tumors (or transfected variants) were implanted subcutaneously in the leg of SCID mice and allowed to reach 60 mm^3 average volume. Mice were then randomized into separate groups (6-7 animals per group) and given 10 µl intratumoral injections of either 2.5 x 10^6 t.u. of oncotyic HSV in PBS or PBS alone. A second similar injection was performed two days later. Tumor volume was measured every 3-4 days and calculated as volume = $\pi AB^2/6$, where A and B are the maximum and minimum diameters, respectively. The time to reach 10 times the volume at treatment was calculated for each tumor.

Multiphoton fluorescence recovery after photobleaching

The diffusion coefficient of $2x10^6$ molecular weight dextran was measured in dorsal chamber tumors using multiphoton fluorescence recover after photobleaching (MPFRAP). A custom-built multiphoton microscope (11) was adapted for MPFRAP based on a previous design (13). One half microliter of tetramethylrhodamine-labeled dextran (Invitrogen, Carlsbad, CA) was injected at a concentration of 2 mg/ml at a depth of 200 µm below the surface of the tumor. Injections were performed using glass micropipettes that were pulled to obtain a 20 µm inner diameter tip (6). Injections were performed at nearly constant flow rate over 2-3 minutes.

MPFRAP was performed approximately 30 minutes after injection. The laser was set at 800 nm and a 40X/0.75 NA objective lens was used with a 525/100 filter between 405 and 605 high pass dichroics. The multiphoton laser was focused on locations in the

extracellular space 40-70 μm below the surface of the tumor. During each bleach/recovery cycle, the sample was bleached with a 160 μs pulse train of light, followed by an ~40 ms recovery monitored in 40 μs time bins. The length of the bleach and the time bins for monitoring recovery were chosen to avoid significant error due to diffusion during these two time periods. Based on the analysis of Brown *et al.* (13), the systematic error in the detected fluorescence intensity due to diffusion during the bleach pulse and over the course of recovery is $\sim 1.05(\Delta t/\tau_D)$ where Δt is the length of the bleach pulse or monitoring time bin and τ_D is the time constant for diffusive recovery. The characteristic fluorescence recovery time of $2x10^6$ molecular weight dextran *in vivo* was found to be ~10 ms. Thus, a bleaching pulse length of 160 μs is short enough to avoid significant diffusion during the bleach pulse (error of ~1.68%) and a monitoring time bin of 40 μs is short enough to accurately monitor the recovery (error of ~0.42%).

The monitoring power was chosen such that photobleaching did not occur. The bleaching power was chosen such that excitation saturation did not occur. Each bleach/recovery cycle was repeated 500 to 1000 times for a given spot/measurement. Approximately 10 to 20 measurements were taken for each individual tumor. Data acquisition typically lasted 2 hrs. The recovery curves were fit to the following equation, derived in Brown *et al.*, which gives the time-dependent detected fluorescence signal due to diffusion into the focal volume:

$$F(t) = F_0 \sum_{n=0}^{\infty} \frac{m^{3/2}(-\beta)^n}{n!} \frac{1}{(m+bn+(bnmt/\tau_D)} \frac{1}{\sqrt{m+bn+(bnmt/R\tau_D)}}.$$

$F(t)$ is the time-dependent fluorescence signal, F_0 is the prebleach equilibrium fluorescence signal, m is the number of photons required to generate a fluorescence photon, β is the bleach depth parameter, b is the number of photons absorbed in a bleaching event, t is the time, R is the square ratio of the $1/e^2$ beam dimensions (w_z^2/w_r^2) and τ_D is the characteristic radial diffusion time of the fluorophore, defined as $w_r^2/8D$, where D is the diffusion coefficient. The beam dimensions for for the objective lens at a wavelength of 840 nm was calculated theoretically, with $w_z = 1.929 \times 10^{-6}$ m and $w_r^2 = 3.382 \times 10^{-7}$ m.

Hydraulic conductivity

Measurements were performed using an apparatus based on one designed previously by Swabb *et al.* (14). Discs of 3 mm diameter and 1 mm thickness were cut from tumor tissue. The tissue was ensured grossly free of necrosis and hemorrhage. The tissue was placed in a tissue clamp and secured in place on both sides with a 3 mm disc of polyester mesh (90 μm thickness, 80 μm mesh opening, 39% open area, Spectrum Laboratories, Rancho Dominguez, CA). Both sides of the tissue in the clamp were filled with fetal bovine serum. An o-ring sealed the interior of the clamp to prevent leakage of fluid. The inlet and outlet of the clamps were connected to polyethylene tubing with an inner diameter of 0.58 mm. The tubing leads to head tanks, which were filled with water. A pressure drop was established by adjusting the height of the inlet and outlet head tanks, and the flow rate of an air bubble in the inlet tubing was measured. The measurement was taken for two pressures (range 5-10 cm water) to ensure a linear increase in hydraulic conductivity with pressure. Measurements were completed in ~ 2 hours. The hydraulic

conductivity was calculated by using Darcy's law for one-dimensional flow through porous media with the following equation:

$$K = \frac{vA_{cap} / A_{tiss}}{\Delta P / \Delta x}$$

Where K is the hydraulic conductivity, v is the velocity of the bubble, A_{cap} is the cross-sectional area of the capillary tube, A_{tiss} is the cross-sectional area of the tissue in the clamp, ΔP is the applied pressure drop and Δx is the thickness of the tissue. Experiments were performed at room temperature.

Cell proliferation assay

1 x 10^4 mock and MMP-transfected HSTS26T cells were seeded in 96 well plates in quadruplicate with 100 μl media (DMEM with 10% FBS). After a 48 hr incubation, the media was replaced with 10 μl of WST-1 reagent (Roche, Basel, Switzerland) in 90 μl serum free DMEM. The cells were incubated for 2 hours at 37°C, 5% CO_2. The plate was shaken for 1 minute and the absorbance at 450 nm was measured.

Viral titer

4 x 10^5 mock and MMP-transfected HSTS26T cells were seeded in 12 well plates. 24 hours later, cells were infected with the oncolytic HSV vector MGH2 at an MOI of 0.1. After 48 hour incubation, cells and supernatant were collected, subjected to three rounds of freeze/thaw in a dry ice/ethanol bath and the cell debris pelleted by centrifugation. Confluent HSTS26T cells in a 96 well plate were infected with serial dilutions of this

virus prep to titer the virus. EGFP-expressing cells were counted 48 hours after infections and the viral titer expressed as transducing units.

Sulfated GAG content

Sulfated glycosaminoglycans (GAGs) was measured using the Blyscan assay (Biocolor, Newtownabbey, Ireland) based on the binding of the cationic dye 1,9-dimethylmethylene blue (15). Briefly, tumor tissue was harvested and snap frozen in liquid nitrogen and stored at -80°C. Tissue was solubilized in digest buffer containing 125 μg/ml papain, 0.1 M sodium phosphate, 5 mM Na_2EDTA and 5 mM cysteine-HCl, pH 6.0. One milliliter of buffer was used for 50 mg of tissue. Tissue was incubated in digest buffer for 18 hrs at 60°C. 25 μl of solubilized sample was added to 1 ml dye reagent and mixed for 30 minutes at room temperature. The samples were centrifuged at 14,000 x g for 10 minutes to pellet the precipitated polysaccharide-bound dye. The pellet was solubilized in 1 ml of dissociation reagent and absorbance of the dye measured at 656 nm. Chondroiton 4-sulphate was used as a standard.

Results

Development of MMP-1 and MMP-8 expressing tumors

Human soft tissue sarcoma HSTS26T cells were stably transfected with full length human MMP-1 and MMP-8 via retroviral transduction and tumors were grown subcutaneously in the flank of SCID mice. A western blot of the tumor lysate showed that while each MMP is expressed, the majority is in the latent, inactive form (Fig. 5.2A). For both MMPs, the zymogen retains the propeptide domain and is thus ~10 kDa larger than

the active form and runs higher on the gel. An *in vitro* collagenase activity assay was performed on tissue lysate from mock and MMP-transfected tumors (Fig. 5.2B). The collagenase activity in both MMP-expressing tumors was not significantly different than mock-transfected tumors. When the MMP-activating agent trypsin was added, the activity in the lysates from MMP-expressing tumors increased significantly compared to both lysate without trypsin and the mock transfected tumor lysate ($P < 0.05$ for all cases). These results are consistent with the western blot analysis; they suggest that the MMP-expressing tumors contain latent collagenases that are not activated in the interstitial space and that maximal collagenase activity has not been achieved.

One other mechanism that may reduce collagenase activity is the presence of MMP inhibitors in the tumor. Activity assays were performed to assess the presence of inhibitors in both the mock and MMP-transfected tumors (Fig. 5.2C). The activity of corneal collagenase was measured in the presence and absence of 100 μg of tumor lysate. Collagenase activity was not reduced significantly compared to the collagenase control for any of the tumors, with no apparent effect of dose. While this does not rule out that inhibitors are present, it does suggest that any inhibitors present are already bound to collagenases in these tumors. In total, these activity assays suggest that activation – rather than inhibition – limits overall collagenase activity. Interestingly, MMP-1 and -8 expression does not appear to trigger an increase in the expression of inhibitors in these tumors.

A

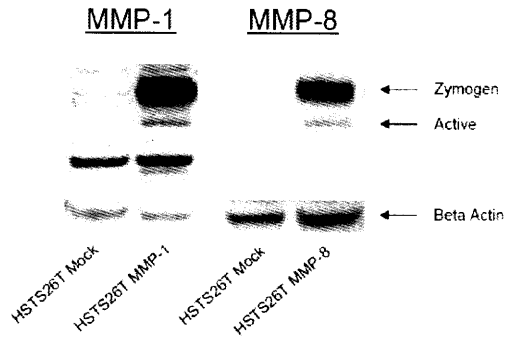
MMP-1
MMP-8
Zymogen
Active
Beta Actin
HSTS26T Mock
HSTS26T MMP-1
HSTS26T Mock
HSTS26T MMP-8

B

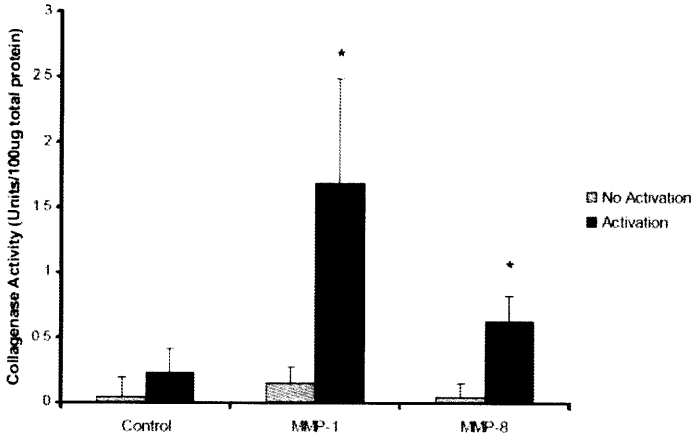
Collagenase Activity (Units/100ug total protein)
3
2.5
2
1.5
1
0.5
0
*
*
No Activation
Activation
Control
MMP-1
MMP-8

C

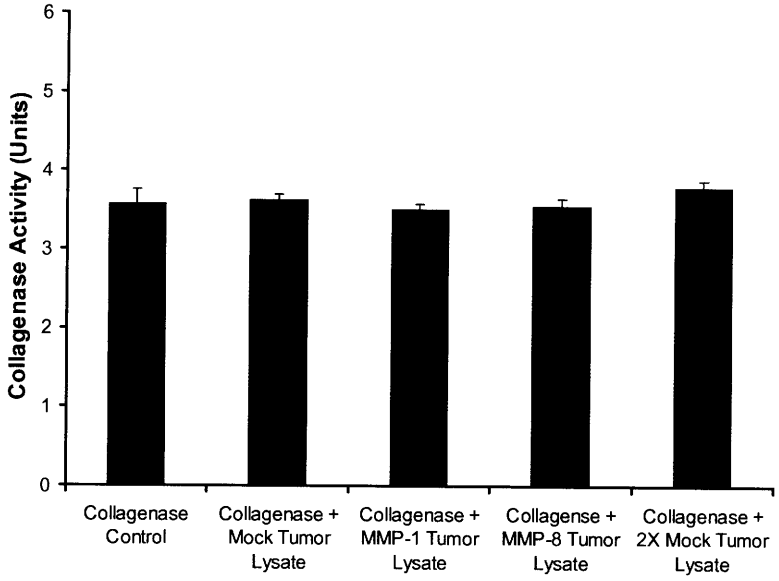
Collagenase Activity (Units)
6
5
4
3
2
1
0
Collagenase Control
Collagenase + Mock Tumor Lysate
Collagenase + MMP-1 Tumor Lysate
Collagense + MMP-8 Tumor Lysate
Collagenase + 2X Mock Tumor Lysate

Figure 5.2. Expression and activity of MMP-1 and MMP-8 in HSTS26T tumors. (A) Western blots of tumor lysates from mock-transfected, MMP-1 expressing and MMP-8 expressing tumors. Arrows denote the full length/zymogen and active forms of each enzyme. For both MMP-1 and -8, enzyme is predominantly in the inactive state. (B) Collagenase activity of tumor lysates from the three tumor types, with and without activation of samples with trypsin. There is no significant difference between non-trypsin activated samples. Trypsin activated tumor lysates from MMP-1 and MMP-8 expressing tumors have significantly greater activity than both their non-activated counterparts and trypsin activated mock-transfected tumor lysate ($P < 0.05$ all cases). (C) Presence of inhibitors in the three tumors assessed by adding corneal collagenase to tumor lysates and measuring the change in activity compared to control. For all three tumor types, there is no significant decrease in collagenase activity compared to control. The amount of tumor lysate tested was equivalent to that used in the activity assays in (B). Mean values and standard errors shown in (B) and (C).

Effect of MMP expression on interstitial collagen

Next we assessed the effect of MMP-1 and -8 expression on tumor collagen. While the activity assays and western blot showed that the majority of the MMPs were not in the active state, even a small active fraction may have an effect on tumor collagen, especially with chronic expression throughout the course of tumor development. Several assays were performed to assess tumor collagen. First, a western blot was performed to determine the presence of cleaved collagen I in the tumor (Fig. 5.3). A polyclonal

antibody targeted to the N-terminus of the ¼ α1 fragment of MMP-cleaved collagen type I was obtained from Eunice Lee (Shriners Hospital for Children, Montreal, Canada). The specificity of the antibody to MMP-1 and -8 cleaved collagen type I was confirmed by comparing SDS/PAGE and western blots of MMP-cleaved collagen (Fig. 5.3A). The antibody is clearly specific for the N-terminal neoepitope of the ¼ αI chain of collagen I. Western blot analysis of tumor lysates detected no difference in the presence of this cleavage fragment between mock and MMP-transfected tumors (Fig. 5.3B).

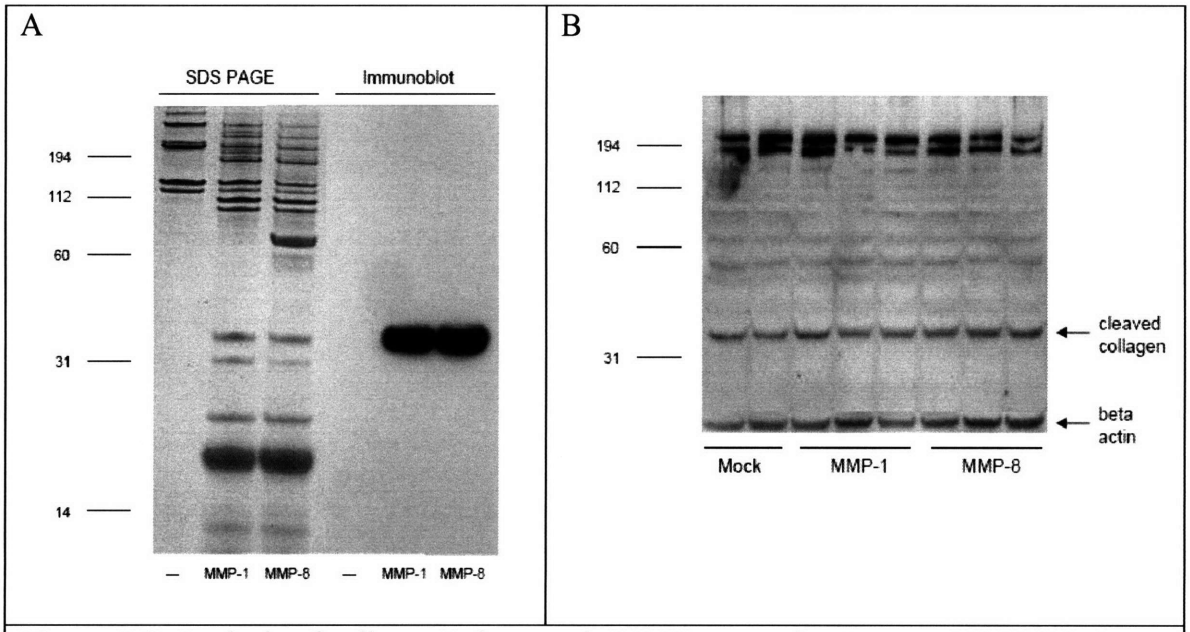

Figure 5.3. Analysis of collagen I cleavage in MMP-expressing tumors. (A) Validation of a polyclonal antibody targeted to the N-terminal neoepitope of the MMP-cleaved α1 chain of collagen type I. SDS/PAGE stained with Coomassie blue (left) and western blots (right) of intact and MMP-1 and MMP-8 cleaved collagen I. The αI and αII chains are slightly higher than the 112 kDa band of the ladder, while the ¾ cleavage fragments are slightly below it. The ¼ cleavage fragments are ~30 kDa in size. The antibody appears specific to the αI ¼ fragment of cleaved collagen I. (B) Western blots of tumor lysate

from mock and MMP-1 and -8 transfected HSTS26T tumors. A western blot of beta actin is also shown. There is no major difference in the amount of cleaved collagen between tumor types.

In a second assay to assess changes in collagen induced by MMP-1 and MMP-8 expression, tumor sections were immunostained for collagen type I. Analysis was performed on images of stained tissue sections and the fraction of tissue that was stained for collagen was compared between tumor types. There was no significant difference in the fraction between each tumor type (Fig. 5.4A). Finally, *in vivo* multiphoton imaging of second harmonic generation (SHG) was performed to determine the amount of collagen in living tumors. Consistent with the previous results, there was no significant difference in the total SHG signal between the tumor types (Fig. 5.4B). In total, these results show that MMP-1 and MMP-8 expression in HSTS26T tumors does not significantly affect interstitial fibrillar collagen.

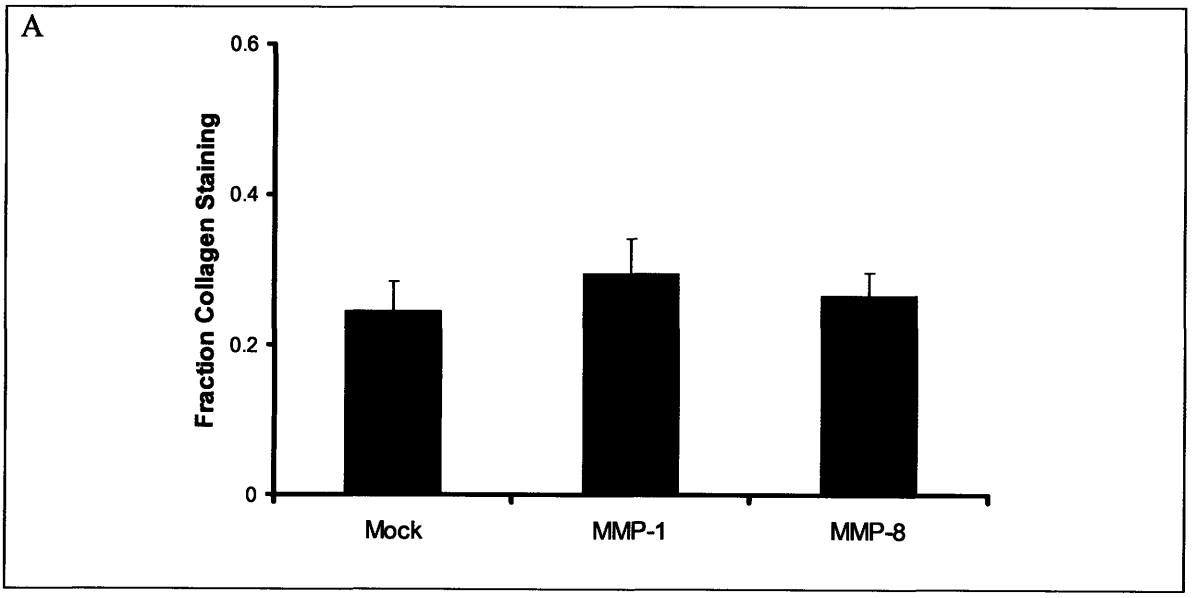

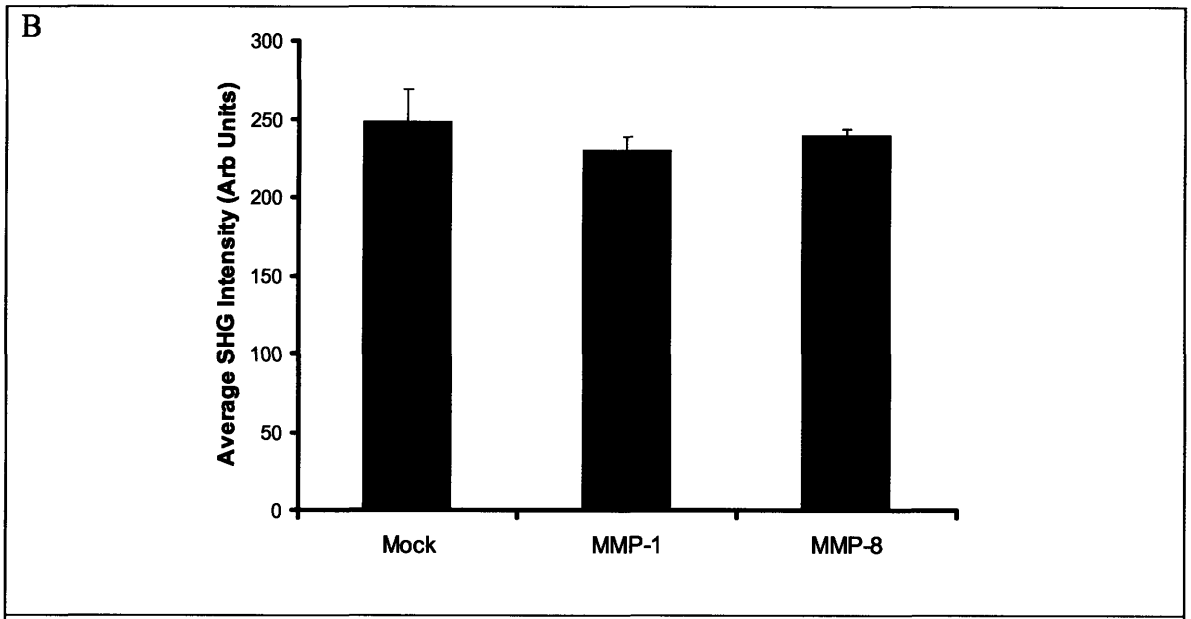

Figure 5.4. Interstitial collagen I level in MMP-expressing HSTS26T tumors. (A) Comparison of the fraction of area containing collagen I immunostaining for mock and MMP-1 and -8 transfected tumors. Image analysis was performed on maximum intensity projections of multiphoton image stacks taken for each tumor section. There is no statistically significant difference between tumor types. (B) Comparison of the average SHG signal from dorsal chamber tumors. Image stacks 130 μm deep were taken of each tumor and total SHG signal was quantified. There is no statistically significant difference between tumor types. Mean values and standard errors shown in both cases.

Effect of MMP expression on tumor GAG content

While MMP-1 and -8 expression had no major effect on collagen, this does not rule out that changes occurred in other ECM components. We next measured the effect of MMP expression on both nonsulfated GAGs (HA) and sulfated GAGs. HA content was measured by quantification of tumor tissue staining. Sulfated GAG content was assessed

biochemically using a 1,9-dimethylmethylene blue dye-binding assay. We found that there was no difference in HA content between mock and MMP-expressing tumors (Fig. 5.5B). However, MMP-1 and MMP-8 expression caused a significant reduction in sulfated GAG content (Fig. 5.5A). This is an unexpected result since MMP-1 and -8 have been traditionally identified as type I collagenases and we found that the overexpressing tumors showed little collagenase activity. However, it is not entirely surprising since these MMPs also have various other matrix substrates, the catabolism of which is not well studied or understood.

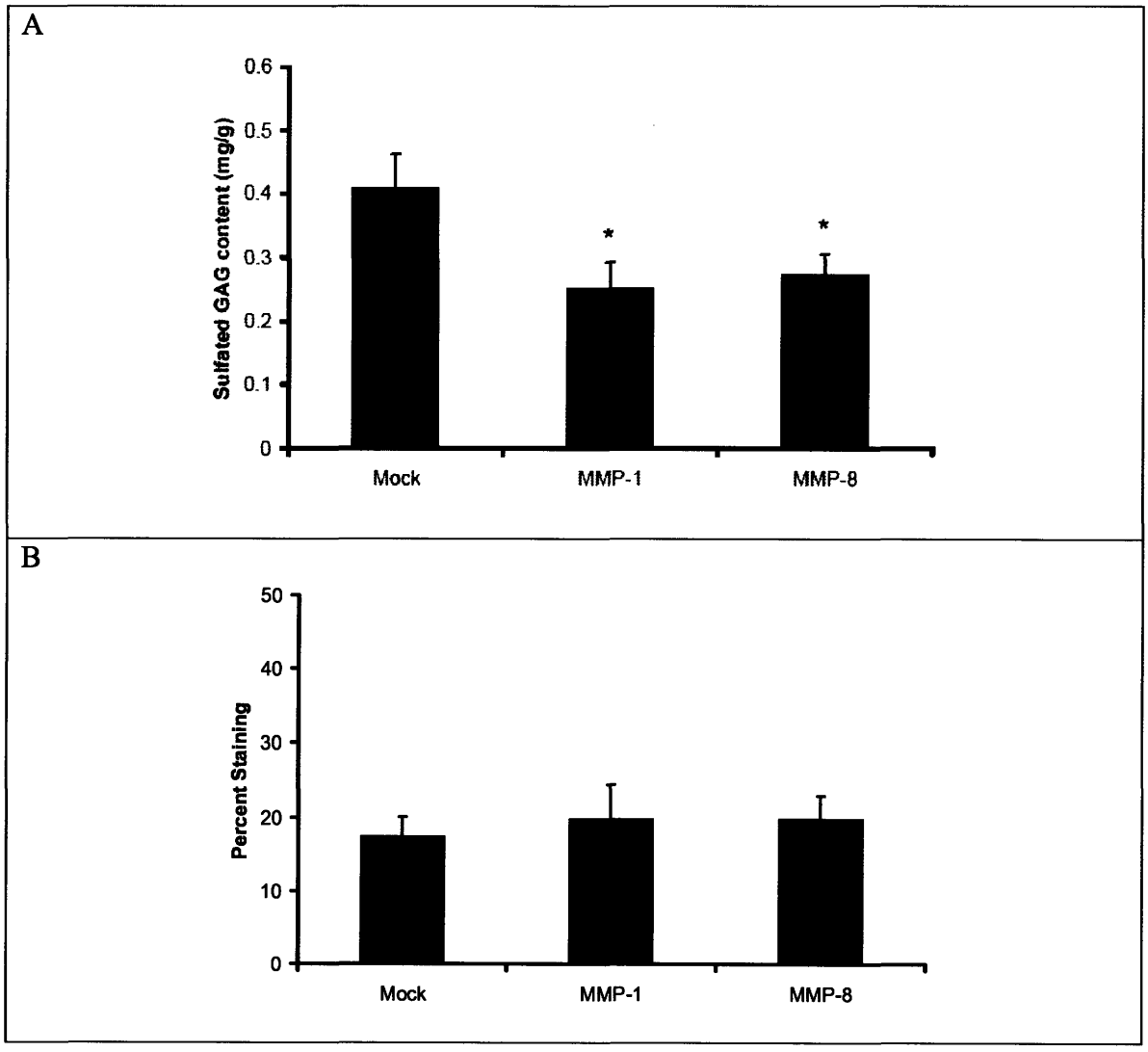

Figure 5.5. Glycosaminoglycan content in MMP-expressing tumors. (A) Tissue content of sulfated GAGs in mock and MMP-expressing HSTS26T tumors assessed with a biochemical assay. Concentrations expressed in terms of equivalent mass of hexuronic acid/g wet tissue. MMP-expressing tumors contain significantly less sGAGs than mock ($P < 0.05$). (B) Comparison of HA content in tumors by quantification of the area fraction of tissue sections containing HA staining. There is no significant difference between tumors. Mean values and standard errors shown.

Effect of MMP expression on interstitial transport

Next we assessed the effect of this change in the tumor matix induced by MMP-1 and -8 expression on interstitial transport. The diffusion coefficient of $1x10^6$ molecular weight dextran was measured with multiphoton fluorescence recovery after photobleaching for each tumor type (Fig. 5.6). No difference in the diffusion coefficient was observed between mock and MMP-transfected tumors. This result is expected, as our labs has previously shown that there is a strong correlation between diffusion and collagen content, but not GAG content (5, 6). On the other hand, it has been shown that convective transport is strongly regulated by the tissue GAG content (16, 17). Thus we also measured the hydraulic conductivity of these tumors. Indeed, we found that in MMP-1 and -8 expressing tumors, the hydraulic conductivity was more than two-fold greater than the mock-transfected (Fig. 5.7). It appears that MMP expression can enhance convective transport in tumors by depletion of sulfated GAGs.

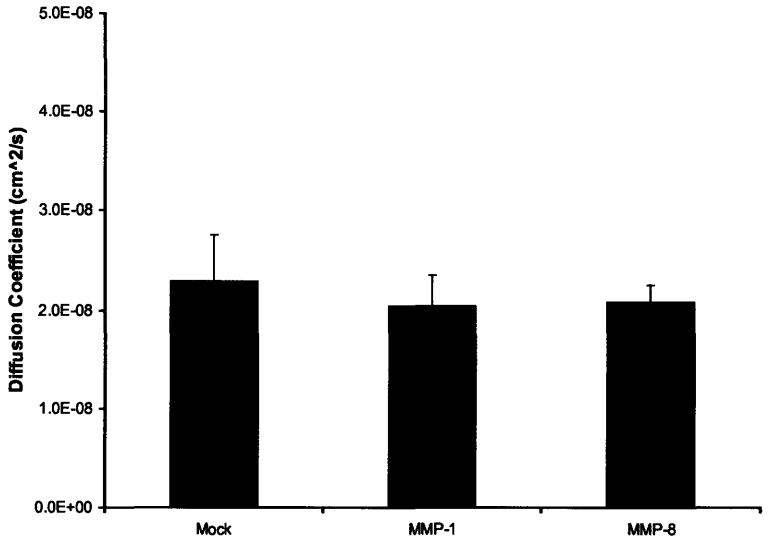

Figure 5.6. Effect of MMP expression on interstitial diffusion. The effective diffusion coefficient of $1x10^6$ molecular weight dextran in mock and MMP-1 and MMP-8 transfected HSTS26T tumors grown in the dorsal chamber was measured by MPFRAP. Mean values and standard errors shown. There is no statistically significant difference between the three tumor types.

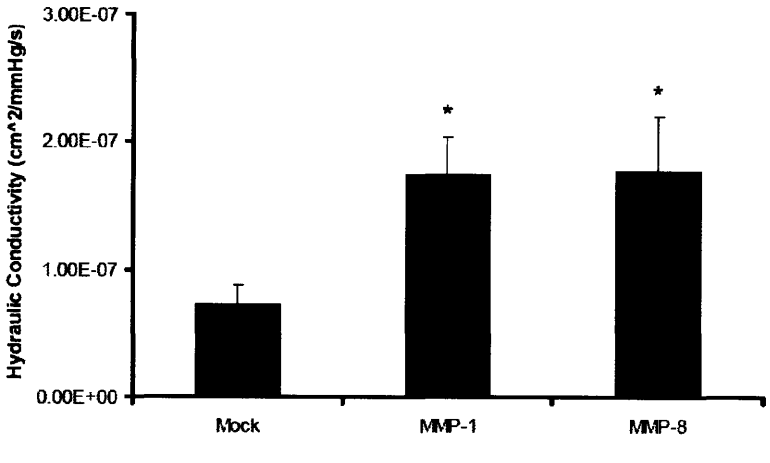

Figure 5.7. Hydraulic conductivity of MMP-expressing tumors. Mock-transfected and MMP-expressing HSTS26T tumors were grown subcutaneously and the hydraulic conductivity of tissue sections measured. Mean values and standard errors shown. MMP-1 and MMP-8 tumors exhibit a significantly greater hydraulic conductivity compared to mock ($P < 0.05$).

Effect of MMP expression on oncolytic HSV

Based on these encouraging – albeit unexpected – findings, we next sought to determine if MMP-1 and -8 expression could enhance the efficacy of oncolytic HSV therapy. In theory, an increase in hydraulic conductivity could enhance the flow of intratumorally injected HSV particles into the tumor tissue, improving distribution and efficacy. To test this hypothesis, mock and MMP-expressing HSTS26T tumors were grown subcutaneously in the leg of SCID mice. For all three groups, tumors were treated with two intratumor injections of either 2.5×10^6 t.u. of the oncolytic HSV vector MGH2 or PBS control. Tumor growth in each of the six groups was monitored following treatment and the time for tumors to grow to ten times the size at treatment was compared (Fig. 5.8). Tumor growth was significantly delayed in the treatment group compared to control in only MMP-1 and MMP-8 expressing tumors and not in the mock-transfected tumors.

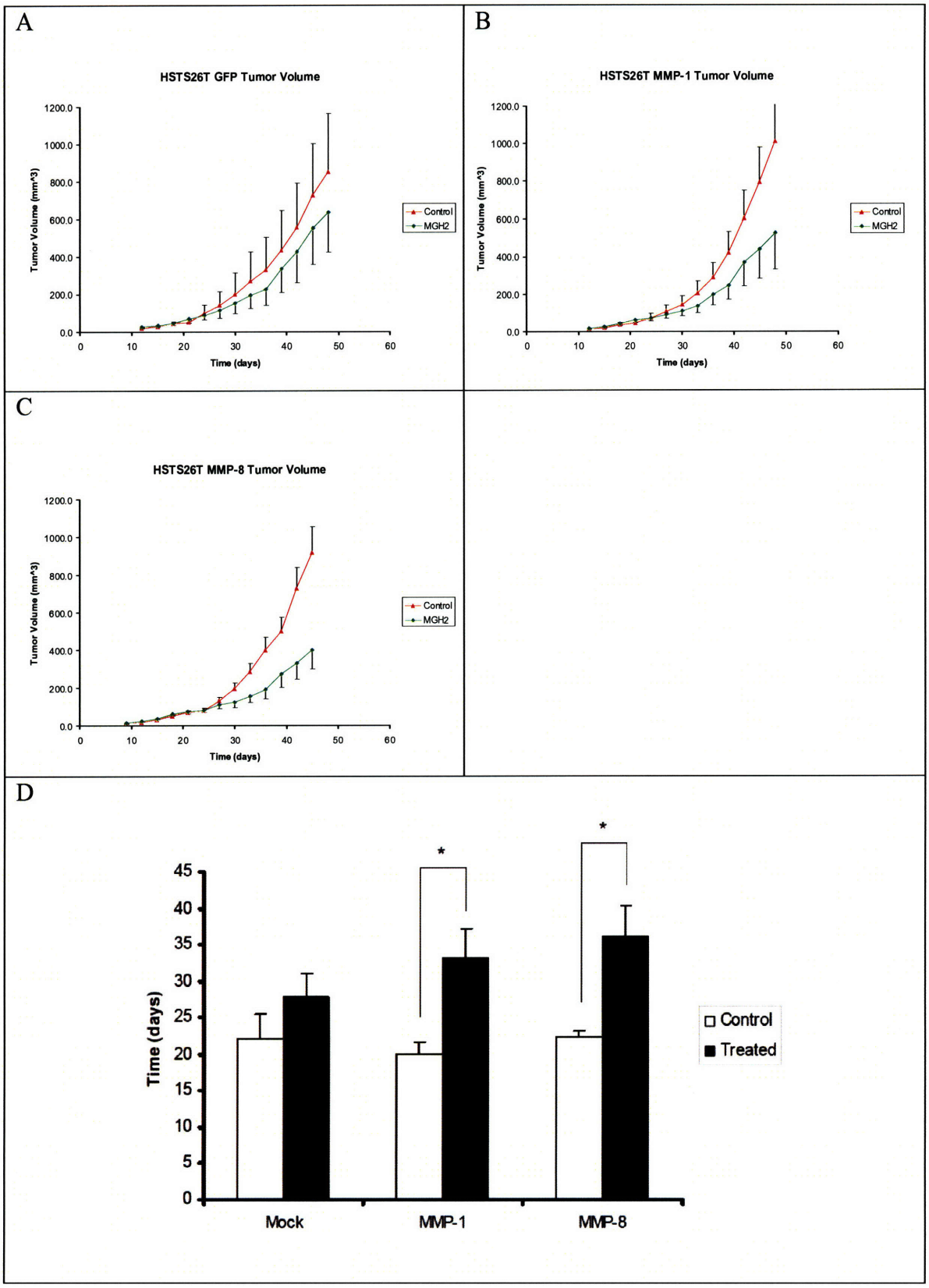
A
HSTS26T GFP Tumor Volume
Tumor Volume (mm^3)
Time (days)
Control
MGH2
B
HSTS26T MMP-1 Tumor Volume
Tumor Volume (mm^3)
Time (days)
Control
MGH2
C
HSTS26T MMP-8 Tumor Volume
Tumor Volume (mm^3)
Time (days)
Control
MGH2
D
Time (days)
Mock
MMP-1
MMP-8
Control
Treated
*
*

Figure 5.8. Effect of MMP expression in HSTS26T tumors on oncolytic HSV-induced growth delay. (A-C) Mean tumor volume of treated (green) and non-treated (red) mock transfected (A), MMP-1 expressing (B) and MMP-8 expressing (C) HSTS26T tumors. (D) Comparison of time for tumors to reach ten times the initial size at treatment. Mean and standard errors shown. Mock transfected tumors show no significant growth delay for MGH2-treated tumors. MMP-1 and MMP-8 expressing tumors showed a significant growth delay between control and MGH2-treated tumors ($P < 0.05$). Mean values and standard errors shown in all cases.

To gain insight into the differential response to MGH2 treatment and to determine if this effect is indeed transport-related, HSV immunostaining was performed on tumors 7 days following treatment with a single injection of MGH2. In mock-transfected HSTS26T cells, HSV particles were present only in the periphery of the tumor. In contrast, for MMP-1 and MMP-8 expressing tumors, HSV particles were located in both the periphery and center of the tumor (Fig. 5.9A). The fraction of tumor area containing HSV staining was quantified (Fig. 5.9B). As expected from the growth delay results, MMP-expressing tumors had significantly more HSV staining than mock. When the tissue HSV staining was subdivided into "periphery" and "middle" subfractions, we found that the majority of the difference was due to the increase in HSV staining in the middle of the MMP-expressing tumor sections. The lack of HSV staining in the center of the mock-transfected tumor sections is interesting since MGH2 was injected directly into the center of the tumors. It appears that in mock-transfected tumors, virus found preferential pathways through the tumor and distributed outside of the tumor, rather than in the

center. Thus infection is only observed at the edge of the tissue section. This could occur with HSTS26T, which has been found to be a very stiff tumor, with high resistance to fluid flow leading to highly non-uniform distributions of infused agents (18). By reducing the resistance to fluid flow, MMP-1 and -8 expression has allowed for greater distribution of injected virus in the center of these tumors around the needle tip.

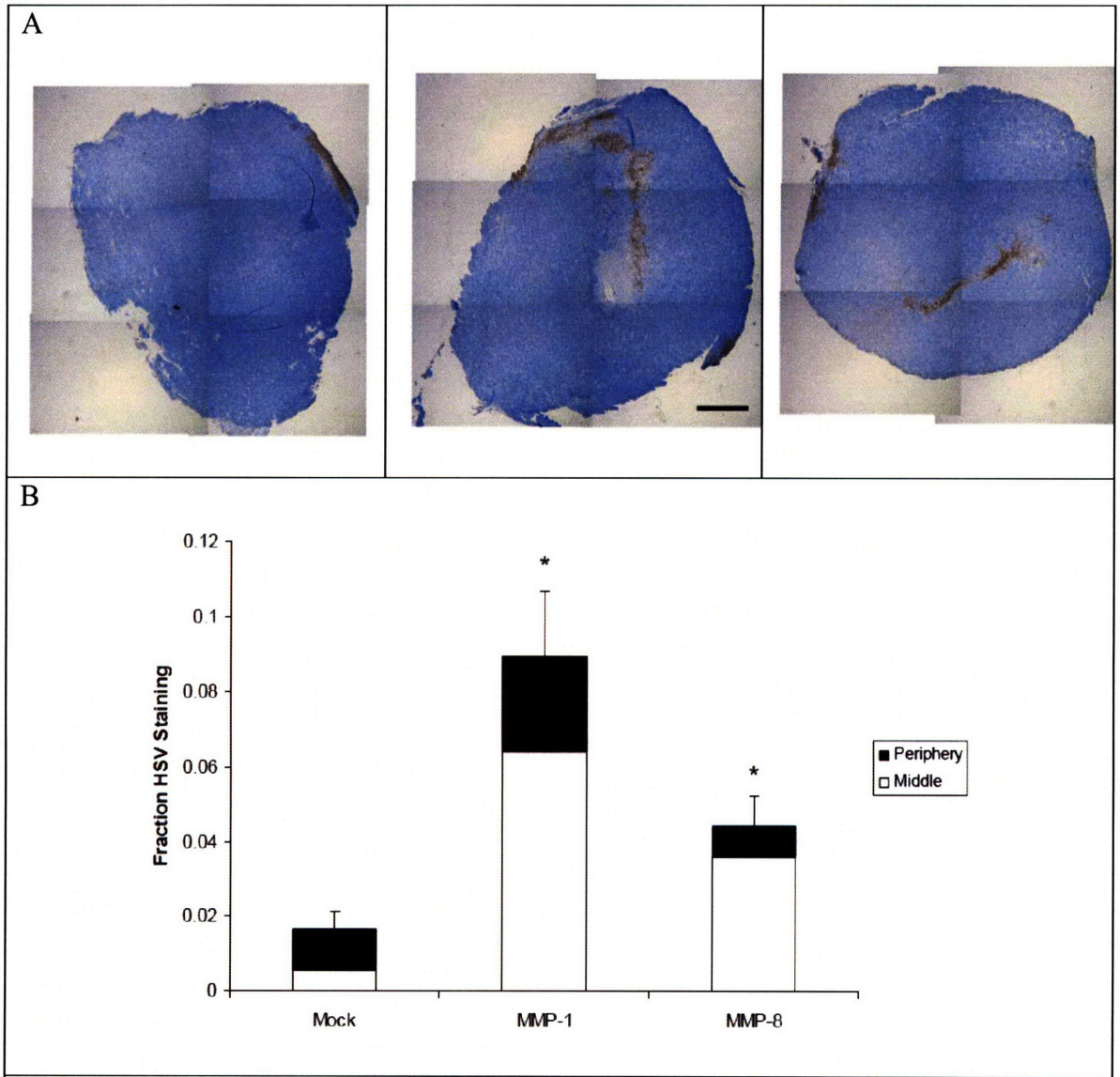

Figure 5.9. HSV staining of MGH2-treated tumors. (A) Representative images of HSV-1 (brown) and nuclei (blue) staining 7 days following intratumor injection of MGH2. Mock

transfected (left), MMP-1 expressing (middle) and MMP-8 expressing (right) tumors. Tissues sections are taken from the center of the tumor, perpendicular to the needle tip. The scale bar in the middle panel is 1 mm. While HSV staining is found in the center of MMP-1 and MMP-8 expressing tumors, it is found only in the periphery of the mock transfected. (B) Quantification of HSV staining. The total area of tissue stained for HSV and the fraction found in the periphery and middle of the sections were quantified. Mean values and standard errors shown. MMP-expressing tumors have significantly greater HSV staining than mock transfected ($P < 0.05$) and show a dramatic increase in the fraction in the middle of the tumor section.

Effect of MMP expression on cell proliferation and HSV infectivity

Since MMPs can have pleiotropic effects – sometimes playing a role in cell signaling as well as matrix catabolism – it is important to determine if MMP-1 and -8 expression induced any biological response in these tumors. First we tested whether MMP-1 and MMP-8 expression affected cell proliferation and tumor growth. Analysis of the rate of tumor growth for control treated tumors showed that MMP expression did not have a significant effect (Fig. 5.8A). A WST-1 assay showed that cell proliferation and viability *in vitro* are also not affected by MMP-1 or -8 expression (Fig. 5.10A). Next we tested if the MMP-transfected cells differ from the mock-transfected in either HSV infectivity or burst size. The viral titer of the three cell lines 48 hours following infection at an MOI of 0.1 was compared. There was no significant difference between mock and MMP-transfected cells (Fig. 5.10B). These results show that the enhanced response of MMP-1

and -8 expressing tumors to oncolytic HSV is not due to a modulation in cell viability or the infectivity of HSV. Rather it appears that MMP expression enhances the therapeutic effect of oncoltyic HSV by increasing the hydraulic conductivity and improving the distribution of virus in the tumor.

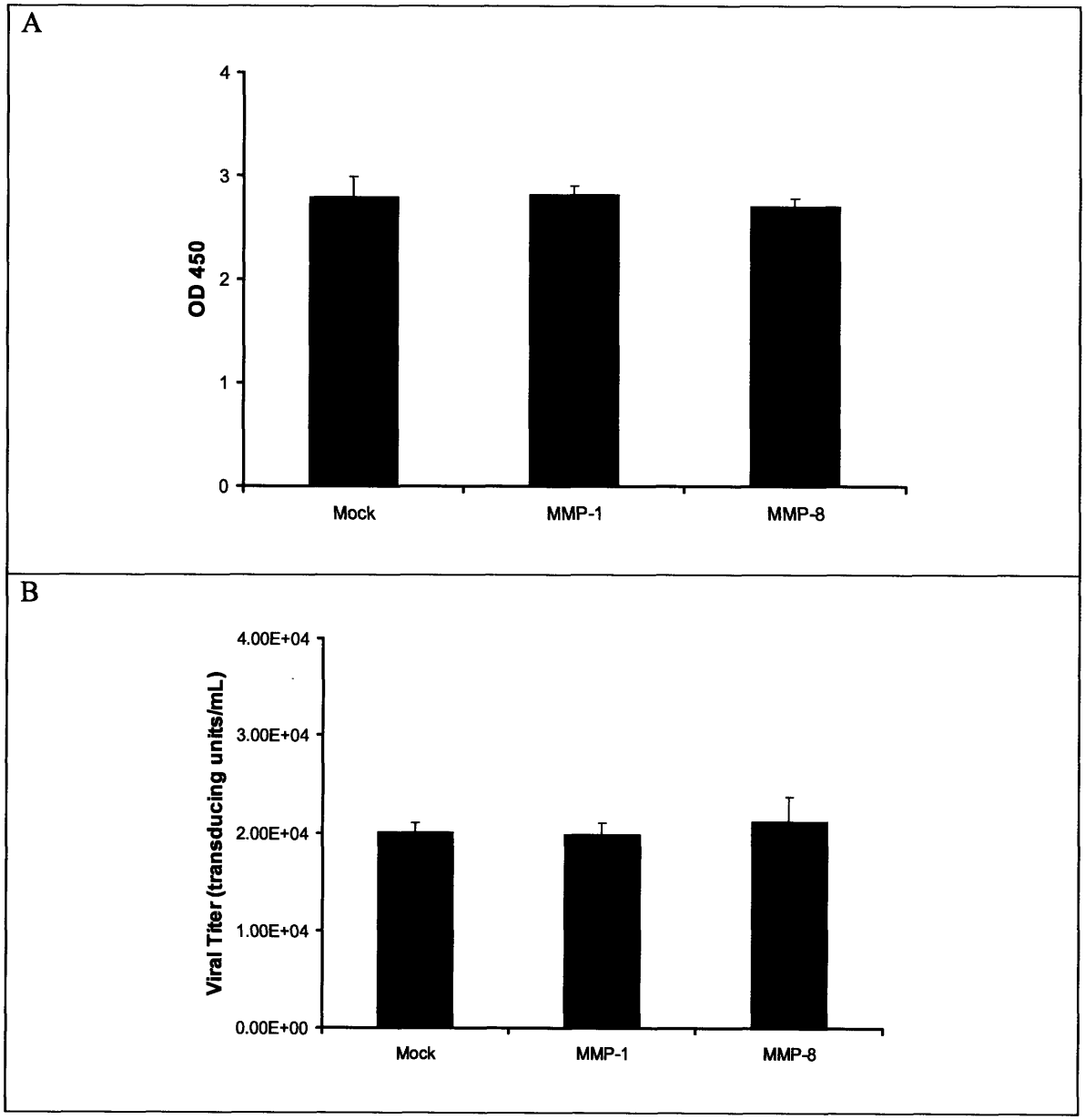

Figure 5.10. Effect of MMP-1 and -8 expression on HSTS26T cell proliferation and response to MGH2 infection. (A) WST-1 cell proliferation assay performed on mock, MMP-1 and MMP-8 transfected cells. Cells were allowed to grow for 48 hours following seeding and the absorbance of 450 nm light was measured following application of WST-1. There is no significant difference between cell lines. (B) Comparison of the viral titer 48 hours following infection at an MOI of 0.1. There is no significant difference between cell lines. Mean values and standard errors shown in both cases.

MMP-expressing oncolytic HSV vectors

Finally, in order to apply the matrix-modifying approach in a clinically-relevant manner, we generated novel oncolytic HSV vectors which express either MMP-1 or MMP-8. While the MMP-expressing tumors are valuable experimental tools, stable transfection of tumor cells in this manner is obviously not a feasible approach in the clinic. The alternative is to generate oncolytic HSV vectors which contain expression cassettes for these MMPs. When tumors are treated with these vectors, MMP-1 or MMP-8 will be expressed and secreted from infected tumor cells prior to their lysis. We applied the HSVQuik system developed by Terada *et al.* (12) to generate these oncolytic vectors. The three vectors generated (HsvQ1 expressing no transgene, HsvQ1-MMP-1 expressing MMP-1 and HsvQ1-MMP-8 expressing MMP-8) are similar to MGH2 in that they contain deletions in both copies of the *γ34.5* gene and transgene insertion at the *UL39* locus. First, we confirmed expression of MMP-1 and MMP-8 in cells infected with these recombinant vectors (Fig. 5.11A). Then we treated wild type HSTS26T tumors with each

of these three vectors to assess if MMP-expression from infected cells could enhance the transport of the viral vectors and overall treatment effectiveness. We found that there was no significant difference in tumor growth between treatment groups (Fig. 5.11B,C).

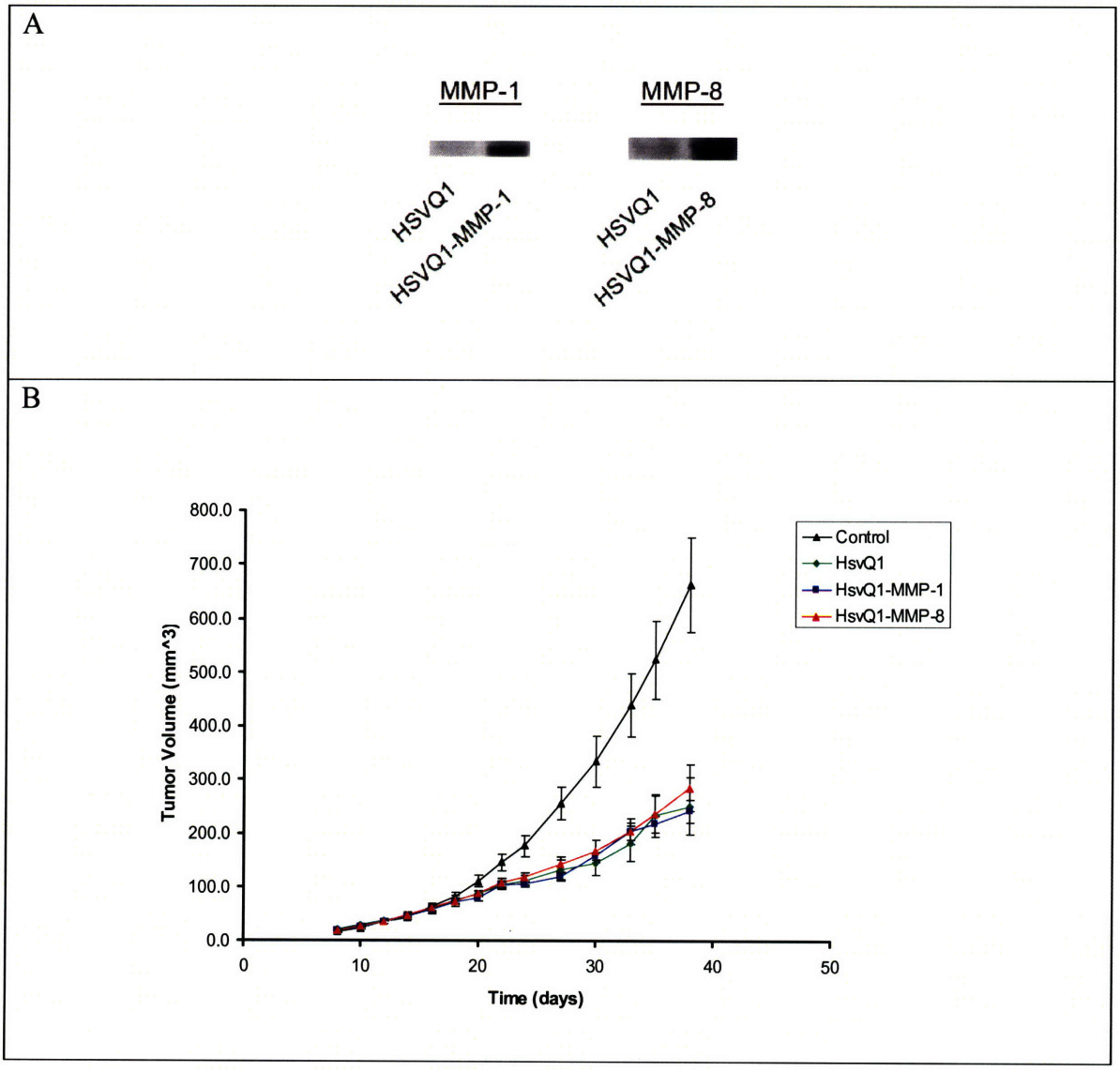

C

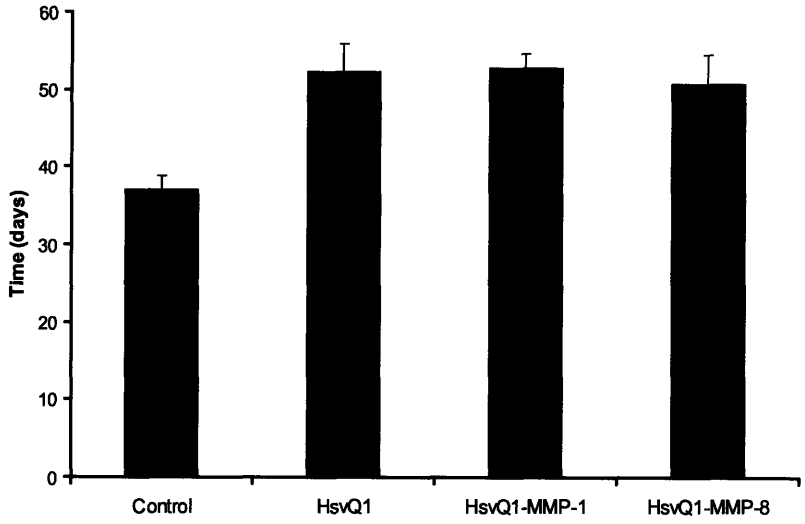

Figure 5.11. Treatment of HSTS26T tumors with MMP-expressing oncolytic HSV vectors. (A) Confirmation of MMP expression in infected cells. Vero cells were infected with either recombinant oncolytic HSV vector HsvQ1 or HsvQ1 variants which express MMP-1 (HsvQ1-MMP-1) and MMP-8 (HsvQ1-MMP-8). MMP-1 (left) and MMP-8 (right) western blots were performed. Significant amounts of MMP-1 and MMP-8 were observed in HsvQ1-MMP-1 and HsvQ1-MMP-8 infected cells, respectively, compared to control. (B-C) Wild type HSTS26T tumors were grown subcutaneously in the leg of SCID mice and treated with two intratumor injections of either PBS, HsvQ1, HsvQ1-MMP-1 or HsvQ1-MMP-8. (B) Mean tumor volume of treated and control tumors. (C) Growth delay induced by oncolytic HSV treatment, given as the time for the tumor to grow to ten times the size at treatment. There is no significant difference in the growth delay between HsvQ1 and HsvQ1-MMP-1 or HsvQ1-MMP-8 treated tumors. Mean values and standard errors shown.

Discussion

Enzyme activity in MMP-expressing tumors

Using multiple methods we have shown that MMP-1 and -8 expression in HSTS26T tumors does not lead to significant changes in tumor collagen. Inhibition of collagenase activity by TIMPs has been ruled out as the cause since our activity assay showed no inhibition of corneal collagenase activity by any of the three tumor lysates. Western blot analysis shows that only a small proportion of the enzyme is in the active state. When an activating agent was added to tumor lysates, the activity in these samples increased significantly. These data suggest that the likely reason why changes in tumor collagen were not observed is because the secreted enzymes are insufficiently activated. However, one other possibility is that MMP-1 and -8 are being activated but simply are not particularly potent collagenases *in vivo*, at least with respect to the amount of degradation desired for our application. These MMPs exists in three main structural states: zymogen, active form and intramolecularly degraded inactive form (19, 20). It may be that the steady state concentration of active enzyme is low even in the presence of copious amounts of activating agents, resulting in a faint active enzyme band on western blots and low "instantaneous" activity in our collagenase assays. Then why did we not observe changes in tumor collagen? Well, we have been using as a standard for significant changes in collagen the amount of degradation induced by bacterial collagenase treatment. However, we have found that bacterial collagenase is a significantly more effective collagenase than either MMP-1 or MMP-8 both *in vitro* and *in vivo* when they are delivered as recombinant proteins. Bacterial collagenase differs in its collagenolytic

activity than MMP-1 and -8: it cleaves at multiple sites rather than one and possesses potent gelatinase activity (21-24). Thus, it is possible that MMP-1 and -8, by themselves, may not be able to induce similar dramatic changes in tumor fibrillar collagen.

Regardless of whether insufficient activation or lack of potency is the main cause of limited collagen degradation, collagenolysis can likely be improved by increasing the proportion of MMP-1 and -8 found in the active state. There are several approaches to accomplish this. An indirect method is to grow MMP-expressing tumors in host tissues which are more likely to contain proteases which can activate the latent enzymes. Both MMP-1 and -8 have been successfully used to treat liver fibrosis (25, 26). In these studies, latent MMP-1 and -8 delivered via adenoviral vectors were activated in the liver and led to a significant reduction in collagen. This suggests that tumors grown in the liver may be amenable to treatment with collagenases. A more direct application of this approach is to combine MMP expression with application of an activating agent. *In vitro* studies have identified a host of enzymes and chemicals which can activate MMP-1 and -8 (27-32). The difficulty with this approach is that these agents can be toxic (*e.g.* APMA), require proteolytic activation themselves (*e.g.* MMP-3) or have ECM substrates, themselves (*e.g.* trypsin), which can lead to confounding and unwanted effects. The most promising approach may be to modify these MMPs genetically. These MMPs have a unique domain structure which lends them to genetic manipulation to attain constitutively active forms. The generation of such mutant forms of MMP-1 and -8 is the focus of the following chapter.

HSV distribution in MMP-expressing tumors

The observation that HSV vectors showed minimal distribution around the site of injection in the center of the tumor is not entirely surprising given the low hydraulic conductivity in these tumors. Netti *et al.* measured the elastic modulus and hydraulic conductivity in four tumors and found that HSTS26T was the hardest and had the greatest resistance to flow (5). Our measurement of the hydraulic conductivity of HSTS26T using the tissue clamp method concurs with the measurement in that study from confined compression tests. The extreme stiffness of this tumor likely causes the unique distribution of injected agents. Boucher *et al.* found that when they infused Evans blue-labeled albumin into the center of HSTS26T tumors at a flow rate of 0.05 μl/min, it distributed asymmetrically from the source and often in necrotic regions (18). Fluid accumulation was found away from the infusion site – including at the surface of tumors – with channels of fluid connecting regions of accumulation. Limited necrosis was observed in the tumors studied in this work, likely because *in vitro* measurements were performed on relatively small tumors (100-200 mm^3) to match the size at treatment with oncolytic HSV. However, the pattern of flow of fluid through preferential pathways rather than bulk flow to the surrounding tissue is consistent with their findings. When the authors of this study performed similar injections in the colon adenocarcinoma LS174T, which has a 5-fold greater hydraulic conductivity than HSTS26T, they found that dye distributed symmetrically around the infusion needle in the center of the tumor. Thus, our results suggest that an increase in hydraulic conductivity in this tumor – which is particularly stiff and resistant to fluid flow – can significantly enhance the delivery of injected viral vectors.

What causes this change in hydraulic conductivity? Fluid flow is believed to be regulated chiefly by the GAG content of the tissue (16, 17). Both Swabb *et al.* and Levick showed a strong negative correlation between tissue GAG concentration and hydraulic conductivity (14, 33). In particular, the non-sulfated GAG HA has been found to be a significant source of hindrance to fluid flow (34, 35). However, Levick's analysis shows that GAGs alone – or even GAGs and collagen alone – cannot account for all of the resistivity to fluid flow in most tissues. When corneal stroma was treated with both trypsin and hyaluronidase, trypsin caused a greater depletion of sulfated GAGs and greater increase in hydraulic conductivity (34). Unlike hyaluronidase, trypsin is a protease with broad substrate specificity that can act on proteoglycan core proteins as well as glycoproteins. Thus, this study suggests that perhaps GAGs other than HA – the sulfated GAGs – and other glycoproteins may affect tissue hydraulic conductivity. It is possible that MMP expression increased hydraulic conductivity by modifying one of these components.

While both MMP-1 and MMP-8 are commonly known as type I collagenases, they have multiple other ECM substrates (4). Degradation of an alternative substrate – perhaps even one yet to be identified – may be responsible for the change in hydraulic conductivity that was observed with the MMP-overexpressing tumors. Both MMP-1 and MMP-8 have been shown to be able to degrade the proteoglycan aggrecan (36). Aggrecan contains both chondroiton sulfate and keratin sulfate chains and up to 100 monomers interact with hyaluronic acid via an N-terminal globular domain (37-39). Cleavage occurs in the interglobular domain near the HA binding site, releasing the portion of the core protein that is GAG-bound. Aggrecan is found mainly in cartilage, where its complex with HA creates a hydrated, space-filling gel that plays a role in cyclical load bearing. While

aggrecan is not typically found in neoplastic tissue, tumors are often found to have elevated levels of other chondroiton sulfate proteoglycans (40-42). The likely proteoglycan found in tumors is versican, which is in the same family of proteoglycans as aggrecan, has a similar domain structure and binds HA to form aggregates (43). While versican has yet to be explored as a substrate for MMP-1 or -8, link protein – which stabilizes the interaction of both aggrecan and versican with HA – has been found to be cleaved by MMP-1 (44). Furthermore, aggrecanases of the ADAMTS (a disintegrin and metalloprotease with thrombospondin type 1 motifs) family of proteases have been found to be able to cleave versican, as well (45-48). These results suggest that degradation of proteoglycans in the MMP-1 and -8 expressing tumors is possible. However, there are a host of other candidate ECM proteins whose degradation may lead to alteration of tumor hydraulic conductivity, since these MMPs have been found to cleave various other fibrillar collagens (49-52) and glycoproteins (53-56).

The finding that convective transport was enhanced by MMP-1 and -8 expression but not diffusive transport is consistent with the change observed in tumor GAG but not collagen. We have previously shown that there is a positive correlation between tumor collagen content and both diffusive hindrance (57, 58) and resistance to flow (59). However, disruption of tumor GAG with hyaluronidase has been shown to increase hydraulic conductivity in various tissue (16, 34, 60), but has been found to only slightly affect diffusive transport, and in the opposite direction (Trevor McKee, personal communication). Furthermore, Netti *et al.* measured hydraulic conductivity and the diffusion coefficient of tracer molecules in a panel of tumors and found that there was no strong correlation between diffusive and convective transport in a given tumor (5). It is

becoming increasingly clear that collagen and GAGs play an interconnected role in regulating interstitial transport and that there are no simple relationships connecting collagen with diffusion and GAGs with convection.

Implications for tumor therapy

While the novel MMP-expressing oncolytic HSV vectors developed in this study showed no improvement over the wild type vector, this result is not entirely discouraging and in fact supports the other findings about the effect of MMP expression on tumor interstitial transport. Our results suggest that chronic MMP-1 and -8 expression improves the initial delivery of virus – by enhancing convection into the tissue during intratumor injection – but would not significantly enhance subsequent propagation, which is affected by diffusion rather than convection. With the recombinant vectors, MMPs are not expressed until after the initial infection of tumor cells. Thus, the initial distribution would be expected to be similar to that of virus injected into the mock-transfected tumors. The subsequent distribution of progeny virus and therapeutic efficacy would not be enhanced since MMP expression does not significantly affect diffusion and also because the poor initial distribution into the periphery of the tumor limits the number of initially infected cells.

These results point to the importance of initial virus distribution in determining overall treatment outcome, a phenomenon we and others have previously observed (1, 61). Therefore, optimizing intratumoral infusion parameters is a promising method to improve the distribution and efficacy of therapeutics. Bobo *et al.* have shown that the use of prolonged infusion can enhance the delivery of macromolecules to the brain, and that the

distribution can be further improved by increasing the volume of infusion (62). However, this may not be a viable method for all tumors. For example, this work as well as the study of Boucher *et al.* (18) show that certain tumors have a matrix composition and structure which makes it difficult to achieve adequate convection during infusion. The findings in this chapter establish a novel technique which may substantially improve the treatment of such tumors. By modifying the tumor, itself, with matrix degrading proteases such as MMPs, the distribution of therapeutic agents during infusion may be enhanced.

Despite this encouraging result, our findings also suggest that there is much room for improvement. The collagenase activity assays showed that the MMPs expressed in these tumors were predominantly in the inactive state. Overcoming this activation barrier may have two positive effects: (1) an increase in collagenase activity which could improve diffusive transport in the interstitium; (2) enhancement of sulfated GAG depletion which could further augment convective transport during intratumor infusion. If such techniques to activate MMPs can be developed, the concept of incorporating matrix proteases into oncolytic viruses to improve the spread of progeny virus may find greater success than achieved here. Using genetic modifications to enhance the ability of MMP-1 and -8 to degrade ECM components and improve diffusive and convective transport is the focus of the next chapter.

References

1. McKee TD, Grandi P, Mok W, *et al.* Degradation of fibrillar collagen in a human melanoma xenograft improves the efficacy of an oncolytic herpes simplex virus vector. Cancer Res 2006 Mar 1;66(5):2509-13.
2. Ohlfest JR, Freese AB, Largaespada DA. Nonviral vectors for cancer gene therapy: prospects for integrating vectors and combination therapies. Curr Gene Ther 2005 Dec;5(6):629-41.
3. Chiocca EA. Oncolytic viruses. Nat Rev Cancer 2002 Dec;2(12):938-50.
4. Sternlicht MD, Werb Z. How matrix metalloproteinases regulate cell behavior. Annu Rev Cell Dev Biol 2001;17:463-516.
5. Netti PA, Berk DA, Swartz MA, Grodzinsky AJ, Jain RK. Role of extracellular matrix assembly in interstitial transport in solid tumors. Cancer Res 2000 May 1;60(9):2497-503.
6. Pluen A, Boucher Y, Ramanujan S, *et al.* Role of tumor-host interactions in interstitial diffusion of macromolecules: cranial vs. subcutaneous tumors. Proc Natl Acad Sci U S A 2001 Apr 10;98(8):4628-33.
7. Leunig M, Yuan F, Menger MD, *et al.* Angiogenesis, microvascular architecture, microhemodynamics, and interstitial fluid pressure during early growth of human adenocarcinoma LS174T in SCID mice. Cancer Res 1992 Dec 1;52(23):6553-60.
8. Au P, Tam, J., Fukumura, D., Jain, R. K. Small Blood Vessel Engineering. In: Hauser H, Fussenegger, M., editor. Tissue Engineering. Totowa, N.J.: Humana Press; 2007.
9. Johnson-Wint B. A quantitative collagen film collagenase assay for large numbers of samples. Anal Biochem 1980 May 1;104(1):175-81.
10. Moses MA, Sudhalter J, Langer R. Identification of an inhibitor of neovascularization from cartilage. Science 1990 Jun 15;248(4961):1408-10.
11. Brown EB, Campbell RB, Tsuzuki Y, *et al.* In vivo measurement of gene expression, angiogenesis and physiological function in tumors using multiphoton laser scanning microscopy. Nat Med 2001 Jul;7(7):864-8.
12. Terada K, Wakimoto H, Tyminski E, Chiocca EA, Saeki Y. Development of a rapid method to generate multiple oncolytic HSV vectors and their in vivo evaluation using syngeneic mouse tumor models. Gene Ther 2006 Apr;13(8):705-14.
13. Brown EB, Wu ES, Zipfel W, Webb WW. Measurement of molecular diffusion in solution by multiphoton fluorescence photobleaching recovery. Biophys J 1999 Nov;77(5):2837-49.
14. Swabb EA, Wei J, Gullino PM. Diffusion and convection in normal and neoplastic tissues. Cancer Res 1974 Oct;34(10):2814-22.
15. Farndale RW, Sayers CA, Barrett AJ. A direct spectrophotometric microassay for sulfated glycosaminoglycans in cartilage cultures. Connect Tissue Res 1982;9(4):247-8.
16. Day T. The permeability of interstitial connective tissue and the nature of the interfibrillary substance. J Physiol 1952;117:1-8.
17. Ogston AG, Sherman TF. Effects of hyaluronic acid upon diffusion of solutes and flow of solvent. J Physiol 1961 Apr;156:67-74.

18. Boucher Y, Brekken C, Netti PA, Baxter LT, Jain RK. Intratumoral infusion of fluid: estimation of hydraulic conductivity and implications for the delivery of therapeutic agents. Br J Cancer 1998 Dec;78(11):1442-8.
19. Knauper V, Osthues A, DeClerck YA, Langley KE, Blaser J, Tschesche H. Fragmentation of human polymorphonuclear-leucocyte collagenase. Biochem J 1993 May 1;291 (Pt 3):847-54.
20. O'Hare MC, Curry VA, Mitchell RE, Cawston TE. Stabilisation of purified human collagenase by site-directed mutagenesis. Biochem Biophys Res Commun 1995 Nov 2;216(1):329-37.
21. Bond MD, Van Wart HE. Characterization of the individual collagenases from Clostridium histolyticum. Biochemistry 1984 Jun 19;23(13):3085-91.
22. Bond MD, Van Wart HE. Purification and separation of individual collagenases of Clostridium histolyticum using red dye ligand chromatography. Biochemistry 1984 Jun 19;23(13):3077-85.
23. Gross J, Harper E, Harris ED, *et al.* Animal collagenases: specificity of action, and structures of the substrate cleavage site. Biochem Biophys Res Commun 1974 Nov 27;61(2):605-12.
24. Hasty KA, Wu H, Byrne M, *et al.* Susceptibility of type I collagen containing mutated alpha 1(1) chains to cleavage by human neutrophil collagenase. Matrix 1993 May;13(3):181-6.
25. Iimuro Y, Nishio T, Morimoto T, *et al.* Delivery of matrix metalloproteinase-1 attenuates established liver fibrosis in the rat. Gastroenterology 2003 Feb;124(2):445-58.
26. Siller-Lopez F, Sandoval A, Salgado S, *et al.* Treatment with human metalloproteinase-8 gene delivery ameliorates experimental rat liver cirrhosis. Gastroenterology 2004 Apr;126(4):1122-33; discussion 949.
27. Knauper V, Murphy G, Tschesche H. Activation of human neutrophil procollagenase by stromelysin 2. Eur J Biochem 1996 Jan 15;235(1-2):187-91.
28. Knauper V, Wilhelm SM, Seperack PK, *et al.* Direct activation of human neutrophil procollagenase by recombinant stromelysin. Biochem J 1993 Oct 15;295 (Pt 2):581-6.
29. Blaser J, Knauper V, Osthues A, Reinke H, Tschesche H. Mercurial activation of human polymorphonuclear leucocyte procollagenase. Eur J Biochem 1991 Dec 18;202(3):1223-30.
30. Suzuki K, Nagase H, Ito A, Enghild JJ, Salvesen G. The role of matrix metalloproteinase 3 in the stepwise activation of human rheumatoid synovial procollagenase. Biol Chem Hoppe Seyler 1990 May;371 Suppl:305-10.
31. Knauper V, Kramer S, Reinke H, Tschesche H. Characterization and activation of procollagenase from human polymorphonuclear leucocytes. N-terminal sequence determination of the proenzyme and various proteolytically activated forms. Eur J Biochem 1990 Apr 30;189(2):295-300.
32. Imai K, Yokohama Y, Nakanishi I, *et al.* Matrix metalloproteinase 7 (matrilysin) from human rectal carcinoma cells. Activation of the precursor, interaction with other matrix metalloproteinases and enzymic properties. J Biol Chem 1995 Mar 24;270(12):6691-7.
33. Levick JR. Flow through interstitium and other fibrous matrices. Q J Exp Physiol 1987 Oct;72(4):409-37.

34. Hedbys BO. Corneal resistance of the flow of water after enzymatic digestion. Exp Eye Res 1963 Apr;2:112-21.
35. Lai-Fook SJ, Rochester NL, Brown LV. Effects of albumin, dextran, and hyaluronidase on pulmonary interstitial conductivity. J Appl Physiol 1989 Aug;67(2):606-13.
36. Fosang AJ, Last K, Knauper V, *et al.* Fibroblast and neutrophil collagenases cleave at two sites in the cartilage aggrecan interglobular domain. Biochem J 1993 Oct 1;295 (Pt 1):273-6.
37. Iozzo RV. Matrix proteoglycans: from molecular design to cellular function. Annu Rev Biochem 1998;67:609-52.
38. Muir H. The chondrocyte, architect of cartilage. Biomechanics, structure, function and molecular biology of cartilage matrix macromolecules. Bioessays 1995 Dec;17(12):1039-48.
39. Vertel BM, Ratcliffe A. Aggrecan. In: Iozzo RV, editor. Proteoglycans: Structure, Biology, and Molecular Interactions. New York: Marcel Dekker, Inc.; 2000. p. 343-77.
40. Alini M, Losa GA. Partial characterization of proteoglycans isolated from neoplastic and nonneoplastic human breast tissues. Cancer Res 1991 Mar 1;51(5):1443-7.
41. Esko JD, Rostand KS, Weinke JL. Tumor formation dependent on proteoglycan biosynthesis. Science 1988 Aug 26;241(4869):1092-6.
42. Yeo TK, Brown L, Dvorak HF. Alterations in proteoglycan synthesis common to healing wounds and tumors. Am J Pathol 1991 Jun;138(6):1437-50.
43. Zimmermann DR. Versican. In: Iozzo RV, editor. Proteoglycans: Structure, Biology, and Molecular Interactions. New York: Marcel Dekker, Inc.; 2000. p. 327-41.
44. Nguyen Q, Murphy G, Hughes CE, Mort JS, Roughley PJ. Matrix metalloproteinases cleave at two distinct sites on human cartilage link protein. Biochem J 1993 Oct 15;295 (Pt 2):595-8.
45. Abbaszade I, Liu RQ, Yang F, *et al.* Cloning and characterization of ADAMTS11, an aggrecanase from the ADAMTS family. J Biol Chem 1999 Aug 13;274(33):23443-50.
46. Sandy JD, Westling J, Kenagy RD, *et al.* Versican V1 proteolysis in human aorta in vivo occurs at the Glu441-Ala442 bond, a site that is cleaved by recombinant ADAMTS-1 and ADAMTS-4. J Biol Chem 2001 Apr 20;276(16):13372-8.
47. Tortorella MD, Burn TC, Pratta MA, *et al.* Purification and cloning of aggrecanase-1: a member of the ADAMTS family of proteins. Science 1999 Jun 4;284(5420):1664-6.
48. Westling J, Gottschall PE, Thompson VP, *et al.* ADAMTS4 (aggrecanase-1) cleaves human brain versican V2 at Glu405-Gln406 to generate glial hyaluronate binding protein. Biochem J 2004 Feb 1;377(Pt 3):787-95.
49. Baici A, Salgam P, Cohen G, Fehr K, Boni A. Action of collagenase and elastase from human polymorphonuclear leukocytes on human articular cartilage. Rheumatol Int 1982;2(1):11-6.
50. Gadher SJ, Eyre DR, Duance VC, *et al.* Susceptibility of cartilage collagens type II, IX, X, and XI to human synovial collagenase and neutrophil elastase. Eur J Biochem 1988 Jul 15;175(1):1-7.
51. Horwitz AL, Hance AJ, Crystal RG. Granulocyte collagenase: selective digestion of type I relative to type III collagen. Proc Natl Acad Sci U S A 1977 Mar;74(3):897-901.

52. Miller EJ, Harris ED, Jr., Chung E, Finch JE, Jr., McCroskery PA, Butler WT. Cleavage of Type II and III collagens with mammalian collagenase: site of cleavage and primary structure at the NH2-terminal portion of the smaller fragment released from both collagens. Biochemistry 1976 Feb 24;15(4):787-92.
53. Fukai F, Ohtaki M, Fujii N, *et al.* Release of biological activities from quiescent fibronectin by a conformational change and limited proteolysis by matrix metalloproteinases. Biochemistry 1995 Sep 12;34(36):11453-9.
54. Imai K, Shikata H, Okada Y. Degradation of vitronectin by matrix metalloproteinases-1, -2, -3, -7 and -9. FEBS Lett 1995 Aug 7;369(2-3):249-51.
55. Mayer U, Mann K, Timpl R, Murphy G. Sites of nidogen cleavage by proteases involved in tissue homeostasis and remodelling. Eur J Biochem 1993 Nov 1;217(3):877-84.
56. Pasternak RD, Hubbs SJ, Caccese RG, Marks RL, Conaty JM, DiPasquale G. Interleukin-1 stimulates the secretion of proteoglycan- and collagen-degrading proteases by rabbit articular chondrocytes. Clin Immunol Immunopathol 1986 Dec;41(3):351-67.
57. Alexandrakis G, Brown EB, Tong RT, *et al.* Two-photon fluorescence correlation microscopy reveals the two-phase nature of transport in tumors. Nat Med 2004 Feb;10(2):203-7.
58. Brown E, McKee T, diTomaso E, *et al.* Dynamic imaging of collagen and its modulation in tumors in vivo using second-harmonic generation. Nat Med 2003 Jun;9(6):796-800.
59. Znati CA, Rosenstein M, McKee TD, *et al.* Irradiation reduces interstitial fluid transport and increases the collagen content in tumors. Clin Cancer Res 2003 Nov 15;9(15):5508-13.
60. Parameswaran S, Brown LV, Lai-Fook SJ. Effect of flow on hydraulic conductivity and reflection coefficient of rabbit mesentery. Microcirculation 1998;5(4):265-74.
61. Jia W, Zhou Q. Viral vectors for cancer gene therapy: viral dissemination and tumor targeting. Curr Gene Ther 2005 Feb;5(1):133-42.
62. Bobo RH, Laske DW, Akbasak A, Morrison PF, Dedrick RL, Oldfield EH. Convection-enhanced delivery of macromolecules in the brain. Proc Natl Acad Sci U S A 1994 Mar 15;91(6):2076-80.

Chapter 6: Genetic Modifications to Enhance MMP Activity

Introduction

In the previous chapter we found that MMP-1 and MMP-8 are not extensively activated by proteases in the extracellular space of HSTS26T tumor xenografts. Thus, they have not reached their full potential as enzymes which can degrade interstitial fibrillar collagen type I and improve the transport characteristics of tumors. Reaching this potential may require modification of these proteins to tip the balance between active and latent enzymes in the tumor.

Both MMP-1 and MMP-8 fall into the "simple hemopexin domain" structural class of MMPs (1). They contain a signal peptide, followed by a propeptide domain, catalytic domain, hinge region and hemopexin domain. The signal peptide directs the protein to the enodoplasmic reticulum and allows for secretion into the extracellular space. The catalytic domain contains the catalytic zinc, which is bound by three His residues (2-4). The hinge region – whose role is still uncertain – links the catalytic domain to the hemopexin domain. The C-terminal hemopexin domain is involved in the recognition of and binding to collagen. Forms of MMP-1 and MMP-8 which lack the hemopexin domain can cleave gelatin (denatured collagen molecules) and short synthetic peptides that correspond to the cleavage site in collagen I, but are not active against collagen itself (5-7). The propeptide domain – which extends from the N-terminus created by the deletion of the signal peptide to the catalytic domain – has been found to interact with the catalytic site and keep the full length enzyme latent. A propeptide cysteine residue in the conserved sequence PRCGVPD is coordinated to the zinc atom in the active site through

the –SH group (8, 9). Collagenase activity is observed only when the propeptide domain-catalytic domain interaction is disrupted or the propeptide domain is cleaved off.

Based on the domain structure of MMP-1 and MMP-8 and the roles each domain plays, one obvious method to develop a constitutively active collagenase is to delete the propeptide domain. This truncated protein would not require activation in the extracellular space. Here we describe our efforts to create such modified MMPs.

Materials and Methods

Construction of expression vectors and MMP mutants

The cDNA coding for human MMP-1 was purchased from ATCC. The cDNA coding for human MMP-8 was a gift from David Tarin (University of California, San Diego). To create an expression vector for the full length enzymes, both MMPs were subcloned into the vector pEAK13 (Brian Seed, Massachusetts General Hospital). For MMP-1 the forward primer 5'-CAGCTGGCTAGCTTCCCAGCGACTCTA-3' and reverse primer 5'GTCGACGCTAGCGACTCACACCATGTG-3' were used with SpeI/BglII restriction digest of the PCR insert and NheI/ BamHI digest of pEAK13. For MMP-8 the forward primer 5'-CAGCTGGGATCCTTTCCTGTATCTTCT-3' and reverse primer 5'-TCTAGAGGATCCTCAGCCATATCTACA-3' were used with NheI/BamHI digest of both the PCR insert and pEAK13. Both MMP-1 and MMP-8 were inserted in frame with the signal sequence in the pEAK13 expression vector.

To generate a truncated version of MMP-1, PCR was performed with the new forward primer 5'-CAGCTGGCTAGCTTTGTCCTCACTGAG-3' and the same reverse primer

used for full length MMP-1 subcloning. The amplified insert was subcloned into pEAK13 in frame with the signal sequence. Similarly, to generate a truncated version of MMP-8, the new forward primer 5'-CAGCTGGGATCCATGTTAACCCCAGGA-3' was used with the same reverse primer for full length MMP-8 subcloning.

To generate the truncated MMP-1 hinge mutant, a strategy adapted from O'Hare *et al* was used (10). The cDNA was modified by PCR in two steps. The forward primer 5'-GACGATCGCAAAATCCTGTCCAGCCCAGCG'3 was paired with the full length enzyme reverse primer to generate the C-terminal half of MMP-1 containing the Ile270Ser mutation. The reverse primer 5'-TTGCGATCGTCCATATAGGGCTTGGAT-3' was paired with the truncated MMP-1 forward primer to generate the N-terminal half of MMP-1 containing the Ile259Leu mutation. In both PCR products, two silent mutations were also introduced in order to generate PvuI restriction enzyme cleavage sites. The two PCR products were inserted into pEAK13 in a three-way ligation with SpeI/PvuI and BglII/PvuI digests of the inserts and NheI/BamHI digest of the vector.

To generate the truncated MMP-8 hinge mutant, the strategy of overlap extension mutagenesis was employed (11, 12). The forward primer 5'-GGAGCTTCAAGCAACCCTGCCCAA-3' was paired with the full length enzyme reverse primer to generate the C-terminal half of MMP-8. The reverse primer 5'-TTGGGCAGGGTTGCTTGAAGCTCC-3' was paired with the truncated MMP-8 forward primer to generate the N-terminal half. Both PCR products contain the Leu243Ala and Ile248Ala mutations. PCR was performed on these two fragments (which contain overlapping sequences) to recover the full length product. This PCR product was

subsequently subcloned into pEAK13 with SpeI/BglII digest of the insert and NheI/BamHI digest of the vector.

Transient and stable cell transfections

293ET and HSTS26T cells were cultured in 6-well plates under standard conditions. Transient transfections were performed with Lipofectamine 2000 (Invitrogen, Carlsbad, CA) according to the manufacturer's instructions. To generate stable HSTS26T transfectants, cells were transfected in 60-mm dishes and passaged at a 1:20 dilution into fresh growth medium 24 hours after transfection. Twenty four hours after passaging the media was replaced with fresh media containing 0.5 μg/mL puromycin. Media with puromycin was changed every 5 to 6 days. Individual colonies were selected, expanded and screened.

A retroviral transfection system was also used to generate stable transfectants. The protocol was adapted from one previously described (13). Briefly, the full length, truncated and mutated-truncated forms of MMP-1 and MMP-8 were subcloned into pMSVCneo (Clontech Laboratories, Mountain View, CA) using the pEAK13 vectors as templates. 80-90% confluent T75 flasks of 293ET packaging cells were transiently transfected with each MSCV vector (15 μg) in combination with plasmids expressing vesicular stomatitis virus glycoprotein (VSVG, 5 μg) and gag/pol (7 μg). After overnight incubation, the 293ET cells were washed three times with PBS and then 10 mL of fresh media was added. The following day the conditioned media containing retrovirus was collected and fresh media added to the flask. The conditioned media was spun down to remove any cell debris and passed through a 0.45 μM filter (Whatman, Middlesex, UK).

Subconfluent HSTS26T cells were incubated with the conditioned media containing retrovirus. The conditioned media from the 293ET packaging cells were collected the following two days and transduction repeated. Transfected cells were selected by culturing with media containing neomycin.

Protein isolation

Cells were pelleted by centrifugation and resuspended in 100 μL RIPA buffer. Samples were kept on ice for 30 minutes and then spun down at 14,000 g for 20 minutes to pellet the cell debris. The supernatant containing cellular proteins was collected. Protein concentration was measured using the Bradford assay (BioRad Laboratories, Hercules, CA) according to the manufacturer's instructions. Pre-diluted BSA (Pierce Biotechnology, Rockford, IL) was used as a protein standard. Protein samples were either used immediately in activity assays or western blots, or were frozen down at -80°C.

Activation and inhibition of MMPs

To activate latent MMPs, samples were incubated with p-aminophenylmercuric acetate (APMA, Sigma, St. Louis, MO). APMA was dissolved in DMSO at a stock concentration of 20 mM and used to activate MMPs at a final concentration of 2 mM. Samples were incubated at 37°C for 1 hr and western blot analysis proceeded immediately afterward. For samples in which activity was assessed, APMA was removed with a centricon filter.

GM6001 (Ryss Lab, Union City, CA) was used to inhibit MMP autoproteolysis in certain transfections. It was prepared by dissolving in DMSO at a stock concentration of 50 mM. 293ET cells were transfected in 6 well plates. 2.5 hrs after transfection, the media was

replaced with 2 mL of fresh media containing either 1:1000 DMSO or 1:1000 50 mM GM6001 (50 μM final concentration). Conditioned media and cells were collected 6 hours later for western blot analysis.

Western blot

Loading buffer containing β-mercaptoethanol was added to the protein samples and they were boiled at 100°C for 5 minutes. Samples were loaded into a 10% Bis-Tris gel (Invitrogen, Carlsbad, CA) and run at 150V for ~ 1 hr. The proteins were transferred to a nitrocellulose membrane in an Invitrogen gel box. The transfer was performed at 30V for 1 hr at room temperature. The membrane was washed with TBST for 10 minutes. The membrane was placed in 20 mL blocking buffer (TBST with 5% milk) and incubated at room temperature for 3 hrs with gently shaking. The membrane was incubated with primary antibody at 4°C overnight with gentle shaking. Polyclonal antibodies AB806 and AB8115 (Millipore, Billerica, MA) were used at a dilution of 1:2,500 for detection of MMP-1 and MMP-8, respectively. The following day, the membrane was washed 3x for 10 minutes with TBST with vigorous shaking. The membrane was then incubated for 1 hr at room temperature with an HRP-conjugated secondary antibody (Amersham). The membrane was washed again with TBST with vigorous shaking and proteins detected using the ECL or ECL Plus kit (Amersham, Buckinghamshire, UK). For cell lysate samples, membranes were stripped by incubating with stripping buffer (Pierce Biotechnology, Rockford, IL) at 37°C and beta actin detected with a polyclonal antibody (Santa Cruz Biotechnology, Santa Cruz, CA).

Collagenolytic activity assay

MMP activity was determined using an *in vitro* collagenolytic activity assay modified from the method of Johnson-Wint *et al.* (14, 15). Briefly, type I collagen was purified from rat tail by solubilization with acetic acid and subsequently acetylated with [^{14}C] acetic anhydride. Fibrils were allowed to form from the radiolabeled collagen and were dried onto wells of a 96-well plate, forming a thin film. Conditioned media samples were added to wells and incubated at 37°C for 2.5 hours. The supernatants containing soluble radiolabeled collagen (from cleavage) were transferred to scintillation vials and counted in a Beckman model LS-3801 scintillation counter. Bacterial collagenase was used as a control to cleave all the radiolabeled collagen in select wells. One unit of activity corresponds to degradation of 10% of the collagen in 2.5 hrs at 37°C.

Results

Generation of truncated MMPs

Truncated versions of both MMP-1 and MMP-8 lacking the propeptide domain were generated as described in Materials and Methods. A schematic diagram of the domain structure of the wild type enzyme and the truncated mutant is shown in Fig. 6.1. Transient transfections were performed to generate the enzyme in 293 cells. Cells were also transfected with the empty vector and with the wild type/full length enzymes as controls. The 12 hour serum-free conditioned media was collected and western blot performed to detect the presence of the protein (Fig. 6.2). The truncated forms are expected to be ~10 kDa smaller than their full length counterparts (57 vs 47 kDa for MMP-1 and 75 vs 64

kDa for MMP-8). No active form of the enzyme appears in the truncated MMP transfection samples. Rather, ~25 kDa proteins were observed. These were believed to be likely products of autoproteolytic degradation.

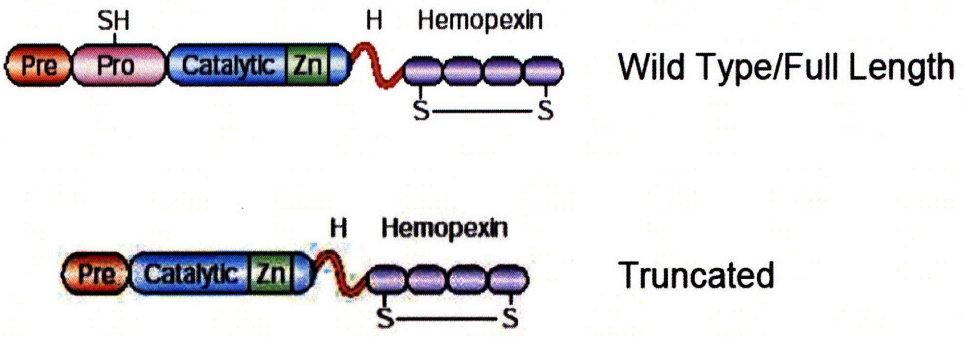

Figure 6.1. The protein structure of wild type and truncated forms of MMP-1 and -8. Both MMP-1 and -8 exhibit the MMP domain structure classified as simple hemopexin domain. The amino-terminal signal sequence (Pre) directs the protein to the endoplasmic reticulum for secretion into the extracellular space. A propeptide domain (Pro) contains a thiol group which can interact with the catalytic site Zn, maintaining the enzyme in the inactive state. A hinge domain (H) connects the catalytic domain with the hemopexin domain, which is believed to be involved in substrate recognition and binding. In the truncated form, the propeptide domain has been deleted.

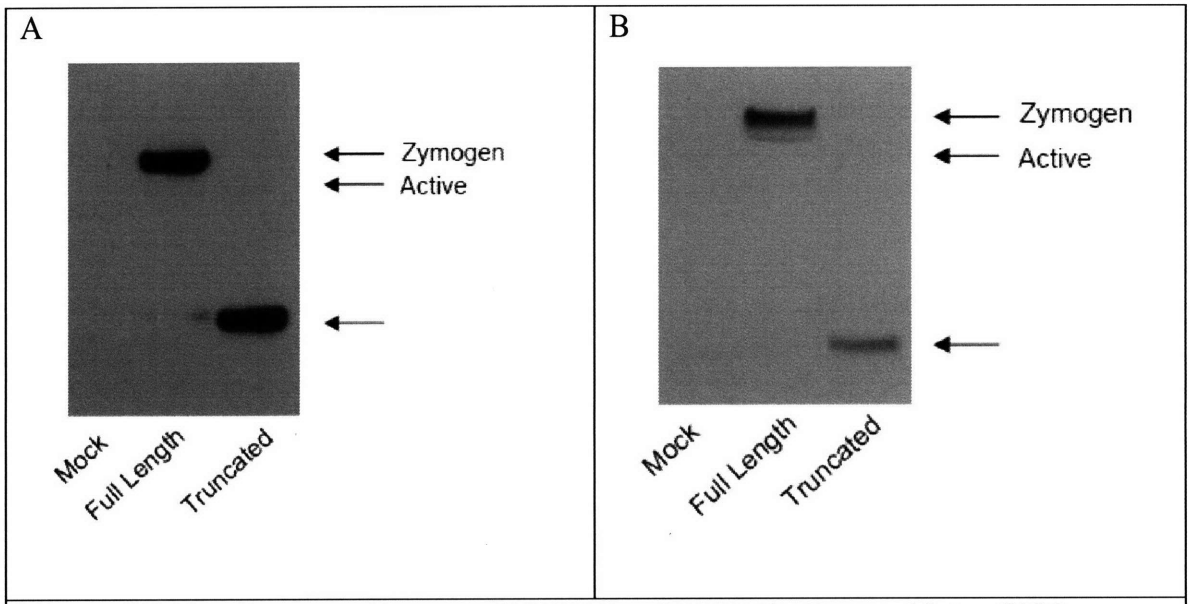

Figure 6.2. Development of truncated MMP-1 and MMP-8. Western blots of 12 hr conditioned media from 293 cells transiently transfected with empty vector, vector expressing full length MMP and vector expressing truncated MMP, for MMP-1 (A) and MMP-8 (B). The arrows refer to the expected location of the full length zymogen, truncated/active enzyme and putative autoproteolytic degradation product. In both cases, the truncated protein is in the degraded form in the conditioned media.

To confirm that these small proteins are indeed degradation products and that this process is not simply a phenomenon of these truncated proteins, the full length enzymes were activated with p-aminophenylmercuric acetate (APMA) and the resultant protein fragments analyzed by western blot. APMA is commonly used to activate MMPs *in vitro* (16). This organomercurial disrupts the interaction between the propeptide and catalytic domains and activation is achieved via autoproteolytic removal of the propeptide domain. A 1-hr incubation with 2 mM APMA at 37°C resulted in partial activation of both the MMP-1 and MMP-8 zymogens (Fig. 6.3). Rapid autoproteolytic degradation also occurs,

as the presence of significant amounts of the degraded protein fragments are detected. Thus, the small proteins found with the truncated mutants are indeed degradation products of the active enzymes, and the process of autoproteolytic degradation appears to occur quite rapidly for both MMP-1 and MMP-8.

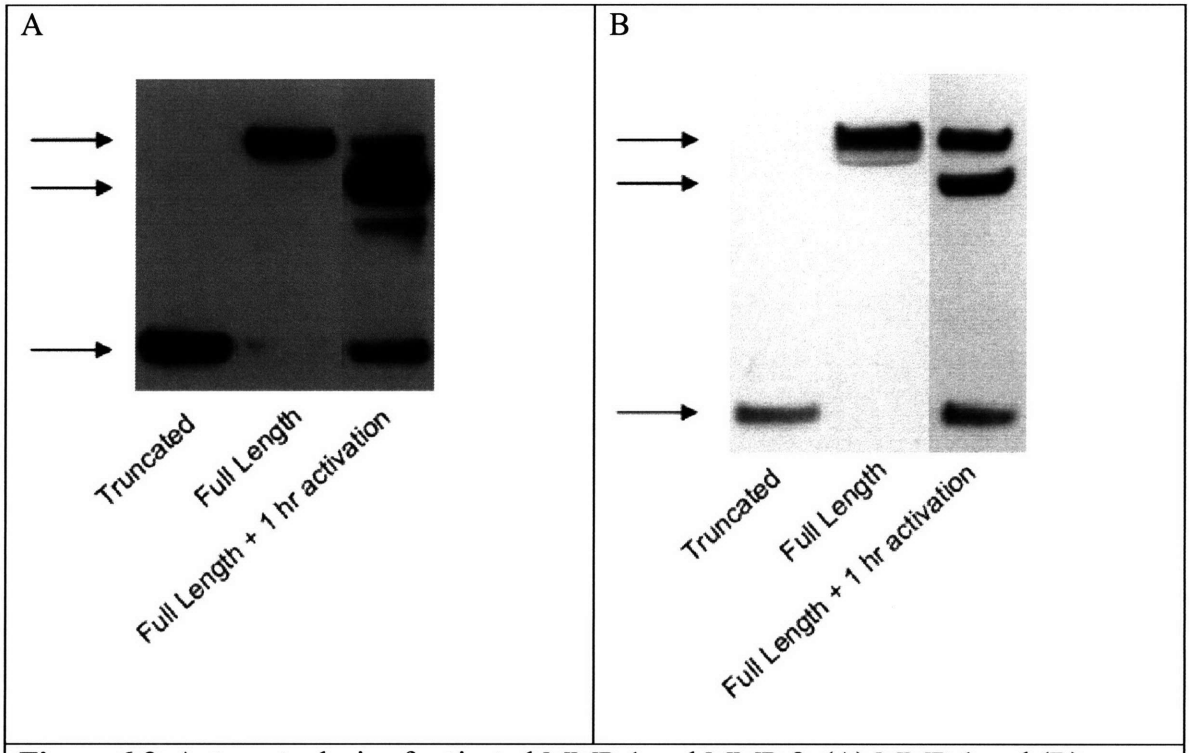

Figure 6.3. Autoproteolysis of activated MMP-1 and MMP-8. (A) MMP-1 and (B) MMP-8 western blots of 12 hr conditioned media of transiently transfected 293 cells. The right lane is conditioned media from full length MMP transfectants following 1-hr incubation with the activating agent APMA. The arrows refer to the expected location of the full length zymogen (top), truncated/active enzyme (middle) and autoproteolytic degradation product (bottom). In both cases, 1-hr activation yields both active and degraded forms.

Published reports have suggested that the degraded forms of both MMP-1 and MMP-8 lack activity against collagen molecules, although the isolated catalytic domains are still able to cleave the small peptides mimicking the collagen I cleavage site (5-7). Since these mutant enzymes are being developed as tools to degrade fibrillar collagen type I in tumors, we assessed the ability of the various fragments to cleave reconstituted collagen fibrils. The samples shown in Figs. 6.2 and 6.3 were tested in this collagenolytic activity assay (Fig. 6.4). As expected, both the truncated and full length samples showed no activity. Only the full length form incubated with the activating agent APMA could cleave the collagen fibers.

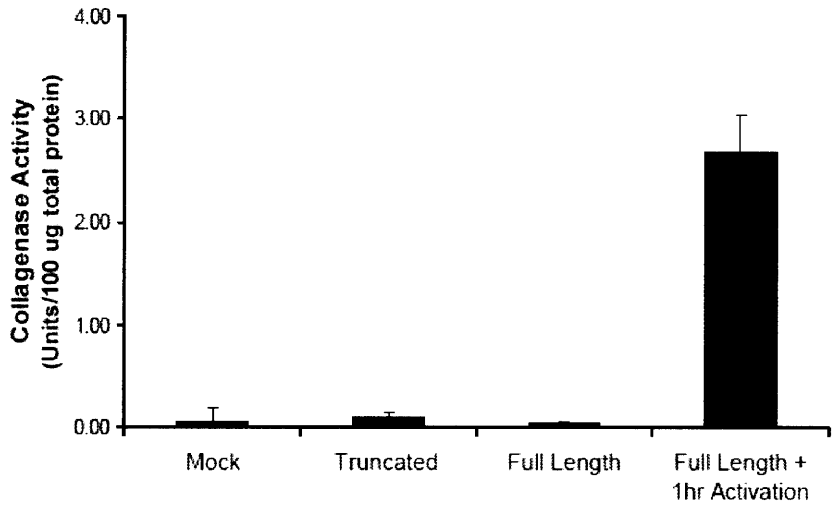

Figure 6.4. Collagenase activity of truncated and full length MMP-1. 12-hr conditioned media of 293 cells transfected with empty vector, truncated MMP-1 and full length MMP-1 were collected and assayed for collagenolytic activity. The full length MMP-1 sample was also activated by incubation with 2 mM APMA for 1 hr at 37°C. One unit of activity is defined as the degradation of 10% of the total collagen in each well with 2.5 hrs incubation at 37°C. Mean values and standard errors shown. Negligible activity is

observed except in the APMA-activated full length MMP-1 sample.

Inhibition of autoproteolytic degradation with cleavage site mutations

In order to overcome this issue of autodegradation and develop forms of MMP-1 and MMP-8 that are truly constitutively active, we sought to develop forms of each enzyme that would be more resistant to autoproteolysis. Previous research had identified the amino acid sequence in both MMP-1 and MMP-8 that appeared to be the sites of autodegradation. The putative cleavage site is located in the hinge region of each protein, which connects the catalytic and hemopexin domains. In these studies site-directed mutagenesis was used to identify amino acids which affect the rate of autoproteolytic cleavage. Based on these findings, we chose mutations that appeared to stabilize each MMP the most and incorporated them into the truncated versions of each protein. The specific point mutations for each "mutated-truncated" MMP are shown in Fig. 6.5. Mutated-truncated MMP-1 appeared to be more stable than the truncated form, while mutated-truncated MMP-8 showed no improvement (Fig. 6.6).

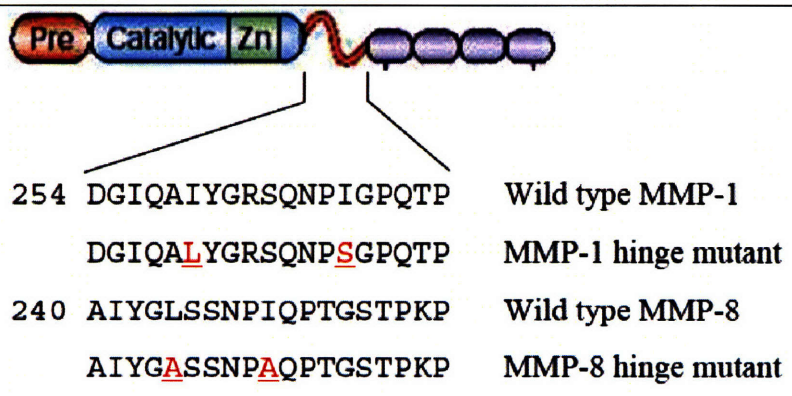

Figure 6.5. Sequences of wild type and mutant MMP-1 and MMP-8. The sequence

modifications for each hinge mutant are shown with underlined amino acid residues in single letter code.

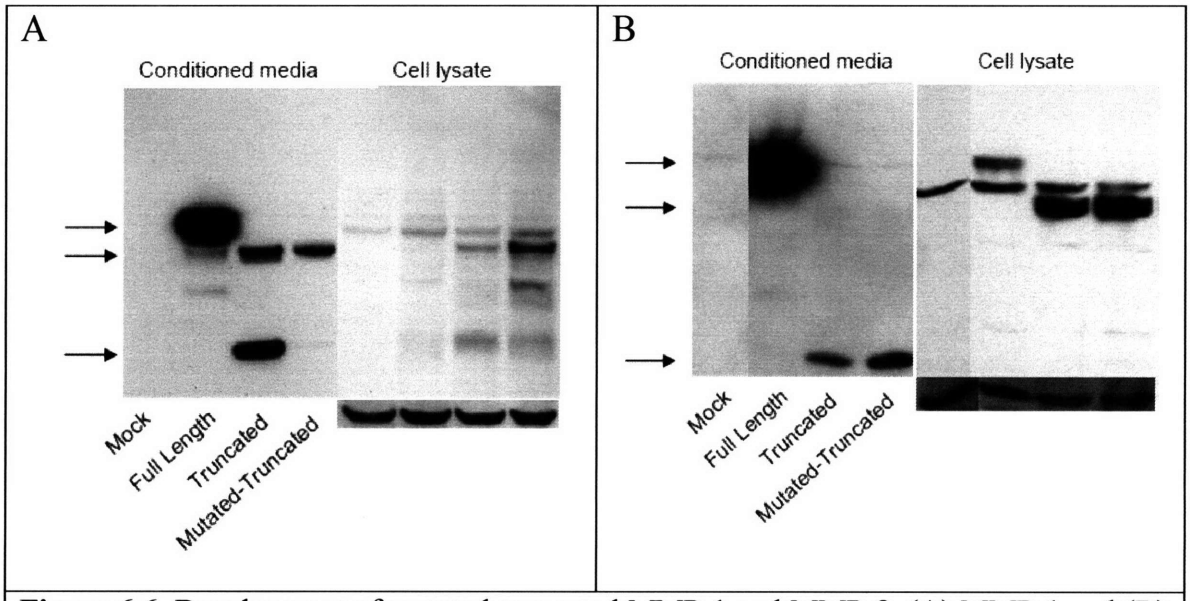

Figure 6.6. Development of mutated-truncated MMP-1 and MMP-8. (A) MMP-1 and (B) MMP-8 western blots of 12 hr conditioned media of transiently transfected 293 cells. Conditioned media is shown on the left side and cell lysate on the right. Detection of beta actin in the cell lysates is shown at the bottom. Arrows show the expected location of bands for full length (high), active (middle) and degraded (low) forms. Mutated-truncated MMP-1 appears to be more stable than the truncated form. Mutated-truncated MMP-8 shows no improvement in stability compared to full length MMP-8. Wild type enzymes are secreted in significantly greater amounts that truncated forms. Substantially more truncated forms are found intracellulary than wild type.

Beyond autoproteolytic degradation, we noted another issue that could have negative consequences for the use of these altered MMPs *in vivo*. For identical experimental conditions (*i.e.* same expression vector/promoter and transfection conditions) significantly more wild type enzyme was secreted than truncated and mutated-truncated forms (Fig. 6.6). Furthermore, much more of the truncated forms of the MMPs were found in the cell lysate compared to the full length, wild type form. We hypothesized that intracellular autoproteolytic degradation could reduce the amount of enzyme secreted from the cell. To test this we transiently transfected 293 cells with both the full length and truncated MMP-1 constructs in the presence and absence of the MMP inhibitor GM6001 (17), which can diffuse into cells. Conditioned media and cells were collected after 6 hours of incubation, a duration that was experimentally determined to be short enough that secretion of truncated enzyme into the media was not substantial. This early time point ensures that any change in the level of non-degraded truncated MMP-1 in the conditioned media will arise from increased secretion of this form, rather than reduced degradation in the media. We found that in the presence of the inhibitor, the amount of "active" truncated MMP-1 in both the cell lysate and conditioned media increased (Fig. 6.7). This indicates that intracellular degradation of the protein occurs and contributes to the reduction in the amount of active protein secreted. However, even in the presence of the inhibitor, the amount of secreted protein was less than that of the wild type protein in both the extracellular and intracellular fractions. This suggests that intracellular degradation is not the only reason for the significantly reduced secretion. Most likely diminished expression and/or impaired intracellular processing are responsible.

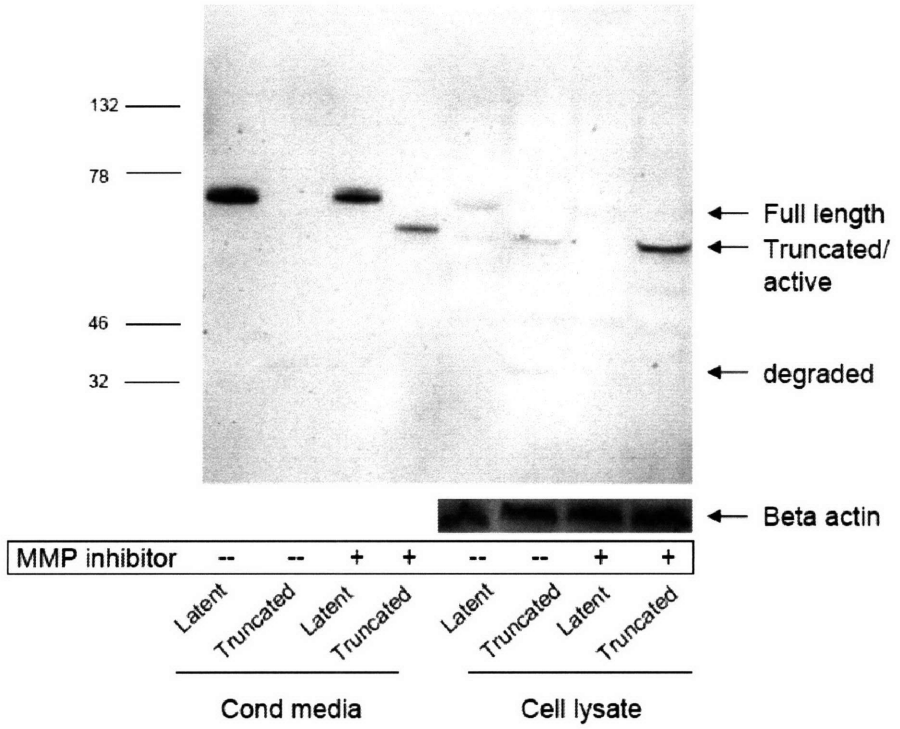

Figure 6.7. Transfection of 293 cells with full length and truncated forms of MMP-1 in the absence and presence of an MMP inhibitor. The inhibitor reduces intracellular degradation of the truncated mutant (lane 8 vs lane 6) and increases the amount of active enzyme secreted into the conditioned media (lane 4 vs lane 2). Significantly less truncated protein is secreted compared to full length (lane 4 vs lane 3). Significantly more truncated MMP-1 remains in the cell compared to full length (lane 8 vs lane 7).

Since the kinetics of autoproteolytic degradation and the amount of secreted protein in these *in vitro* assays may not accurately reflect what happens in a tumor, the next goal was to study the effect of these modified MMPs on fibrillar collagen and interstitial transport *in vivo*. To do so, HSTS26T human soft tissue sarcoma cells were transfected with the wild type, truncated and mutated-truncated versions of MMP-1 and MMP-8.

Two separate expression vectors were used: a retroviral vector with a murine stem cell PCMV LTR promoter and a plasmid expression vector with a CMV promoter. In both cases negligible amounts of the truncated MMPs relative to wild type were detected by western blot in all of the clones screened. A representative sample of the clones from transfection with the plasmid expression vector is shown in Fig. 6.8. The autodegradation and impaired processing of these mutated forms appear to prevent the secretion of appreciable amounts of active enzyme in cancer cells. Thus, the generation of constitutively active forms of MMP-1 and MMP-8 for *in vivo* work via genetic mutations was not successful.

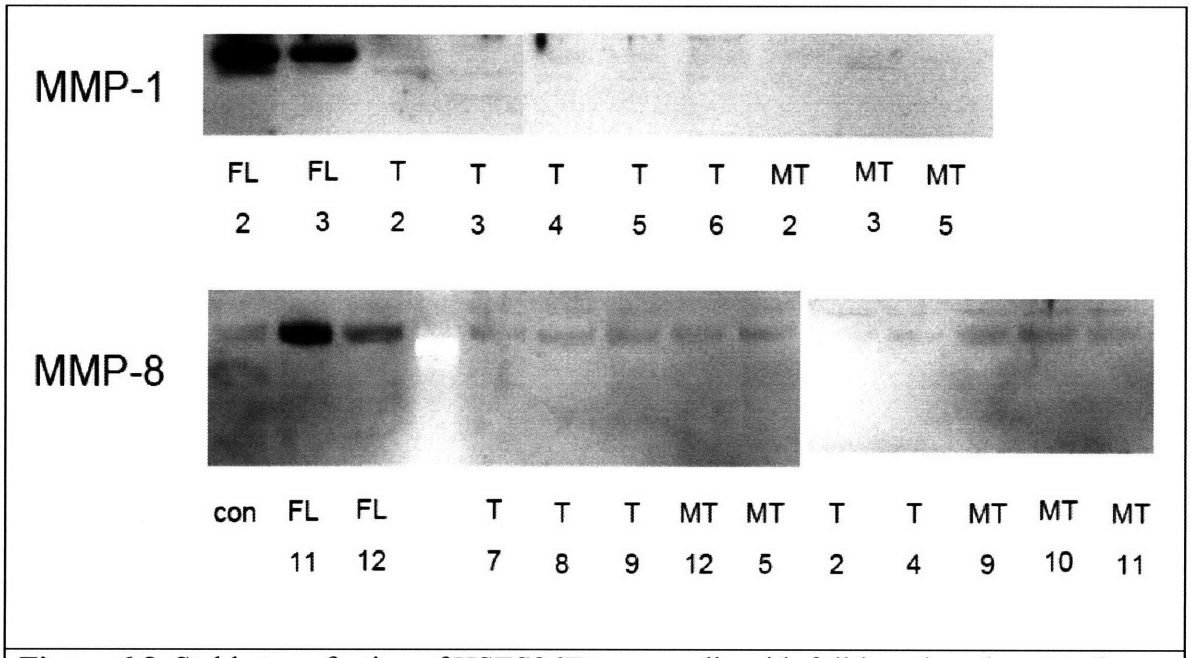

Figure 6.8. Stable transfection of HSTS26T tumor cells with full length and mutated forms of MMP-1 and MMP-8. MMP-1 and -8 western blots of conditioned media from representative clones transfected with either empty vector (con), full length MMP (FL), truncated MMP (T) or mutated-truncated MMP (MT).While the full length forms are expressed and secreted, very little truncated and mutated-truncated enzyme is secreted.

Future Directions: Furin-activatable MMPs

One final genetic approach to creating a constitutively active MMP is to enhance its activation by inserting a furin consensus sequence between the propeptide and catalytic domains. Furin is a ubiquitously expressed enzyme involved in the secretory pathway of cells (18). It cleaves proteins containing the consensus sequence at the trans-Golgi. It plays a role in processing certain cell surface-bound enzymes and has been found to activate other MMPs (*e.g.* MMP-11 and MMP-14) (19, 20). We believe that this version will have advantages over the truncated version for several reasons. First, furin-mediated activation is a naturally occurring process for several other MMPs, both membrane-bound and soluble. Second, the insertion of the 10 amino acid consensus sequence will likely disrupt proper protein folding and processing less than complete removal of the propeptide domain. And finally, activation by furin cleavage occurs in the trans-Golgi, providing less time for intracellular autoproteolytic degradation.

A form of MMP-1 containing the inserted furin consensus sequence has already been developed (19). The secretion of what appeared to be the active form was verified, but detailed analysis of its activity relative to the wild type enzyme had not been performed. At our urging, the creators of this recombinant enzyme recently performed this analysis in order to determine the suitability of this mutant construct for degradation of tumor collagen *in vivo*. Strangely, the secreted enzyme was dramatically less active against collagen I than wild type MMP-1. The mechanism of this reduced activity is not yet known. It is believed that perhaps structural changes induced by the peptide insertion caused the furin-cleaved propeptide to remain attached to the catalytic domain,

preserving the enzyme in the inactive state (S. Weiss, personal communication). Thus, development of furin-activatable forms of MMP-1 and MMP-8 has not been successful and requires more extensive research.

Discussion

Based on their domain organization, the creation of constitutively active forms of MMP-1 and -8 seemed like a straightforward exercise. In practice, however, it is quite problematic and our findings highlight the complexity involved in the balance between active and inactive forms of these enzymes. We found that the truncated forms of each protein were secreted in much smaller quantities than the wild type enzymes, with greater amounts remaining inside the cell. This may be due to improper protein folding or some other type of impaired processing. While these truncated forms were not overtly harmful to cells (*i.e.* no massive cell death of transfected cells was observed in culture), their toxicity has not been ruled out. In addition, the truncated mutants were also found to go through rapid inactivating autoproteolysis both extracellularly and intracellularly.

These observations support the idea that the steady state concentration of active MMPs – and by extension the level of collagenase activity –is tightly regulated in tumors. We have documented in the previous chapter that even when copious amounts of MMP-1 and -8 are expressed in a tumor, limited amounts are converted to the active form. It has been shown *in vitro* that activation of these MMPs can be a multi-step process and that various serine proteases and MMPs (MMP-2, -3, -7, -10, -11) may be part of the process (21-28). That each of these MMPs requires activation, itself, suggests that MMP-1 and -8 activation is a highly controlled event that occurs only when collagenase activity is

needed. Once activated, MMP-1 and -8 can rapidly break down into smaller forms. In contrast to the activation process, this autoproteolysis is not well studied beyond several papers that have identified the putative cleavage sites for each MMP (6, 10, 12). While for our purposes this autoproteolysis can be considered an inactivating cleavage (since type I collagenase activity is lost), this may not be the only, or true, role *in vivo*. Isolated catalytic domains have been found to retain their activity against certain substrates (5-7), so removal of the hemopexin domain may serve a specific biological role. Alternatively, autoproteolysis may be a built-in regulatory mechanism to prevent an overabundance of collagenase activity, which may be harmful in many tissues. In any event, maintaining high levels of active (*i.e.* propeptide-free) MMP-1 and -8 in the tumor may be difficult to achieve.

So what does this mean for engineering constitutively active forms of these collagenases? There are several possible routes going forward. First, a greater understanding of the activation processes of these two collagenases is needed, particularly if a rational approach to protein engineering is taken. While much research has gone into understanding the activation process of MMP-1 and -8 *in vitro*, the actual method of activation *in vivo* is still unknown. Identifying the proteases responsible for activation *in vivo* and elucidating the mechanism would help us understand how best to approach the engineering of these MMPs. Perhaps even co-transfecting MMP-1 or -8 with such an activating agent may be an effective approach.

A second method to improve activation is to use targeted mutation of the propeptide domain to disrupt the inactivating interaction it has with the catalytic site Zn. Studies

which have identified the amino acids in the propeptide domain responsible for the interaction provide preliminary targets for such mutations (9). These mutations would likely disrupt proper protein folding and intracellular processing less than truncation of the enzyme, and thus may hold greater potential. Finally, the method of proteolytic activation via furin-mediated cleavage of the propeptide domain still holds hope. Further research should provide insight into why limited activity was observed and how this can be improved. We should also note that the recovery of full collagenase activity relative to the activated wild type enzyme is not a requirement. Collagenase activity is a function of both the inherent activity of the enzyme and also its concentration. Thus, an engineered form of MMP-1 or -8 that has reduced activity may still be advantageous if greater amounts are present in the tumor compared with the wild type enzyme, which is activated in low proportions.

Regardless of how activation of these MMPs is improved, one limiting factor may be autoproteolytic inactivation. Targeted mutations still provide the best approach to limit this process. As mentioned previously, autoproteolysis has not been extensively studied. The stabilizing mutations made in this work were motivated by this existing work and are likely suboptimal. Further research should identify the proper sets of mutations that reduce autodegradation while maintaining collagenase activity.

Lastly, an alternative to protein engineering by rational design is the method of directed evolution. In this approach, a protein is altered at the genetic level and screened for advantageous characteristics (29). Essentially the process of Darwinian evolution is carried out in the test tube with the selective pressure applied by the scientist. Directed

evolution has been used in such applications as enhancing the activity of enzymes (30) and altering the binding characteristics of proteins (31). The ability to develop robust, high-throughput screens is critical and will be the limiting step with MMP engineering. If screens can be developed for both enzyme stability and collagenase activity, this may be the most effective way to engineer a constitutively active collagenase.

References

1. Egeblad, M. and Werb, Z. New functions for the matrix metalloproteinases in cancer progression. Nat Rev Cancer, *2:* 161-174, 2002.
2. Bode, W., Reinemer, P., Huber, R., Kleine, T., Schnierer, S., and Tschesche, H. The X-ray crystal structure of the catalytic domain of human neutrophil collagenase inhibited by a substrate analogue reveals the essentials for catalysis and specificity. Embo J, *13:* 1263-1269, 1994.
3. Lovejoy, B., Cleasby, A., Hassell, A. M., Longley, K., Luther, M. A., Weigl, D., McGeehan, G., McElroy, A. B., Drewry, D., Lambert, M. H., and et al. Structure of the catalytic domain of fibroblast collagenase complexed with an inhibitor. Science, *263:* 375-377, 1994.
4. Windsor, L. J., Bodden, M. K., Birkedal-Hansen, B., Engler, J. A., and Birkedal-Hansen, H. Mutational analysis of residues in and around the active site of human fibroblast-type collagenase. J Biol Chem, *269:* 26201-26207, 1994.
5. Clark, I. M. and Cawston, T. E. Fragments of human fibroblast collagenase. Purification and characterization. Biochem J, *263:* 201-206, 1989.
6. Knauper, V., Osthues, A., DeClerck, Y. A., Langley, K. E., Blaser, J., and Tschesche, H. Fragmentation of human polymorphonuclear-leucocyte collagenase. Biochem J, *291 (Pt 3):* 847-854, 1993.
7. Lowry, C. L., McGeehan, G., and LeVine, H., 3rd Metal ion stabilization of the conformation of a recombinant 19-kDa catalytic fragment of human fibroblast collagenase. Proteins, *12:* 42-48, 1992.
8. Springman, E. B., Angleton, E. L., Birkedal-Hansen, H., and Van Wart, H. E. Multiple modes of activation of latent human fibroblast collagenase: evidence for the role of a Cys73 active-site zinc complex in latency and a "cysteine switch" mechanism for activation. Proc Natl Acad Sci U S A, *87:* 364-368, 1990.
9. Windsor, L. J., Birkedal-Hansen, H., Birkedal-Hansen, B., and Engler, J. A. An internal cysteine plays a role in the maintenance of the latency of human fibroblast collagenase. Biochemistry, *30:* 641-647, 1991.
10. O'Hare, M. C., Curry, V. A., Mitchell, R. E., and Cawston, T. E. Stabilisation of purified human collagenase by site-directed mutagenesis. Biochem Biophys Res Commun, *216:* 329-337, 1995.
11. Ho, S. N., Hunt, H. D., Horton, R. M., Pullen, J. K., and Pease, L. R. Site-directed mutagenesis by overlap extension using the polymerase chain reaction. Gene, *77:* 51-59, 1989.
12. Knauper, V., Docherty, A. J., Smith, B., Tschesche, H., and Murphy, G. Analysis of the contribution of the hinge region of human neutrophil collagenase (HNC, MMP-8) to stability and collagenolytic activity by alanine scanning mutagenesis. FEBS Lett, *405:* 60-64, 1997.
13. Au, P., Tam, J., Fukumura, D., Jain, R. K. Small Blood Vessel Engineering. *In:* H. Hauser, Fussenegger, M. (ed.), Tissue Engineering. Totowa, N.J.: Humana Press, 2007.
14. Johnson-Wint, B. A quantitative collagen film collagenase assay for large numbers of samples. Anal Biochem, *104:* 175-181, 1980.

15. Moses, M. A., Sudhalter, J., and Langer, R. Identification of an inhibitor of neovascularization from cartilage. Science, *248:* 1408-1410, 1990.
16. Stricklin, G. P., Jeffrey, J. J., Roswit, W. T., and Eisen, A. Z. Human skin fibroblast procollagenase: mechanisms of activation by organomercurials and trypsin. Biochemistry, *22:* 61-68, 1983.
17. Galardy, R. E., Cassabonne, M. E., Giese, C., Gilbert, J. H., Lapierre, F., Lopez, H., Schaefer, M. E., Stack, R., Sullivan, M., Summers, B., and et al. Low molecular weight inhibitors in corneal ulceration. Ann N Y Acad Sci, *732:* 315-323, 1994.
18. Steiner, D. F. The proprotein convertases. Curr Opin Chem Biol, *2:* 31-39, 1998.
19. Pei, D. and Weiss, S. J. Furin-dependent intracellular activation of the human stromelysin-3 zymogen. Nature, *375:* 244-247, 1995.
20. Sato, H., Kinoshita, T., Takino, T., Nakayama, K., and Seiki, M. Activation of a recombinant membrane type 1-matrix metalloproteinase (MT1-MMP) by furin and its interaction with tissue inhibitor of metalloproteinases (TIMP)-2. FEBS Lett, *393:* 101-104, 1996.
21. Crabbe, T., O'Connell, J. P., Smith, B. J., and Docherty, A. J. Reciprocated matrix metalloproteinase activation: a process performed by interstitial collagenase and progelatinase A. Biochemistry, *33:* 14419-14425, 1994.
22. Imai, K., Yokohama, Y., Nakanishi, I., Ohuchi, E., Fujii, Y., Nakai, N., and Okada, Y. Matrix metalloproteinase 7 (matrilysin) from human rectal carcinoma cells. Activation of the precursor, interaction with other matrix metalloproteinases and enzymic properties. J Biol Chem, *270:* 6691-6697, 1995.
23. Knauper, V., Murphy, G., and Tschesche, H. Activation of human neutrophil procollagenase by stromelysin 2. Eur J Biochem, *235:* 187-191, 1996.
24. Knauper, V., Wilhelm, S. M., Seperack, P. K., DeClerck, Y. A., Langley, K. E., Osthues, A., and Tschesche, H. Direct activation of human neutrophil procollagenase by recombinant stromelysin. Biochem J, *295 (Pt 2):* 581-586, 1993.
25. Murphy, G., Segain, J. P., O'Shea, M., Cockett, M., Ioannou, C., Lefebvre, O., Chambon, P., and Basset, P. The 28-kDa N-terminal domain of mouse stromelysin-3 has the general properties of a weak metalloproteinase. J Biol Chem, *268:* 15435-15441, 1993.
26. Nicholson, R., Murphy, G., and Breathnach, R. Human and rat malignant-tumor-associated mRNAs encode stromelysin-like metalloproteinases. Biochemistry, *28:* 5195-5203, 1989.
27. Suzuki, K., Nagase, H., Ito, A., Enghild, J. J., and Salvesen, G. The role of matrix metalloproteinase 3 in the stepwise activation of human rheumatoid synovial procollagenase. Biol Chem Hoppe Seyler, *371 Suppl:* 305-310, 1990.
28. Windsor, L. J., Grenett, H., Birkedal-Hansen, B., Bodden, M. K., Engler, J. A., and Birkedal-Hansen, H. Cell type-specific regulation of SL-1 and SL-2 genes. Induction of the SL-2 gene but not the SL-1 gene by human keratinocytes in response to cytokines and phorbolesters. J Biol Chem, *268:* 17341-17347, 1993.
29. Farinas, E. T., Bulter, T., and Arnold, F. H. Directed enzyme evolution. Curr Opin Biotechnol, *12:* 545-551, 2001.

30. Chen, K. and Arnold, F. H. Tuning the activity of an enzyme for unusual environments: sequential random mutagenesis of subtilisin E for catalysis in dimethylformamide. Proc Natl Acad Sci U S A, *90:* 5618-5622, 1993.
31. Maheshri, N., Koerber, J. T., Kaspar, B. K., and Schaffer, D. V. Directed evolution of adeno-associated virus yields enhanced gene delivery vectors. Nat Biotechnol, *24:* 198-204, 2006.

Chapter 7: Conclusion

Interstitial collagen type I has previously been shown to be the primary source of diffusive hindrance in tumors (1-4). Interestingly, Pluen *et al.* found that this hindered diffusion became increasingly more dramatic as the size of the macromolecule being probed rose (4). Based on this result, we hypothesized that the effectiveness of most novel cancer therapeutics – such as antibodies and liposomal and viral vectors – could be significantly impaired due to limited distribution in tumors resulting from their large size. The first goal of this thesis was to confirm this theory. The second goal was to answer the following question: can we do anything about this in a clinical setting?

We first addressed the issue of impaired therapeutic efficacy with a mathematical model. A 1D reaction-diffusion model was developed to determine the distribution of a specific therapeutic, an HSV vector, in a solid tumor. While the model did not explicitly consider collagen, its effect was incorporated in the diffusion of the viral particles. The model predicted that HSV vectors would spread only minimally from the injection site following intratumor infusion. Hindered diffusion and rapid binding were responsible for this. Importantly, the model predicted that an improvement in diffusion from modulation of tumor collagen could enhance vector distribution several fold.

These intriguing findings were supported by our experimental results. *In vivo* imaging of intratumorally injected HSV vectors showed that their distribution was limited by the collagen in tumors. The effect appeared to be size dependent, as smaller macromolecules distributed more uniformly in the tumors. Furthermore, the collagen network limited the propagation, and thus efficacy, of oncolytic HSV vectors. These images showed, for the first time, the direct effect tumor collagen can have in limiting the distribution and

efficacy of a cancer therapeutic. The second main finding from this study was that collagen degradation with bacterial collagenase could be used to enhance vector transport and efficacy. Thus, these results provided proof of principle that the technique of tumor collagen degradation for enhanced interstitial transport could be used to positively influence treatment outcome.

However, in order for this concept to advance to the clinic, a human, rather than bacterial, enzyme needs to be used. MMP-1 and MMP-8 were identified as two potential human enzymes that could be used in replacement of bacterial collagenase. Unfortunately, our studies with recombinant MMPs showed that these enzymes are significantly less potent than their bacterial counterpart. The enhancement of interstitial transport and efficacy of oncolytic HSV found with bacterial collagenase was not duplicated by either MMP. It was concluded that in order for these enzymes to effect the changes in collagen and diffusion necessary to enhance therapeutic efficacy, the dose needed to be increased substantially.

Genetic delivery of MMPs offered a potential solution to this problem: tumor cells would be converted to factories producing and secreting these human collagenases. However, while copious amount of these MMPs were generated and secreted, another problem arose. These enzymes were insufficiently activated in the extracellular space and thus no changes in collagen and diffusion were observed. The mechanism of activation of these MMPs in physiological settings is still unknown. However, *in vitro* studies suggest that the mechanism may be quite complex and tightly regulated, as many other MMPs, which themselves require activation, can cleave MMP-1 and -8 in the propeptide domain (5).

Thus, the observation that only a small proportion of the MMPs were activated is not entirely surprising, especially considering the large amount of protein being secreted in this overexpression model. On the other hand, this result could hardly have been predicted. In their only other use as enzymes to degrade collagen *in vivo*, both MMP-1 and MMP-8 were found to be activated in the tissue to which they were delivered (6, 7).

Based on the domain organization of these two enzymes, we proposed a genetic method of bypassing this activation barrier: deletion of the inactivating propeptide domain. However, this method of generating constitutively active MMPs was hampered by two phenomena. First, the truncated/active form of both enzymes went through inactivating autoproteolysis, both intracellularly and extracellularly. Second, impaired intracellular processing – possibly from improper protein folding – significantly reduced the amount of enzyme secreted. In combination, these two effects limited the gains we sought from deleting the propeptide. Our attempts to reduce autoproteolytic degradation with stabilizing mutations were unsuccessful. It appears that our understanding of the autoproteolytic cleavage of MMPs is still in the nascent stages and more research is needed to effectively block this process.

One intruiging and unexpected result came from our analysis of the MMP-expressing tumors. While collagen and diffusion were not affected, MMP-1 and -8 expression reduced the sulfated GAG content in tumors and increased tumor hydraulic conductivity. This led to a significant improvement in the efficacy of an oncolytic HSV vector. This finding has several important implications. First, it highlights the significance of initial intratumoral distribution in regulating the overall efficacy of oncolytic HSV therapy. It

echoes the findings from our modeling work (Chapter 2) and the bacterial collagenase study (Chapter 3). This thesis has clearly shown that the physicochemical properties of HSV and the tumor extracellular matrix combine to severely limit the intratumor distribution of infused particles. Second, this finding has identified a novel approach to improve the efficacy of oncolytic viral treatment: enhancing convection during intratumoral infusion by modifying the tumor matrix with MMPs. By using both bacterial collagenase to degrade fibrillar collagen and MMPs to deplete tumor sulfated GAGs, this thesis has highlighted the significant impact that an improved initial viral distribution can have on the therapeutic outcome of oncolytic viral therapy. However, this work also emphasizes the pleiotropic nature and complexity of the MMP family of enzymes. Since they have a host of matrix substrates, it may be difficult to use MMPs to specifically degrade a single matrix component. Care must be taken in their use since it is likely that unintended effects will arise.

The use of MMP-1 and -8 to modulate sulfated GAGs and hydraulic conductivity is an exciting new approach which has the potential to improve the treatment of tumors. However, oncolytic viral therapy would be further enhanced if this approach could be combined with a method which improves diffusive transport in tumors. Enhanced convection would improve the initial viral distribution, while increased diffusion would allow progeny virus to spread more broadly throughout the tumor. While our efforts to improve diffusion through collagen degradation were not entirely successful, they provide valuable lessons and delineate several options going forward. First, our results have identified several limiting steps in achieving sustained collagenase activity with MMPs and points to several steps necessary to engineer more efficient enzymes. Clearly,

a greater understanding is needed in two key areas: the activation and degradation of MMPs. Knowledge of which proteases activate these two MMPs in physiological settings would open up the possibility of co-delivery of a set of enzymes to overcome the hurdle of extracellular activation. While we showed that simple deletion of the propeptide domain leads to problems in intracellular processing, mutations in the propeptide domain (to make it more susceptible to cleavage or less prone to interaction with the catalytic site) or the insertion of a different cleavage site (such as one that leads to intracellular activation by furin) are still viable options. As for autoproteolytic degradation, a more thorough analysis of the hinge region would allow us to better stabilize these enzymes with mutations. A second option is to apply these MMPs to the treatment of different – more responsive – tumors, rather than modify them to improve their activity in all tumors. Both MMPs have been shown to be activated in the liver (6, 7). Thus, perhaps only certain tumors – those growing in a host site that contains the proper factors for MMP activation – can be treated with this approach. Recently, Cheng *et al.* incorporated MMP-8 into a non-replicating adenoviral vector (8). Infection of human lung cancer cells led to the production of the active form of the protein and the treatment of lung xenografts reduced the amount of tumor collagen and enhanced the efficacy of oncolytic adenoviral therpay. This further suggests that MMP activation is dependent on the tumor type. Third, our findings may suggest that MMP-1 and -8 are more effective as modulators of tumor sulfate GAGs and that other agents must be identified to modulate collagen. Within the MMP family, MMP-14 – which has unique properties like an intracellular activation mechanism and potential resistance to inhibitors as a membrane-bound protein (9, 10) – may be better suited as a tumor collagenase. Outside of the MMP

family of enzymes, cathepsin K may also be an ideal candidate since its acidic pH activity dependence makes it "targeted" to tumors (which generally have low pH) and it has not been linked to tumor cell invasion or metastasis. While it was not a potent collagenase in our *in vitro* assays, these studies were performed with conditioned media samples which may have promoted degradation and inhibition. More success may be found by applying recombinant cathepsin K directly to tumors. In addition, there are alternative methods to modulate tumor collagen that do not involve the direct use of collagenases at all. Upstream effectors may be identified which can initiate the entire expression and processing cascade that is needed to degrade collagen *in vivo*. This would bypass the need to develop methods to activate and stabilize the enzymes. Another approach is to focus on inhibiting collagen deposition, perhaps by blocking TGF-β, which has been associated with collagen production in tumor fibroblasts (11, 12).

Regardless of which path is taken, this thesis serves as a necessary first attempt to develop clinically relevant techniques to overcome the barrier to interstitial transport posed by collagen and sulfated GAGs. It has exposed the difficulties and limitations in this technique and has identified critical processes that need to be addressed in future attempts. The negative effect of the tumor ECM on therapeutic delivery and efficacy has garnered very little attention despite its substantial potency and its broad applicability among both tumors and therapeutics. We hope that in some small measure this work shines light on this problem and provides insight into how to overcome it.

References

1. Alexandrakis G, Brown EB, Tong RT, Campbell RB, Boucher Y, Jain RK. Two-photon fluorescence correlation microscopy reveals the two-phase nature of transport in tumors. Nature Medicine 2003.
2. Brown E, McKee T, diTomaso E, *et al.* Dynamic imaging of collagen and its modulation in tumors in vivo using second-harmonic generation. Nat Med 2003;9: 796-800.
3. Netti PA, Berk DA, Swartz MA, Grodzinsky AJ, Jain RK. Role of extracellular matrix assembly in interstitial transport in solid tumors. Cancer Res 2000;60: 2497-503.
4. Pluen A, Boucher Y, Ramanujan S, *et al.* Role of tumor-host interactions in interstitial diffusion of macromolecules: cranial vs. subcutaneous tumors. Proc Natl Acad Sci U S A 2001;98: 4628-33.
5. Sternlicht MD, Werb Z. How matrix metalloproteinases regulate cell behavior. Annu Rev Cell Dev Biol 2001;17: 463-516.
6. Iimuro Y, Nishio T, Morimoto T, *et al.* Delivery of matrix metalloproteinase-1 attenuates established liver fibrosis in the rat. Gastroenterology 2003;124: 445-58.
7. Siller-Lopez F, Sandoval A, Salgado S, *et al.* Treatment with human metalloproteinase-8 gene delivery ameliorates experimental rat liver cirrhosis. Gastroenterology 2004;126: 1122-33; discussion 949.
8. Cheng J, Sauthoff H, Huang Y, *et al.* Human Matrix Metalloproteinase-8 Gene Delivery Increases the Oncolytic Activity of a Replicating Adenovirus. Mol Ther 2007.
9. Owen CA, Hu Z, Lopez-Otin C, Shapiro SD. Membrane-bound matrix metalloproteinase-8 on activated polymorphonuclear cells is a potent, tissue inhibitor of metalloproteinase-resistant collagenase and serpinase. J Immunol 2004;172: 7791-803.
10. Yana I, Weiss SJ. Regulation of membrane type-1 matrix metalloproteinase activation by proprotein convertases. Mol Biol Cell 2000;11: 2387-401.
11. Berking C, Takemoto R, Schaider H, *et al.* Transforming growth factor-beta1 increases survival of human melanoma through stroma remodeling. Cancer Res 2001;61: 8306-16.
12. Lohr M, Schmidt C, Ringel J, *et al.* Transforming growth factor-beta1 induces desmoplasia in an experimental model of human pancreatic carcinoma. Cancer Res 2001;61: 550-5.

Appendix: Treatment of Liver Tumors

Previous studies have shown that MMP-1 and MMP-8 can be used to treat liver fibrosis (1, 2). Replication deficient adenoviral vectors were used to genetically deliver the full length enzymes. While neither MMP was activated *in vitro* when expressed in liver cells, both were activated in the extracellular space of the liver *in vivo*. In both cases, the amount of collagen in the liver was markedly reduced. These findings led us to hypothesize that perhaps the activation of these MMPs is dependent on the tumor host site, with the liver being particularly amenable. In support of this hypothesis, various proteases have shown the ability to activate (or partially activate) these MMPs *in vitro*, and the presence and amount of these proteases – as with many proteins – likely varies by organ site. To test this hypothesis we performed the following preliminary experiments.

We first tested whether MMPs expressed in tumors would be differentially activated depending on the site of tumor implantation. MMP-1 and MMP-8 overexpressing HSTS26T cells (developed in Chapter 5) were implanted in the liver of SCID mice by direct injection of ~$5x10^5$ cells into a single lobe. Tumors were also grown subcutaneously in the leg, a site in which we previously observed limited MMP activation (Chapter 5, Fig. 5.2A). Mock-transfected tumors were grown in both sites as a control. After 3-4 weeks, tumors were harvested and western blot performed on the tumor lysate to determine the levels of active and latent MMPs. For MMP-1, the western blot shows that for tumors grown in both the liver and subcutaneously, enzyme is primarily in the latent form (Appendix Fig. 1A). In contrast, MMP-8 was found to be primarily in the active form in the liver, but in the latent form in subcutaneous tumors (Appendix Fig.

1B). For both tumor sites, low background expression of each MMP was observed. Thus, it appears that the activation of MMPs – at least MMP-8 – is tumor host site dependent.

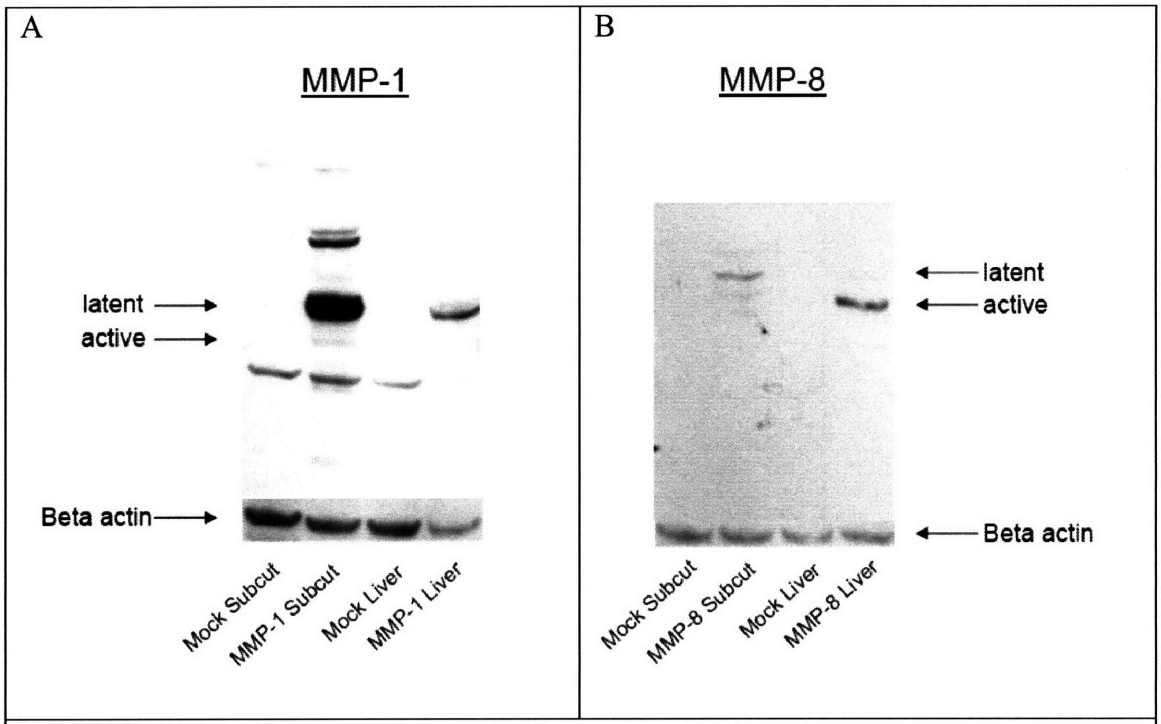

Appendix Figure 1. Expression of MMP-1 and MMP-8 in subcutaneous and liver tumors. (A) MMP-1 and (B) MMP-8 overexpressing HSTS26T cells were implanted in the subcutaneous space or in the liver of SCID mice. Western blot was performed on tumor lysates. The location of bands corresponding to the latent and active forms is denoted by arrows. Beta actin western blots are shown at the bottom for control. There is low background expression of both MMPs in mock-transfected tumors in both sites. While MMP-1 is found predominantly in the latent form in both sites, MMP-8 is found in the latent form in subcutaneous tumors but in the active form in liver tumors.

Based on these encouraging findings, we decided to test whether tumors grown in the liver would respond better to treatment with MMP-expressing oncolytic HSV vectors.

We hypothesized that virus expressing MMP-8 would better spread through the tumor and control its growth. We performed a tumor treatment experiment similar to that performed with subcutaneous tumors (Chapter 5, Fig. 5.12). In that previous experiment we observed no difference in the response to MMP-expressing oncolytic viruses. Here, wild type HSTS26T cells were first stably transfected with Gaussia luciferase via lentiviral vectors (gift from Bakhos Tannous, Massachusetts General Hospital). Tumors were grown in the liver as before. Tumor load was monitored by obtaining 5 μl of blood from each mouse, adding the luciferase substrate coelenterazine and measuring the bioluminescence signal. This bioluminescence signal has been found to correlate well with the tumor load (Xandra Breakefield, personal communication), and provided us with a method to monitor tumor growth without performing invasive surgery multiple times. At an appropriate size, tumors were treated with a single intratumor injection of PBS or 2.5×10^6 t.u. of HsvQ-1, HsvQ1-MMP-1 or HsvQ1-MMP-8. Tumor load was monitored after treatment.

We found that there was no difference in the mean tumor growth rate between treatment groups (Appendix Fig. 2). There was also no difference between any of the treatment groups and the control. This latter result suggests that tumors need to be treated with a higher dose, multiple doses or at a smaller size in order to see a response to the oncolytic virus. We also observed that tumors grew quite heterogeneously. In some cases, tumors grew in the middle of the lobe of the liver. In other cases, tumors grew at the edge and often spread to the abdominal cavity. There were also instances of tumors growing in both the liver and abdominal cavity in the same mouse. Leakage of tumor cells from the liver during implantation was observed and likely contributed to this pattern of growth.

Approximately 1/3 of tumors had significant regions of necrotic tissue at the time of treatment, although tumors were still relatively small in size. Furthermore, nearly ¼ of the mice became sick, a condition that did not correlate with tumor size or treatment with virus. The causes of the unusual behavior are not known. However, to obtain more consistent tumors, it may be necessary to inject less tumor cells at a lower flow rate into the liver.

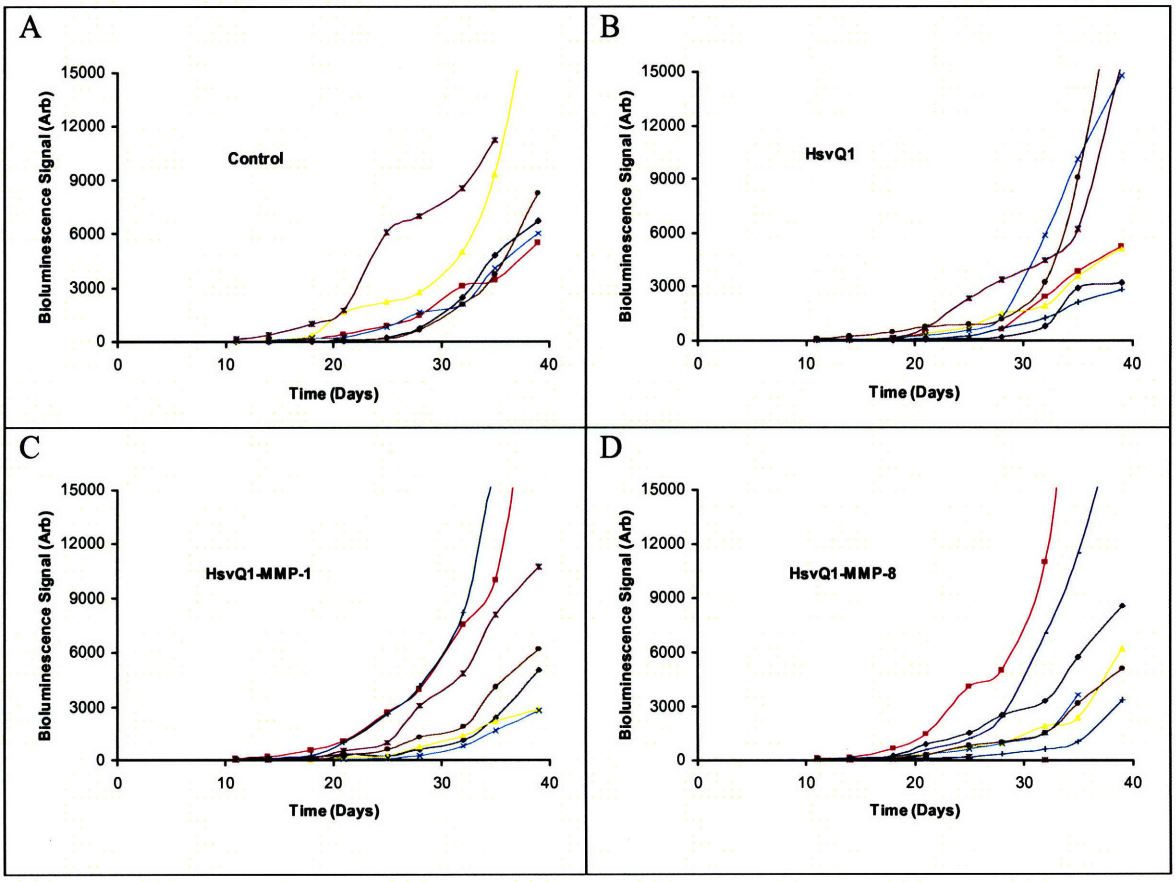

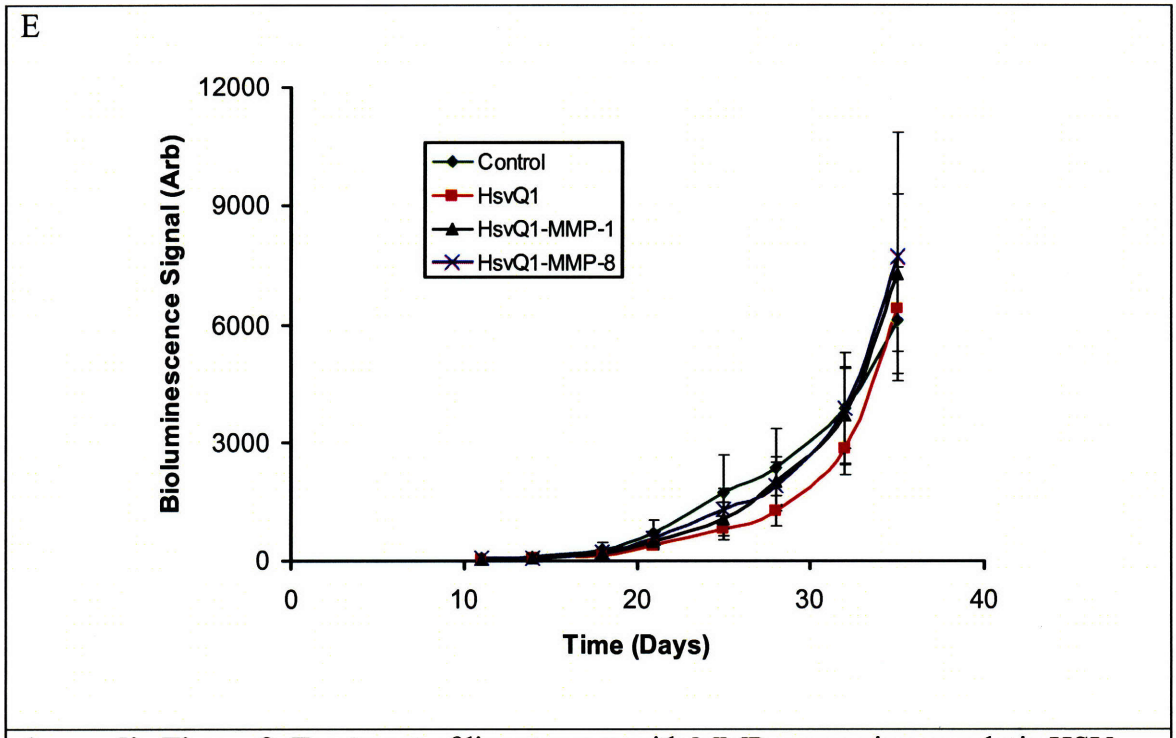

Appendix Figure 2. Treatment of liver tumors with MMP-expressing oncolytic HSV vectors. Tumors were grown in the liver and treated with a single injection of PBS control or 2.5 x 10^6 t.u. of HsvQ-1, HsvQ1-MMP-1 or HsvQ1-MMP-8. Tumor size was monitored by addition of luciferase substrate and measurement of bioluminescence. Tumor size is given as bioluminescence signal in arbitrary units. (A-D) Individual growth curves for control (A), HsvQ1 treated (B), HsvQ1-MMP-1 treated (C) and HsvQ1-MMP-8 treated (D) tumors. (E) Mean tumor size and standard errors for each treatment group. Tumors were treated at a bioluminescence signal of 430 ± 216 (mean ± SD). No significant difference in tumor growth was observed.

In conclusion, no difference was observed in the efficacy of oncolytic HSV treatment of liver tumors with MMP-1 or MMP-8 expression. Substantial improvements to both the experimental model and treatment parameters are needed to definitively assess the

relative effectiveness of the oncolytic vectors in liver tumors. Furthermore, the preliminary results with MMP-1 and MMP-8 expression in liver tumors (Fig. 1) should be confirmed by both western blot and collagenase activity assays and the effect on tumor collagen should be determined.

References

1. Iimuro, Y., Nishio, T., Morimoto, T., Nitta, T., Stefanovic, B., Choi, S. K., Brenner, D. A., and Yamaoka, Y. Delivery of matrix metalloproteinase-1 attenuates established liver fibrosis in the rat. Gastroenterology, *124:* 445-458, 2003.
2. Siller-Lopez, F., Sandoval, A., Salgado, S., Salazar, A., Bueno, M., Garcia, J., Vera, J., Galvez, J., Hernandez, I., Ramos, M., Aguilar-Cordova, E., and Armendariz-Borunda, J. Treatment with human metalloproteinase-8 gene delivery ameliorates experimental rat liver cirrhosis. Gastroenterology, *126:* 1122-1133; discussion 1949, 2004.